ABSTRACT

Title of Dissertation: A SYNTHETIC TMRNA PLATFORM FOR ELUCIDATION OF BACTERIAL PROTEOME REMODELING UNDER STRESS

Dissertation directed by: Professor & Chair, Kevin S. McIver

Cell Biology and Molecular Genetics

Translational reprogramming is a key component of the bacterial stress response and is a function of mRNA stability, protein turnover and proteolysis. Total proteome measurements give a view of the stable proteome but can fail to capture dynamic changes under stress, including incomplete polypeptides that result from cleaved mRNAs or stalled translation events. Bacteria employ a nearly ubiquitous native ribosome rescue system, transfer-messenger RNA (tmRNA), that rapidly resolves stalled translational complexes and tags the incomplete polypeptides for degradation. Characterization of these tmRNA-tagged polypeptides could reveal previously unknown aspects of the bacterial stress response. To address this information gap, we have developed a synthetic tmRNA platform that reprograms the native system to allow for co-translational labeling of the incomplete polypeptides in live bacteria. A short tag reading frame (TRF) encoded on native tmRNA facilitates the addition of a natural peptidyl degradation tag to the polypeptides, and therefore offers an attractive modular domain to introduce synthetic peptide tag sequences and study the “degradome”. To study translational remodeling under stress, we modified the native tmRNA with an 6x-HIS isolation tag with the specific purpose of stabilizing, isolating, and characterizing the degradome in *Escherichia coli*. Using our inducible system, we have successfully isolated 6xHis-tagged proteins, verified dynamic controlled tagging, assessed broad-spectrum tag introduction with mass spectrometry. Our results capture known tmRNA substrates and excitingly show that tagged protein profiles are markedly different under stress. We investigated the shifting degradome in cells experiencing translational stress associated with serine starvation induced by serine hydroxamate. In cells lacking RelE, the mRNA interferease toxin that

cleaves mRNA in the ribosome A site, we find a dramatic shift away from catalytic protein degradation and distinct, disparate enrichment of ribosomal proteins in the degradome under stress. These latter results suggest a new specific role for RelE in regulating ribosome protein abundance under translational stress conditions.

A SYNTHETIC TMRNA PLATFORM FOR ELUCIDATION OF BACTERIAL PROTEOME REMODELING UNDER STRESS

by

Randi Laine Turner

Dissertation submitted to the Faculty of the Graduate School of the University of Maryland, College Park, in partial fulfillment of the requirements for the degree of

Doctor of Philosophy

2022

Advisory Committee:

Professor Kevin McIver, Chair

Professor Jonathan Dinman

Associate Professor Jiqiang Ling

Professor Wade Winkler

Professor Eric Haag, Dean's Representative

ACKNOWLEDGEMENTS

I would first and foremost like to extend my gratitude my committee members: Dr. Kevin McIver, Dr. Jonathan Dinman, Dr. Wade Winkler, Dr. Jiqiang Ling, and Dr. Eric Haag. My road to my defense has been paved with uncertainty and turmoil, and you have been unendingly empathetic, patient, and helpful throughout. You have served as indispensable support in my time of need and gone above and beyond to help me reach my final goals. I would not have had a positive outcome to my graduate career without your guidance and assistance.

I would also like to thank my former advisor Dr. Daniel Dwyer. You created an environment that allowed me to thrive as an independent researcher. Under your advisement, I developed essential project and lab management skills, gained an understanding of establishing and maintaining a research lab, and learned the value of self-motivation, independent scholarship, and perseverance. My career will forever be informed by these lessons.

I would like to thank the former members of the Dwyer, particularly Aubrey Geer, Allison Daitch, and Dr. Sean Mack, and the friends I made at UMD. You offered camaraderie and laughter even in the most disheartening times. My graduate experience would not have been the same without you.

I would like to thank the BISI-MOCB program and staff for funding my research and supporting me for these seven years. I would like to specially thank Gwen Warman, Dr. Zakiya Whatley, and Elizabeth Pepper for their administrative support. You were there whenever I needed a last-minute TA spot or a quickly filed form. I am forever grateful for your efforts, though I apologize for the stress I put on you.

I would also like to thank Nick Paladino and One Frame Link. My love of data science, analysis, and graphical presentation began here in the most unlikely of places. Your companionship and passion inspired me at a time when I was struggling. Our work drove me to expand my horizons and bettered me academically. I can honestly say my academic scholarship and analysis would not be the same without the experience you offered me.

To my parents, thank you for supporting and driving me through my career. It has been a winding road, but through your support and love, I have made it to a very bright horizon. From an early age, you instilled hard work and perseverance. The skills and values you taught me have been instrumental in my success.

And finally, to my partner Joseph Kendra. You have taken on so many roles throughout our time together. You have been my rock, my cheerleader, my sympathetic ear, and most recently my editor-in-chief. Truly, I would not be here without you. You have held my hand through the dark and guided me to a bright horizon. I look forward to many better years in our future.

TABLE OF CONTENTS

LIST OF TABLES

LIST OF FIGURES

LIST OF ABBREVIATIONS

6xHIS	6x-Histidine epitope
AB	Antibody
ABC	ATP binding cassette
AME	Aminoglycoside modification enzyme
AMR	Antimicrobial resistance
ArfA	Alternative release factor A
ArfB	Alternative release factor B
aTc	Anhydrous tetracycline
CDC	Centers for Disease Control
DDA	Data-dependent acquisition
DNA	Seoxyribonucleic acid
EF-G	elongation factor G
EF-Tu	elongation factor Tu
GO	gene ontology
GSK	GlaxoSmithKline
IDT	Integrative DNA Technology
IP	immunoprecipitation
LC-MS/MS	liquid chromatography tandem mass spectrometry
LFQ	label-free quantification
M/z	mass-to-charge ratio
MATE	multi-drug and toxin extrusion
MDR	Multi-drug resistance
MFS	major facilitator superfamily
mg	milligram
mL	milliliter
MLD	mRNA-like domain
mRNA	messenger RNA
MRSA	methicillin resistant staphyloccocus aureus
PBP	penicillin binding protein
PK	pseudoknot
PPP	Pentose phosphate pathway
PQ	paraquat
PTC	peptidyl transferase center
RBS	ribosome binding site
RNA	ribonucleic acid
RNAP	RNA polymerase
RND	resistance nodulation-division
SHX	serine hydroxamate
SmpB	small molecule protein B
SMR	small multidrug resistance
TLD	tRNA-like domain
tmRNA	transfer messenger RNA
TRF	tag reading frame

tRNA	transfer RNA
TTC	transcriptional-translational complex
µg	microgram
µL	microliter
UT	untreated
WB	western blot
WT	wildtype MG1655

CHAPTER 1: INTRODUCTION

Antibiotics

Humans have been locked in a deadly battle with microbial pathogens for the entirety of our existence. We are constantly besieged by microscopic entities that want to invade and infect us, from viruses, bacteria, fungi, and parasites. Bacteria are omnipresent in our environment, abundant in our soil, water, and even on our skin and in our bodies. Most of these do not harm us and some are even beneficial, like those in our digestive tracts. Yet even here, there is a delicate balance between a commensal relationship and a pathogenic invasion. *Staphylococcus aureus,* for example, is a bacterium often found in the natural biota of our skin and typically thrives there without threat. However, if allowed to enter our bodies, this same bacterium can cause skin lesions, pneumonia, endocarditis, and sepsis.[1] We have evolved defenses to maintain the balance. Our skin prevents pathogens from entering; our immune system attacks those that slip through; genetic mutations provide diversity in immune responses and targets of pathogens. But we are not the only ones evolving solutions. Pathogens are constantly evolving along-side of us, developing better infectivity, greater pathogenicity, and even evading our defenses. And so, we remain locked in this ever-evolving arms race.

About 100 years ago, we got the upper hand. In 1928, the Scottish physician, Alexander Fleming discovered a compound that inhibited the growth of bacteria.[2–4] Fleming had just been appointed as the Chair of Bacteriology at St. Mary's Hospital in London and was conducting research on *Staphylococcus* species.[5] In September, he returned from a month long vacation with his family to find his culture plates contaminated.[6] He noticed that the bacteria growing in close proximity to this contaminant had begun to turn translucent and were lysing. Further isolation and testing revealed that the mold excreted a compound that had "marked bactericidal and bacteriolytic properties."[7] He named this compound penicillin after the genus of the mold that produced it, *Penicillium.* It would prove nothing short of a medical miracle.

During the first world war (1914-1918), over 4 million American soldiers were deployed around the world. The trench warfare that defined this conflict proved to be a breeding ground for infection and disease, with little meaningful medical recourse. By the end of the war, 57,460 American soldiers had died of disease,

eclipsing the 50,280 deaths from combat related injuries.[8] When World War II broke out twenty years later, penicillin was becoming widely available and utilized in the medical field. [9] More than 11 million American soldiers were deployed throughout the war. All told, 220,823 of these soldiers died of combat injuries and only 14,904 died of disease. The employment of antibiotics was a pivotal victory over infectious diseases, which has since not been a significant contributor to American warzone deaths.[8]

Despite being a landmark discovery in the field of medicine, penicillin was not the first antibiotic to be used by humans to treat microbes. Traces of tetracycline have been found in Egyptian mummies and skeletons from Sudanese Nubia from 350 AD.[10–12] Mold has been used in numerous cultures for wound treatments.[2,3,13] British herbalists commonly used a concoction of moldy bread and milk; Chinese medicine men used moldy soy beans; and Aboriginal peoples in Australia used mold from eucalyptus trees.[14] In 1910, a synthetic arsenic-based compound, salvarsan, was discovered and used to treat syphilis.[2–4] This discovery was the first instance of using a synthetic compound library to screen for substances with antimicrobial properties, an approach that continues to be used today.[3] Thus, while not entirely novel, Fleming's discovery nonetheless rapidly changed the face of the medical field and kicked off a surge in antibiotic development.

From 1940-1970, there was a rapid expansion of the antibiotic arsenal that became known as the Golden Age of Discovery. This generation of drugs were largely isolated natural products (Table 1). These

Antibiotic Class	Example Compound	Originating Species	Target Pathway	Molecular Target
β-lactams	Penicillin G	Penicillium	Cell wall synthesis	Peptidogylcan
Aminoglycosides	Kanamycin	Actinomycetes	Protein synthesis	30S ribsomal subunit
Macrolides	Erythromycin	Actinomycetes	Protein synthesis	50S ribosomal subunit
Tetracyclines	Tetracycline	Actinomycetes	Protein synthesis	30S ribsomal subunit
Glycopeptides	Vancomycin	Actinomycetes	Cell wall synthesis	Lipid II
Lipopeptides	Daptomycin	Actinomycetes	Cell membrane	Cell membrane disruption
Polyketides	Rifamycin SV	Actinomycetes	Nucleic acid synthesis	RNA polymerase
Sulfonamides	Sulfamethoxazole	Synthetic	Folate synthesis	Dihydroptreroate
Fluoroquinolones	Ciprofloxacin	Synthetic	DNA synthesis	DNA gyrase and topoisomerase IV
Oxazolidinones	Linezolid	Synthetic	Protein synthesis	50S ribosomal subunit

Table 1. Major classes of antibiotics as determined by molecular structure and target. Classes listed with an example compound from the class, the originating species, and molecular target of action.

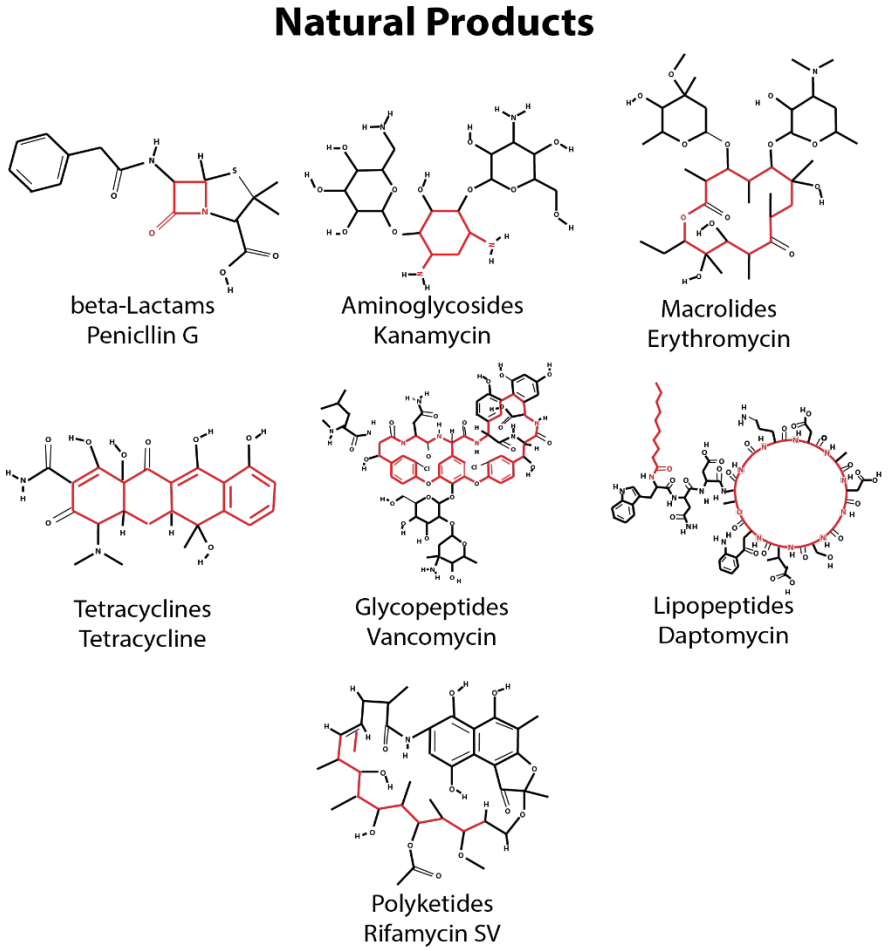

Figure 1. Representative compound structures of each major antibiotic class. The core structures that characterize each class are highlighted in red.

compounds targeted bacterial-specific molecules and worked to inhibit essential functions. Seven major classes of natural antimicrobial compounds were discovered. (Table 1, Figure 1) These classes were determined by the core structure and molecular target.

Penicillin founded the most well-known class, the β-lactams. These compounds all have a characteristic four-membered ring in their structure and target the proteins used in peptidoglycan synthesis. Aminoglycosides, like kanamycin, contain a 2-deoxystreptamine core and two other attached sugar structures with amino group substitutions. These compounds bind to the 30S subunit of the prokaryotic ribosome to reduce translational fidelity. Tetracyclines also target the 30S subunit, though at a distinct site from the aminoglycosides. Characterized by a four fused six-member rings, they inhibit protein synthesis by preventing stable accommodation of amino acid building blocks into the ribosome. Erythromycin founded the macrolide class. Macrolides, short for macrolactone polyketide, have a core macrolactone ring and interact with the 50S ribosomal subunit to block addition of amino acids during protein synthesis. A related class of polyketides, like rifamycin, have a similar composition to macrolides but are structurally distinct with a chained "bridge" on one face of the molecule. These inhibit RNA polymerase and prevent transcription. Glycopeptides, like vancomycin, have a hepta-peptide backbone that is cross-linked to its sidechains. This forms a cup-like structure that prevents cell wall assembly by binding to the peptidoglycans used to compose it. Like the glycopeptides, lipopeptides have a polypeptide backbone but are modified

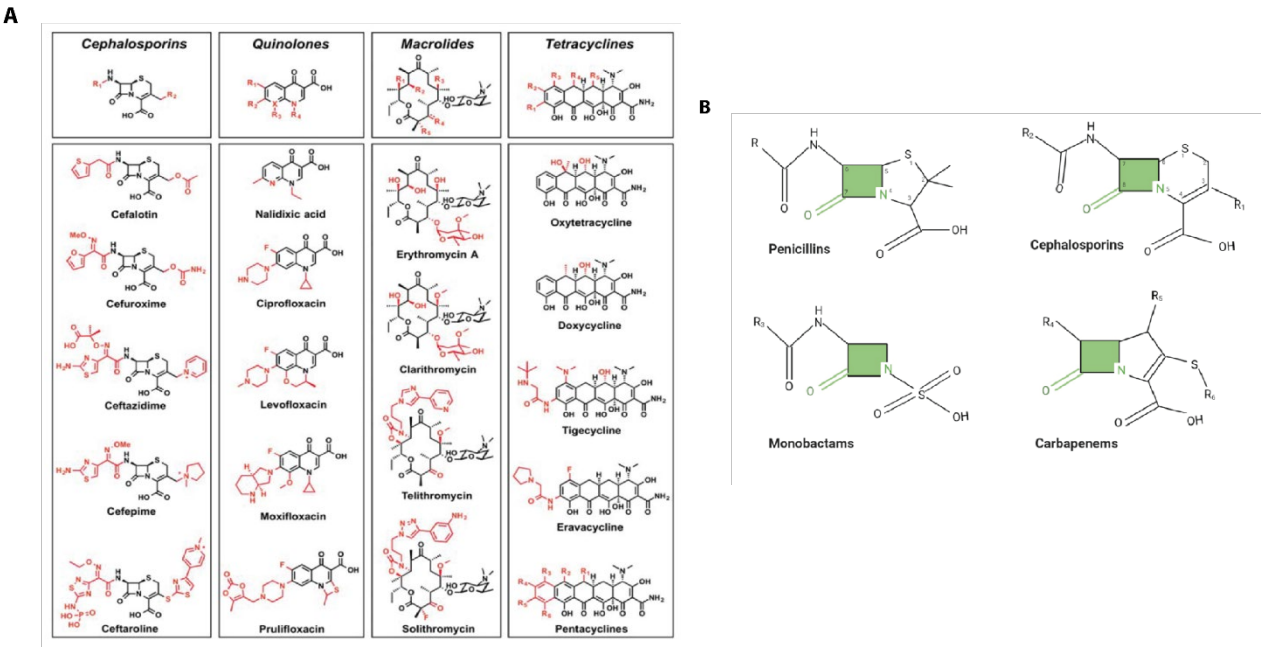

Figure 3. Antibiotic structure modification by generation. (A) Representative antibiotic structures from different classes and structural modifications made through each generation (red). Originally appears in Walsh and Wencewicz 2014. (B) Representative structures of β-lactam subclasses with core structure in green. Image originally appears in Vrancianu *et al.* 2020.

with lipid chains attached. Lipopeptides like daptomycin work to disrupt cell membrane integrity, though the exact mechanism is not understood.

Fully synthetic antibiotics also appeared early in the discovery age. Sulfonamides, like sulfamethoxazole, were among the first antibiotic compounds to be used in the clinical setting, even before penicillin.[3,4] Similar to their natural counterparts, these targeted bacterial pathways essential to their survival. Sulfonamides have an azobenzesulfonamide scaffold that works to inhibit the synthesis of folate, a key component of nucleic acid synthesis. Fluoroquinolones are considered the most successful class of synthetic antibiotics. They have a core of nalidixic acid and block DNA synthesis through binding to topoisomerase II enzymes. By the end of the 1960s, discovery of new drug classes had slowed, but a new era of chemical modification was on the rise. In the Golden Age of Medicinal Chemistry, development of new antibiotics was focused on improving the pharmacological efficacy of existing compounds. The originally discovered compounds (first-generation antibiotics) became the scaffolds for successive generations. The core bioactive structures remained intact while sidechains and groups were altered. Some modifications were small, while others were more extensive. For example, the difference between oxytetracycline and doxycycline is the removal of a single hydroxyl group from the second ring. Through discovery and modification, the β-lactam class has expanded to include four structural subclasses. (Figure 2). All maintain the core four-membered lactam ring with variations in type of fused bicyclic ring structure, chemical side groups, or even the lack of a bicyclic ring as in the case of monobactams. In more extreme cases, functional groups from multiple classes were combined into one compound. All of these modifications aimed to improve clinical efficacy, stability, bioavailability, and pharmacokinetics. Today, we have fourth- and fifth-generation drugs in clinical use.

Antibiotic Resistance

However, these drugs did not go unchallenged by their targeted pathogens for very long. Penicillin resistance was detected only two years after it became widely available. (Figure 3) Sulfonamide resistance was discovered within three years on clinical implementation. Methicillin resistant *Staphylococcus aureus* (MRSA) was detected in 1960, the same year methicillin was approved for clinical use.[9] Other resistances took longer to manifest. Vancomycin, a glycopeptide targeting cell wall synthesis, did not incur resistance until 30 years after its release. Steadily, resistant bacteria became more prevalent and more deadly. In

2019, the Center for Disease Control (CDC) estimated that MRSA was responsible for over 300,000 infections and more than 10,000 deaths in the US.[9] Worryingly, multiple-drug resistance (MDR) has also been on the rise.[15,16] In addition to methicillin, most current MRSA isolates carry resistance to at least one other class of drug including aminoglycosides, tetracycline, and macrolides.[17,18] In 2018, the United Nations declared antimicrobial resistance (AMR) as a global threat,[19] and a year later, the CDC released its threat report with 18 resistant microbes reported as either urgent, serious, or concerning threats (Table 2).[9]

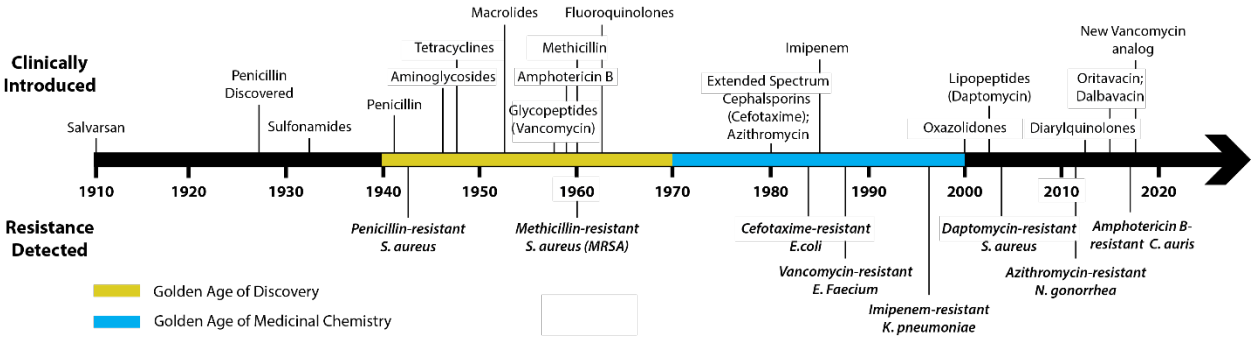

Figure 3. Timeline of antibiotic developments and first detection of clinically resistant bacterial strains. Top: years that antibiotic compounds were approved for clinical use. Bottom: year that first resistant species were detected.

Unfortunately, development of AMR was inevitable. In 2012, a bacterial survey sample was conducted in a highly isolated section of the Lechuguilla Cave in New Mexico. Lechuguilla is one of the 10 longest caves in the world with over 148 miles of caverns mapped and is famous for its beautiful gypsum formations featured in the BBC Planet Earth series.[20,21] Access to the caverns is strictly regulated by the park service, preserving its pristine environments. Researchers sampled a section of the cave system that they estimated had been isolated from the surface for over 4 million years. They identified microbes that were resistant to 14 commercially used antimicrobials including daptomycin, a drug considered to be a last resort treatment for gram positive bacteria.[22] Even in the near complete absence of human intervention, AMR was diversely present. Resistance is a natural phenomenon.

During the Golden Age of Discovery, 55% of new antimicrobial compounds were isolated from *Streptomyces*, a genus of bacteria commonly found environmentally in soil and water.[23] It is hypothesized that these compounds served as chemical weapons, allowing *Streptomyces* to out-compete other native soil-dwelling bacteria for resources or to protect them from predation by other species.[23–25] Production of

these chemicals means that the producer needs to be to resistant to their effects. Most antibiotic-producing species have multiple ways to evade the mechanism of action of their compound and are considered to have natural resistance.[4] With the presence of antibiotic-producing bacteria comes the selective pressure for co-habitating species to evade these compounds. This is one of the drivers of acquired resistance.

Organisms can use multiple strategies to confer resistance. One of the most common is antibiotic modification or degradation.[26] Aminoglycoside modification enzymes (AMEs) were first identified in aminoglycoside-producing *Streptomyces*.[27,28] These are a diverse class of enzymes that modify the chemical structure through acetylation, phosphorylation or adenylation. While they were first identified as

Threat Level	Organism	Primary Resistance	Other notable resistances
Urgent	Acinetobacter	Carbapenem	Fluoroquinolones, extended-spectrum β-lactam, ampicllin, sulbactam
Urgent	Candida auris	Multiple drugs	Azoles, echinocandin, amphotericin B
Urgent	Clostridioides difficile	Cephalosporins	Fluoroquinolones, erythromycin, clindamycin
Urgent	Enterobacteriaceae	Carbapenem	All β-lactams
Urgent	Neisseria gonorrhoeae	Penicllin, tetracycline	Ciprofloxacin, cefotaxime
Serious	Campylobacter	Ciprofloxacin	Azithromycin
Serious	Candida species	Multiple drugs	Azoles, echinocandin, amphotericin B
Serious	Extended bata-lactamase producing Enterobacteriaceae	β-lactams	Cephalosporins
Serious	Enterococci	Vancomycin	
Serious	Pseuidomonas aeruginosa	Multiple drugs	Fluoroquinolones, polymyxins, aminoglycosides, rifampin
Serious	Nontyphoidal salmonella	Ciprofloxacin	Ceftriaxone, azithromycin, ampicllin, trimethoprim
Serious	Salmonella serotype tyhpi	Ciprofloxacin	Chloramphenicol, ampicillin, nalidixic acid, cephalosporin
Serious	Shigella	Ciprofloxacin	Azithromycin
Serious	Staphylococcus aureus	Methicillin	Other β-lactams
Serious	Streptococcus pneumoniae	Penicillin	Amoxicillin, erythromycin, cefotaxime, cefuroxime, vancomycin, tetracycline, levofloxacin
Serious	Tuberculosis	Isoniazid	Rifampin, pyrazinamide, ethambutol
Concerning	Group A Streptococcus	Erythromycin	Clindamycin
Concerning	Group B Streptococcus	Clindamycin	Eyrthoromycin

Table 2. Global antibiotic threats identified by the CDC in their 2019 report. Threat level of each resistant species and primary resistance of concern of each species are listed. Other notable resistances include additional resistances commonly found with primary resistance.

a natural resistance mechanism, AMEs have also been identified in resistant clinical isolates as well. Modification enzymes are also used to inactivate bleomycin family antibiotics and chloramphenicol. In contrast, resistance to β-lactams is typically conferred by a hydrolyzing β-lactamase. While β-lactamase are a diverse family, they all cleave the four-membered lactam ring at the core of the antibiotic. Similar to AMEs, β-lactamases are also commonly found in *Streptomyces* as well as other pathogenic and non-pathogenic bacteria.[26,29]

Efflux, pumping antibiotic from the cell, is another common resistance strategy. Efflux is typically found in conjunction with other resistance mechanisms, particularly in producer organisms. Active efflux pumps can come from several families: ATP Binding Cassette (ABC), major facilitator super family (MFS) transport proteins, resistance nodulation-division (RND), multidrug and toxin extrusion (MATE), or small multidrug resistance (SMR). The majority of these pump families rely on ion gradient coupled transport, but the ABC proteins utilize ATP to pump substrate from the cell.[30] While some pumps are specific in their substrate, like the Tet pump proteins of the MFS family, every family has pumps that exhibit polyspecificity. For example, OtrC protein from the ABC family is able to transport multiple antibiotic classes such as oxytetracycline, ampicillin, and vancomycin.[26,31] Polyspecific pumps can be found in both clinical resistant isolates and natural produce organisms and can be used in conjunction with specific efflux pumps, resulting in MDR or decreased sensitivity to particular antibiotics.[26,32]

Target modification and protection mechanisms are particularly prevalent and diverse resistance mechanisms in clinical isolates. These can range from target point mutations, enzymatic alterations, post-translational modifications, to by-passing mechanisms. Many clinical MRSA strains contain a classic example of target by-pass. MRSA has an exogenous penicillin binding protein (PBP), PBP2a, whose transpeptidase domain is insensitive to many β-lactams.[33] Macrolide resistance on the other hand is often conferred by one of the erythromycin ribosomal methylation genes, which methylate an adenine in the 23S rRNA. [26] Target protection is a less common, but effective strategy for resistance. Two of the tetracycline resistance mechanisms, the Tet(M) and Tet(O) proteins, act to remove tetracycline from the ribosome using through GTPase activity.

Acquired resistance is resistance that is developed to a compound not produced by the host organism. This can be either through selective mutation or horizontal gene transfer (HGT).[34,35] Bacteria have multiple routes for HGT: transformation, transduction, and conjugation. Transduction and conjugation involve direct transfer of genetic from one organism to another. In transduction, bacteriophage inject genetic material directly into the host bacteria, while in conjugation, two bacteria directly exchange material. In contrast, transformation involve bacteria assimilating DNA from the environment. This process is commonly used in research labs to introduce synthetic plasmids.[34,35]

While natural resistance mechanisms are placed in the chromosome, acquired resistance mechanisms are often found on plasmids. Plasmids represent a particular threat for AMR. They often contain a collection of genes and are capable of self-replicating.[17] In addition, plasmids allow for genetic transfer between a diverse range of bacterial organisms. Recent years have seen a rise in plasmids containing resistance mechanisms to multiple or nearly all classes of antibiotics.[15,16,32] Most concerning is that some of these plasmids contain resistance genes in a transposon element, allowing for recombination and integration into chromosomal DNA.[15,16]

It is unclear what proportion of AMR-related HGT is through transformation, transduction, or conjugation. However, areas with high densities of bacteria, plasmids, and phages are known to be breeding grounds for resistant bacteria.[18] These include waste from hospitals, agriculture, and sewage. In addition to high microbial populations, these areas are contaminated with antibiotics. The agricultural industry is a main contributor to environmental antibiotic contamination. Livestock is often fed antibiotics both to treat and prevent disease in crowded conditions.[2] Excess antibiotic is excreted through feces and urine, seeping into the soil, groundwater, and surfaces surrounding the facility. This creates additional selective pressure and increases the proportion of resistant microorganisms in an already densely populated area.[16]

Issues in Drug Development

Compounding the issue of increasing resistance, development of new antibiotics has begun to dwindle. The last new class of antibiotics to be discovered were the oxazolidinones in 1987 after a nearly 30 year gap.[4,36] The first drug discovered, linezolid, had a completely unique structure to other compounds that existed at the time. It has become the core structure of the class, with additional compounds being created

from chemical modification. Oxazolidinones are known to bind to the 50S subunit of the ribosome to inhibit protein synthesis, but the exact mechanism has been difficult to discern. New compounds continue to release however they primarily are modifications of existing antibiotics.

As the 1990's dawned, there was new hope for antibiotics on the horizon. The Human Genome project launched in 1990 and was shortly followed by campaigns for other model organisms, including *Escherichia coli* and *Bacillus subtilis*. In 1995, the first bacterial genome was sequenced, the pathogenic *Haemophilus influenzae*. By 1999, genomes for *E. coli, B. subtilis, M. tuberculosis,* and *H. pylori* had been sequenced.[37] There was a rush by pharmaceutical companies to capitalize on the new information. In 1995, GlaxoSmithKline (GSK) launched their new "genomics-derived, target-based approach" to antibiotic discovery.[38] In a combination of bioinformatic analysis and high throughput compound library screening, GSK investigated hundreds of potential targets. By 2001, not a single viable broad-spectrum compound had made it to the development pipeline. In 2006, GSK scientists Payne *et. al* published a retrospective review of the program and the challenges facing antibiotic development. "Blind spots in target validation and an inability to find lead compounds from HTS together with the larger problem of making a single compound that has broad-spectrum activity and is safe at the high serum concentrations needed to cover the least susceptible organisms have left an empty industrial antibacterial portfolio."[38] They found that investigating novel chemical structures and continuing pharmacological optimization have been a more cost-effective and successful avenue for discovery.

Research hurdles are not the only barrier for development of new compounds. Many pharmaceutical companies have chosen to discontinue antibiotic discovery programs. In 2018, there were 45 new antibiotic candidates in clinical trials. Only two of them were owned by major pharmaceutical companies.[3] Unfavorable return of investment has been cited as a primary reason for the departure.[39] Antibiotics are designed to be taken for short periods of time and historically have had low cost. New drugs with novel mechanisms of action will likely be reserved as last resort drugs, further limiting potential return of investment.[3] In addition, costs and regulatory requirements for bringing a drug to market have drastically increased. Currently, antibiotic development is primarily performed in academic research labs. [3,38,39]

Recent technological developments have produced promising results. In the Golden Age of discovery, soil-bacteria were a rich source for antimicrobial compounds. However, soil-bacteria are very difficult to cultivate in the laboratory setting. One recent advance was the development a miniature isolation chip based on a diffusion chamber that allowed soil bacteria to be cultured in a natural environment. This allowed for the isolation of thousands of isolates that were able to be screened and the identification of antibacterial peptide teixobactin.[40] Of the 45 candidate antibiotics in clinical trials in 2018, there were a total of 12 classes on antibiotics represented in the compounds. Seven of them were completely novel.[3]

Stress as a Target

To assist the drug development pipeline, novel targets need to be explored. While we have a good understanding of the primary drug-target interactions for most antibiotics, the downstream and global metabolic changes in response to antibiotics are less explored. Developing a deeper understanding of the bacterial stress response could provide potential novel targets and pathways that could be exploited to increase antibiotic sensitivity.

A key part of the stress response is changes to gene expression. While gene expression can be regulated on many levels, transcription is a primary control point. Transcription initiation is highly regulated, mediated by the sigma (σ) subunit of RNA polymerase (RNAP; Figure 4A). As RNAP binds to the gene promoter, σ subunit recognizes two key elements: the -35 (*E. coli* consensus sequence TTGACA) and -10 sites (*E. coli* consensus sequence TATAAT).[41] Every bacteria has a primary σ subunit that regulates transcription of the housekeeping genes (ie σ^{70} subunit in *E. coli*). However, there are alternative σ-subunits that recognize alternative sequences and are used to control genes associated with stress response, stationary growth, and starvation.[42] As RNAP binds to the promoter, a section of the double-stranded DNA surrounding the gene start site is melted to allow single-stranded access for transcription. RNAP closes around one strand of the DNA, which will serve as the template strand for the new RNA. Free ribonucleotides enter the ribonucleoside tri-phosphate tunnel and stably bind to the template DNA strand through complementary base pairing. Once bound, the active site hydrolyzes the ribonucleotide to join it to the 3' end of the previous nucleotide. The σ subunit is ejected after the synthesis of approximately 10 nucleotides, allowing transcription to continue elongating along the template DNA. Transcription

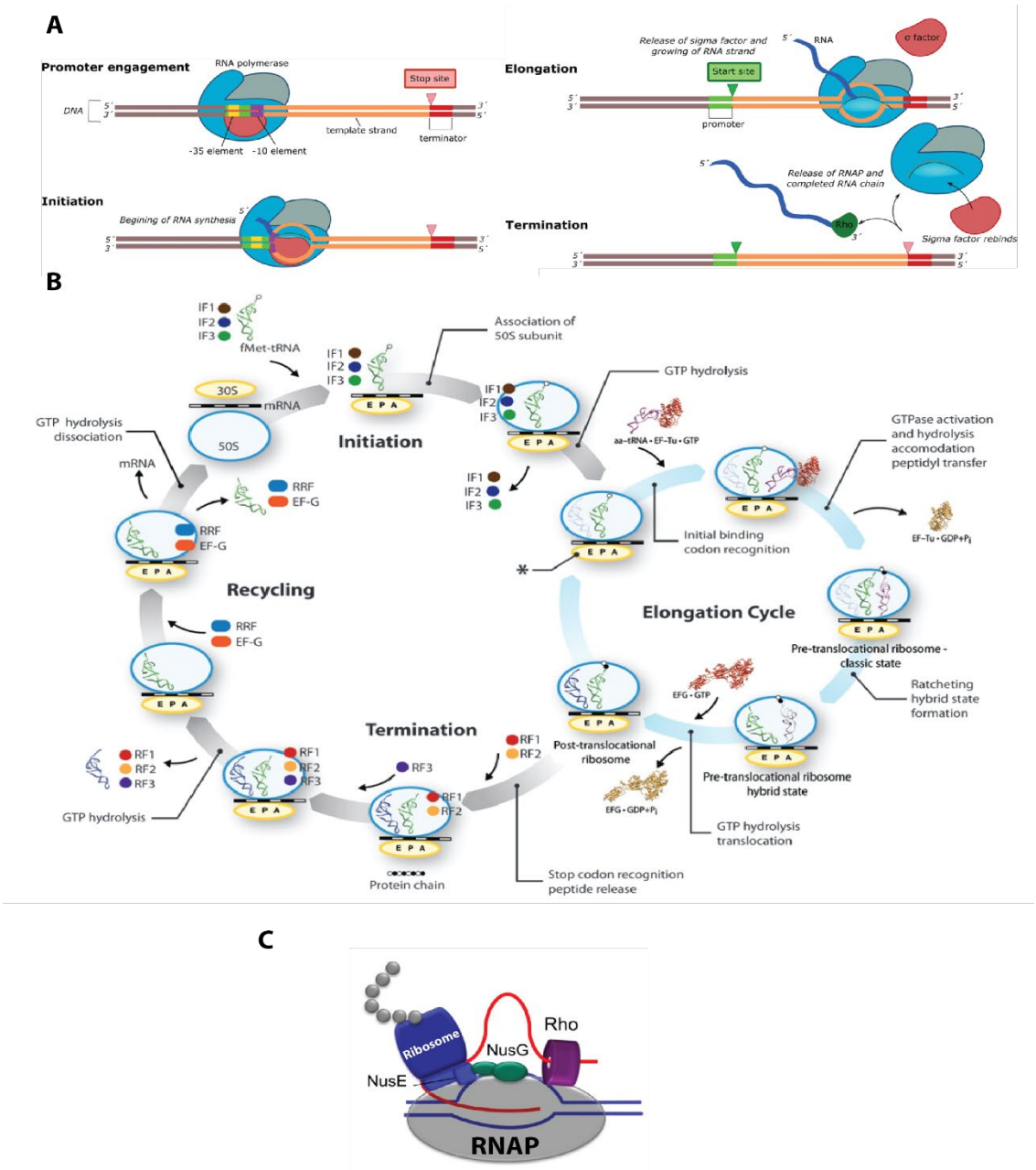

Figure 4. Gene expression in bacteria. (A) Diagram of bacterial transcription. RNA polymerase (RNAP) binds to the promoter region, with the σ-subunit recognizing the -35 and -10 sequence elements. RNAP then melts the double-stranded RNA and initiates transcription. RNAP synthesizes mRNA by adding ribonucleotides from 5' to 3'. Transcription elongation continues until the termination structure is reached. RNAP then dissociates and the newly synthesized mRNA is ejected. Image originally appears in Abril *et. al* 2020.[3] (B) Diagram of bacterial translation steps. The 30S subunit of the ribosome binds to mRNA with the initiator tRNA before recruiting the 50S subunit. Cognate amino-acylated tRNAs bind to the A-site and binding is stabilized through codon-anticodon interactions. As the tRNA is translocated into the P-site, the amino acid is added to the growing peptide chain in the peptidyl-transferase center. Elongation continues until the stop codon is reached. Lastly, release factors are recruited to cleave the final peptide and release the ribosome subunits. Image originally appears in Agirrezabala and Frank 2010.[4] (C) Transcriptional-translational complex. NusG interacts with the head of RNAP and NusE within the ribosome. Image adapted from McGary and Nudler 2013.[5]

termination can be performed in three ways. The most common is called intrinsic termination in which newly synthesized messenger RNA (mRNA) forms a small hairpin. This causes RNAP to pause and eventually dissociate, either through slipping in the active site or a collapse of the transcription bubble. An alternative form of termination is Rho-dependent termination which is used on specific genes. Rho is a homohexameric translocase that binds to the newly formed mRNA and slides along until it hits the Rho-termination binding site. While the exact mechanism is unknown, evidence suggests Rho remains bound to the initial binding site and tracks toward RNAP. Once it interacts with RNAP, it may exert a force that extracts the mRNA from the channel terminating transcription.[43]

Translation of the newly transcribed mRNA is the next major avenue of regulation (Figure 4B). As in transcription, rate of initiation plays a key role in determining translation rate and protein expression level. Initiation begins with a free 30S ribosomal subunit binding to several protein-based initiation factors and an initiator tRNA (formylmethionine RNA). This complex binds to a mRNA and scans along until the initiator tRNA pairs with the AUG start codon. Upstream of the start codon is a ribosome binding sequence (RBS) that is complementary to the 3' end of the 16S rRNA within the 50S subunit. As the 50S subunit binds, the RBS stabilizes the entire translational complex through base pairing. The start codon and initiator tRNA are positioned within the peptide site (P-site) of the ribosome, where peptidyl-transferase activity takes place, and the second codon is positioned within the acceptor site (A-site). A complex of aminoacylated tRNA and elongation factor Tu (EF-Tu) enter the acceptor site and bind to the mRNA through codon-anticodon pairing. Once successfully bound, elongation factor G (EF-G) hydrolyzes GTP to translocate the entire complex 3 nucleotides downstream, and in the process, shifting the newly bound tRNA into the P-site. During translocation, the amino acid attached to the tRNA contacts the peptidyltransfer center (PTC) and is attached to the initiator methionine. The now de-aminoacylated initiator tRNA moves into the exit site (E-site) of the ribosome where it dissociates. Translation continues until it reaches a stop codon (UUA, UAG, UGA), leaving an empty A-site. Release factors will bind to the stop codon and cleave the attached polypeptide. The ribosomal subunits then dissociate and can form new complexes.

Quality Control of Gene Expression

Ensuring quality control of both transcription and translation is critical for cell survival. Eukaryotes utilize compartmentalize these processes to help maintain the quality control. Transcription occurs exclusively within the nucleus of the cell, while translation occurs in the cytoplasm. Before a mRNA can be exported to the cytoplasm, it must be modified with a 7-methyl-guanine nucleotide at the 5' end and a poly-adenylated tail at the 3' end. These modifications increase the stability of the RNA, assist in export to the cytoplasm, and provide scaffolding for eukaryotic ribosomes to initiate translation.

Bacteria lack internal organelles. DNA condenses within the cytoplasm to form a mesh nucleoid structure with pore sizes of approximately 50nm. The pore sizes are sufficiently large enough for RNAP and free ribosomes to enter. Ribosomes can begin translation as soon as the RBS of mRNA has exited RNAP, allowing for transcription and translation to occur simultaneously. Bacteria have streamlined this process by coordinating these processes through a transcriptional-translational complex (TTC; Figure 4C). Binding between the lead ribosome (the first translating ribosome) and RNAP are thought to be mediated through NusG, though the exact binding interface is not entirely clear.[44] Data indicates that the N-terminal domain of NusG binds to the RNAP β' and β subunits, while the flexible C-terminal domain associates with the S10 ribosomal protein, and NusA may be involved in stabilizing the TTC.[44–46] This coordination allows for rapid changes to gene expression and provides protection to the mRNA, decreasing the likelihood of cleavage and degradation. Additionally, it can help moderate transcription dynamics. RNAP is capable of backtracking during transcription and is particularly prone to it within the first 50 nucleotides proximal to the promoter. Ribosomes on the other hand move in one direction and thus when engaged in the TTC may help to push RNAP along and prevent backtracking.

However, coordination of the TTC does not allow for quality control checks of the mRNA before translation begins. This exposes the system to perturbations at both the transcription and the translational level. RNAP pausing and backtracking can be important regulatory functions, but it can also cause premature Rho-dependent termination, resulting in non-stop RNAs. Translation is also prone to pausing. Nearly all mRNAs have secondary structure, which can increase RNA stability and moderate translation rates. Because of this, ribosomes can have RNA helicase activity using the S3 and S4 proteins in the 30S subunit, but rate

of translation is intrinsically linked to complexity of the secondary structure. Additionally, translation can pause due to rare codons, proline runs, and programmed stall sequences like SecM. Most translational pauses are transient, but excessive pausing can lead to decoupling of the TTC. This exposes the mRNA to cleavage and possible generation of non-stop RNAs. Compounding this, most bacterial genes are translated as a polysome, with multiple ribosomes translating a single transcript. Any generation of downstream non-stop transcripts will result in multiple catastrophically stalled translational complexes.

These issues are exacerbated under stress conditions. Nutrient starvation for example interacts with the TTC on multiple levels. Decreased availability of amino acids increases translational pausing as uncharged tRNAs bind to the ribosome. The RelA/SpoT family of proteins recognize this binding and produce the alarmone ppGpp. In turn, ppGpp binds to the β subunit of RNAP to inhibit transcription activity. In addition, bacteria activate RNase toxins like RelE and MazF that cleave and degrade mRNA transcripts. RelE cleaves mRNA within the A-site of the ribosome leading to a catastrophically stalled translational complex.

Resolving catastrophically stalled translational complexes is critical to maintaining a functional pool of ribosomes. [47] Most bacteria have one of two protein-based rescue systems, alternative ribosome-rescue factor A and B (ArfA and ArfB).[48] ArfA binds in the open mRNA channel of the ribosome and recruits RF2. Peptide release and ribosome dissociation are subsequently induced by canonical factors. In *E. coli*, mature ArfA is translated from a non-stop transcript generated by RNase III cleavage.[49] ArfB, on the other hand, has two functional domains: a positively charged tail region and a catalytic domain homologous to the GGQ domain of RF2. The tail domain binds to the open mRNA channel of the ribosome, while the GGQ-domain binds to the peptidyl transfer center of the ribosome to stimulate peptide release. Both ArfA and ArfB only serve to release the ribosomes from the non-stop translational complex. Bacteria have evolved a third system, trans-translation, that uses a specialized RNA-protein complex to both release sequestered ribosomes and tag the aberrant non-stop peptide products for proteolysis.[50–52] This system has been identified in all sequenced bacteria and is the primary method for resolving non-stop translation complexes.

Transfer Messenger RNA (tmRNA)

The main actor of trans-translation is a highly specialized and structured RNA molecule, transfer-messenger RNA (tmRNA) encoded by the ssrA gene.[53–55] While every bacterial species has a unique tmRNA, they all contain three structural domains: tRNA-like domain (TLD), mRNA-like domain (MLD), and a ring of pseudoknots (Figure 5A).[56,57] The TLD contains several structural similarities to a canonical tRNA. The 5' and 3' ends of mature tRNA form an acceptor stem, with the 3' terminus creating a small CCA overhang. [58] This overhang can be charged with an alanine residue by alanyl-tRNA synthetase and is conserved in all tmRNA sequences.[59] The TLD also features a tRNA-like T stem-loop and a reduced D-loop that serve as the primary binding locations for accessory proteins. The MLD is the least structured region of the molecule. The MLD contains a tag reading frame (TRF) that encodes an amino acid tag recognized by proteases. The TRF does not contain a start codon or an upstream ribosome binding site

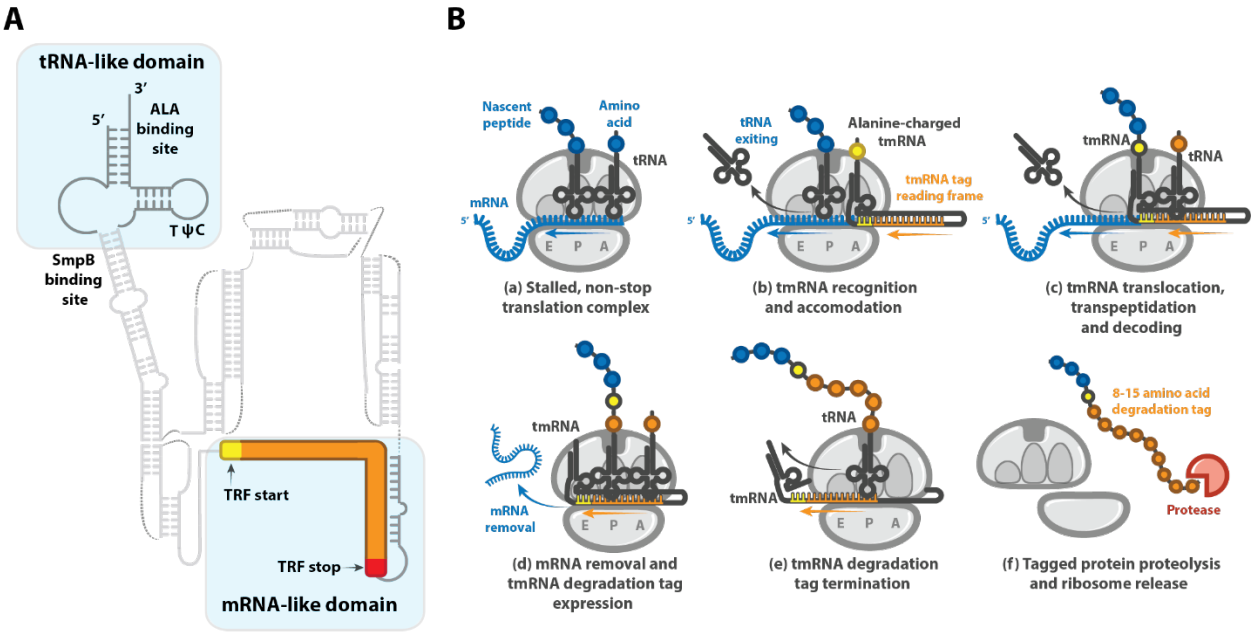

Figure 5. Transfer messenger RNA (tmRNA). (A) Structure of tmRNA in *E. coli*. Locations of the alanyl-synthetase and SmpB are noted in the tRNA-like domain. Tag reading frame (TRF, orange) is located within the mRNA-like domain. The resume codon is noted in yellow and the final codon is in red. (B) Mechanism of *trans*-translation. Stalled translation complexes are recognized by tmRNA, which is accommodated into the empty A-site of the ribosome. During accommodation, the TRF is aligned within the mRNA channel. During translocation, translation shifts from the nascent mRNA to the TRF. Elongation resumes using the TRF as a template. Translation continues until it reaches the stop codon within the TRF and translation terminates normally. The peptide sequence encoded in the TRF is now attached to the C-terminus of the nascent peptide, which is recognized by proteases and degraded.

like canonical mRNA but instead has a resume codon. Though the length and sequence of the TRF varies by bacterial species, nearly all tags begin with alanine or glycine and end with at least one stop codon. The ring of pseudoknots typically consists of four pseudoknots (PKs). PK1 is located upstream of the MLD and is the only PK required for proper tmRNA function. While PKs 2-4 are not essential, they are thought to help ensure proper tmRNA folding and anchor tmRNA to the ribosome during trans-translation.[60,61]

Small molecule protein B (SmpB) is responsible for integrating and orientating tmRNA in the ribosome.[45,46] SmpB is highly conserved among bacterial species. As the critical binding partner for tmRNA, SmpB deletion results in the same phenotype as deletion of tmRNA. The body of SmpB binds to the elbow region of the TLD, stabilizing the structure. The C-terminal tail also contains an RNA binding region that interacts with the ribosomal mRNA channel. In solution, the tail is unstructured but upon entry into the ribosome accommodation adopts an alpha-helix.[62–65]

The TLD region of the tmRNA-SmpB complex resembles a canonical tRNA. The structural similarities allow the complex to utilize many of the canonical translation factors to enter and move through the ribosome (Figure 5B). Prior to accommodation, EF-Tu•GTP interacts with the alanyl-tmRNA-SmpB complex, primarily contacting the TLD. The quaternary complex is guided to the stalled translational complex akin to aminoacylated tRNAs.[62,66] SmpB interacts with the decoding center to mimic the tRNA codon/anticodon pairing, and the C-terminal tail enters the mRNA channel.[54,64,67] Downstream pseudoknots of tmRNA crowd the entrance and anchor to the solvent side of the ribosome. GTP hydrolysis releases EF-Tu•GDP to allow accommodation of the complex. The C-terminal tail allows the main body of SmpB to rotate fully into the A-site. The acceptor arm of the tmRNA TLD swings into the peptidyl transferase center (PTC), and the alanine is transferred to the nascent peptide. EF-G binds to SmpB and tilts the head of the ribosome.[66] This translocates SmpB-TLD into the P-site and expels the nascent mRNA fragment and remaining tRNA. During translocation, the SmpB C-terminal tail moves into the mRNA channel in the E-site. The MLD binds to the vacant mRNA channel. Following dissociation of EF-G, the components return to the canonical position. The resume codon is positioned within the A-site, and translation re-registers on the TRF. Some evidence suggests that the C-terminal tail directly interacts with the MLD and is responsible for the correct framing of the TRF.[64,68] The resume codon is decoded with canonical aa-tRNA and moves into the P-site.

SmpB-TLD does not bind to the E-site but rather passes through and binds to the solvent side of the ribosome.[66] Translation of the TRF continues and terminates canonically with the MLD moving through the RNA channel. SmpB-TLD and the PKD regions remain anchored to the solvent sides of the ribosome. Following termination, the ribosome dissociates, and the aberrant peptide is released with the encoded tag sequence attached to the C-terminus. ClpAP and ClpXP recognize the tag sequence and degrade the aberrant peptides, while the original nonstop mRNA is degraded by RNase R.[69–74]

The length and sequence of the TRF varies by species ranging 8-35 codons in length. Nearly all species use alanine as the resume codon, though there are a few instances when glycine is used. The 5 nucleotides directly upstream from the resume codon have been shown to be critical in proper frame selection. In *E. coli*, the TRF encodes the 10-mer peptide ANDENYALAA. Early studies into degradation of ssrA-tagged proteins determined that the final two amino acids in the tag were critical for targeted proteolysis.[71–73] ClpAP and ClpXP are responsible for most of the ssrA-tag mediated degradation. ClpA subunit recognizes the C-terminal ALA sequence, while ClpX subunit recognizes the LAA C-terminal sequence. More recently, it was discovered that several other cytoplasmic proteases like Lon can also recognize and degrade tagged proteins.[73,75] Modifying the TRF to encode two aspartic acids (ANDENYALDD) produced proteins that were unable to be degraded.[71]

The TRF has been shown to tolerate more extensive sequence modifications. In 2001, Roche and Sauer modified the *E. coli* TRF to introduce an isolation epitope to study which proteins were tagged. They replaced the final six amino acids with a 6x-histidine motif (ANDEHHHHHH) which stabilized the tagged proteins and allowed for affinity purification and mass spectrometry analysis. They identified a broad range of proteins, including LacI repressor, YbeL, and GalE. LacI and YbeL were tagged after their native C-terminus, which implied they were tagged during the termination step.[76] Similar approaches have been used in other organisms to identify native tmRNA substrates, including *B. subtilis* and *C. crescentus*.[77–79] These studies have further confirmed the broad spectrum of proteins tagged by tmRNA and the prevalence of tagging at stop codons.[80,81] Initially it was estimated that 0.4% of all translation events required tmRNA intervention during exponential growth phase. In *E. coli,* that is the equivalent of every single ribosome requiring intervention once per cell cycle. However, it was noted that tmRNA expression did not increase

with artificial increase of nonstop mRNA, indicating that the system likely operates below its peak tagging capacity.[82] More recent estimates have placed tagging frequency at 2-4% of all translation events. A deeper understanding of the factors contributing to catastrophic stalling have emerged. Common substrates often have inefficient translation termination sequences or strings of rare codons or prolines. It is believed that translational stalling exposes downstream mRNA, which is cleaved by RNase II and then chewed to the ribosome edge by endonucleases.[83,84] Additionally, evidence also suggests that tmRNA plays a role in targeting misfolded peptides as they are translation, though the mechanism is not understood.[85–87]

Studies have shown that tmRNA plays significant roles in cellular regulation and this can vary by species. Deletion of the ssrA gene in certain species like *Neisseria gonnorhoeae* and *Shigella flexneri* are lethal,

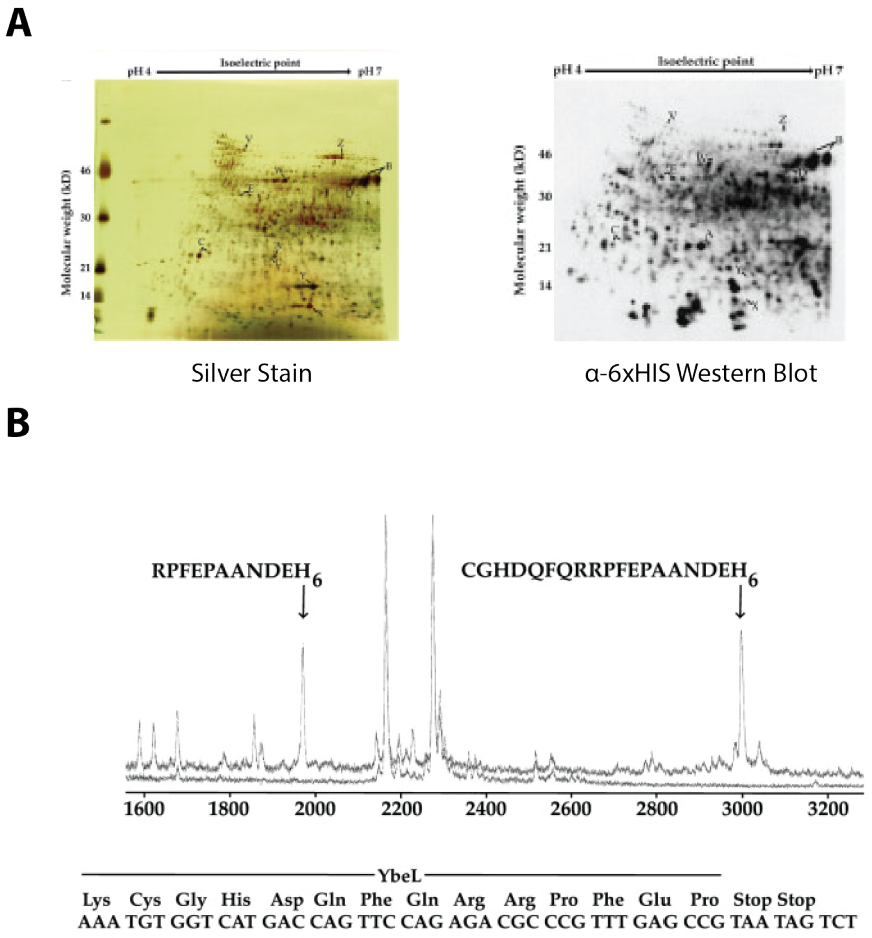

Figure 6. Summary of findings from Roche and Sauer 2001. (A) Two-dimensional gel electrophoresis of Ni21-NTA chromatography purified SsrA-H6-tagged proteins analyzed by silver stain and α-6xHIS western blot. (B) Example mass spectrometry spectra of tagged peptides. Images adapted from Roche and Sauer 2001.

while others like *E. coli*, *B. subtilis,* and *C. crescentus* result in physiological deficiencies.[50,51,84] In *E. coli,* deletion of ssrA results in poor growth, weakened cell membrane, and poor stress response. It also plays a critical role in the stress response. Stress conditions, like antibiotic treatment and starvation, activate a host of RNases that serve to shut down transcription and translation.[88–90] Cleavage by RNases result in nonstop mRNAs and thus catastrophically stalled translational complexes.[91–94] It is essential for rapid stress response and recovery that the stalled complexes are resolved quickly. Under stress conditions, transcription of tmRNA increases rapidly to allow for this response and conserve resources.[48,82,84] Rescue by tmRNA also serves as a regulatory mechanism for alternative rescue factors. ArfA mRNA adopts a hairpin structure that is cleaved by RNase III and produces a non-stop mRNA. Under conditions where trans-translation is in full capacity, tmRNA rescues the stalled translational complex and degrades the ArfA protein. However, when tmRNA is inhibited, another ArfA protein will bind to the ribosome and cause termination and dissociation.[49,95] Thus, when trans-translation is inhibited, it upregulates expression of ArfA.

The tmRNA degradome provides unique insight into the combined dynamics of the TTC in bacteria and plays a critical role in allowing bacteria to respond to and survive stress conditions. Previous studies have shown that the tmRNA TRF can be modified to stabilize normally degraded products and allow for their isolation. However, these studies focused primarily on identifying substrates under steady-state growth conditions. In addition, recent technological advances have drastically increased the sensitivity in protein detection methods. In this study, I engineered an inducible synthetic tmRNA platform that introduced a 6x-Histidine motif to tagged proteins. I utilized this platform in combination with multiple purification techniques and state-of-the-art mass spectrometry equipment to investigate the tmRNA degradome under steady state and oxidative and translational stress conditions.

CHAPTER 2: DEVELOPMENT AND OPTIMIZATION OF SYNTHETIC TMRNA-6XHIS PLATFORM

Introduction

The emerging field of synthetic biology has produced a wide array of platforms enabling the re-programming and robust control of biological systems at all organismal levels.[96,97] The relationship that exists among sequence, structure, and function has made RNA a highly attractive and versatile molecular basis for modular synthetic device design, particularly when employed as an engineered regulator of gene expression. To this end, gene expression regulation by synthetic RNAs has been demonstrated at both the transcription and translation levels, as well as through tuning of mRNA stability. As the diverse and complex roles played by native RNAs in directing biological function are better appreciated, naturally evolved abilities have been increasingly leveraged to develop powerful synthetic modulators and sensors of cellular behaviors. In particular, the ability of RNA to detect and respond to ranging environmental cues framework for predictable and programmable design of uniquely capable experimental tools.[96,98–100]

We identified transfer messenger RNA (tmRNA) as a target for synthetic modification. Natively, this highly specialized RNA serves to rescue stalled ribosomes and target the incomplete polypeptides for degradation.[48] Briefly, tmRNA recognizes stalled translational complexes on nonstop RNA transcripts (Figure 5B). Upon accommodation into the ribosome, translation switches from the nascent RNA onto a short tag reading frame (TRF) contained on tmRNA. When translation resumes, the encoded tag is attached to the C-terminus of the nascent aberrant peptide product, targeting it for proteolysis by the protease ClpP.[62,66,101] These tagged products comprise the tmRNA degradome and are not normally captured. The TRF offers a modular domain for the synthetic modification of the tag sequence. Thus, a synthetic tmRNA will allow for the addition of a predefined tag to be introduced at the ribosome *in vivo*. This approach allows for undirected tagging, as tmRNA acts universally on any nonstop RNA transcript.

One application of this synthetic approach is to modify the TRF to introduce an isolation motif that will stabilize tagged products and allow for targeted study. ClpP recognizes the two terminal amino acids in the TRF. Modification of the C-terminal codons of the TRF to an isolation epitope would prevent proteolysis, causing tagged products to accumulate, and enable isolation of these products for identification. Bacteria can regulate translation by altering gene expression, RNA stability, and translation dynamics, which are further affected under stress with the activation of RNase toxins and changes to nutrient availability.[90,102–

[105] tmRNA plays a key role in resolving issues arising from these modifications and preventing aggregation of the resulting aberrant peptide products.[84,106,107] Studying the tmRNA degradome could close the information gap between transcription and translation and provide novel insight into the bacterial stress response.

Tagged proteins can then be identified using liquid chromatography tandem mass spectrometry (LC-MS/MS). In a bottom-up proteomics approach, proteins are digested with a protease that cleaves at specific amino acids to generate peptide fragments (Figure 7).[108,109] The pool of peptide fragments is then temporarily separated using liquid chromatography. This produces a steady stream of microscopic droplets that are ionized and injected into the mass spectrometer. Within the mass spectrometer, it first takes a reading of the mass-to-charge ratio (m/z) of all the peptides contained within the droplet known as the MS1 spectrum. The peptides are then fragmented, and the fragments are separated by m/z before passing to the detector to create the MS2 spectrum. The peptide sequence determines the way that peptides fragment and provides a unique fingerprint.[109–111] From the MS2 spectrum, the sequence of the peptide can be inferred. Typically, this is accomplished using a search algorithm that uses the raw mass spectrometry files along with a reference proteome of the organism the proteins originated from.[112,113] Each search algorithm

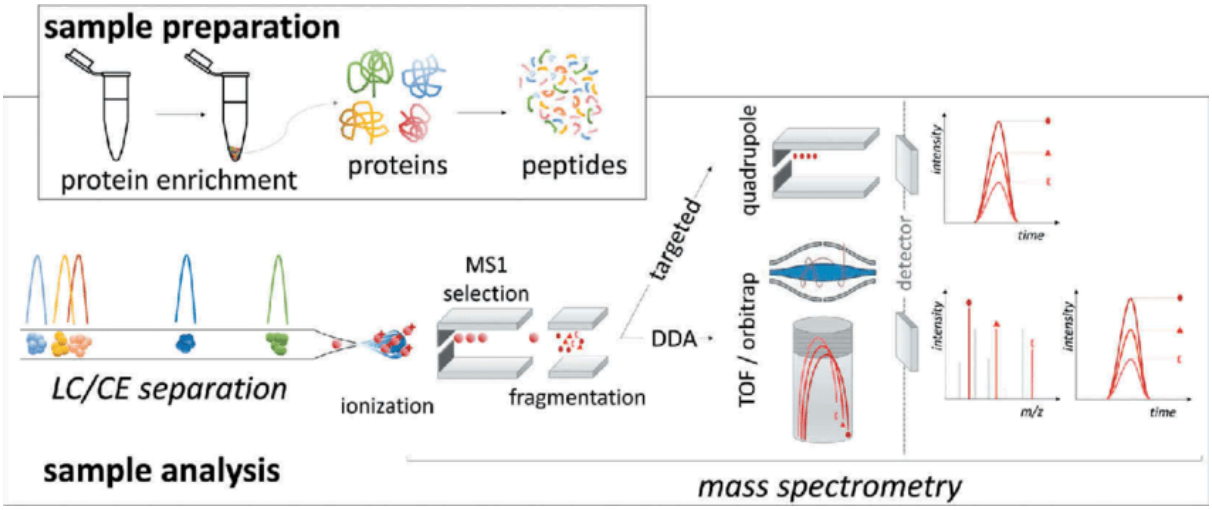

uses unique parameters to identify peptide fragments, so it is common to use two or more to increase data

Figure 7. Diagram of example bottom-up proteomics using tandem mass spectrometry (LC-MS/MS). Proteins are digested to form peptides, which are separated using liquid chromatography. Peptides are expelled from the column as droplets and ionized before entering the mass spectrometer. Mass-to-charge ratios (M/z) of peptides are measured to generate a MS1 spectrum. Peptides are then selected and fragmented. The M/z of peptide fragments are measured to generate a MS2 spectra. The peptide sequence can be derived from MS2 spectra. Image originally appears in Gool *et al* 2020.[8]

coverage. There are three main approaches to creating MS2 spectra. The most common is data-dependent acquisition (DDA). In DDA, the most abundant peptides are selected for fragmentation. The number of peptides that can be selected and efficiently resolved depends on the sensitivity and selectivity of the instrument, though commonly the top 10 or 20 peptides are selected.[109] In data-independent acquisition (DIA), every peptide present in the MS1 is selected for fragmentation, which gives the greatest coverage of peptide identification. However, this produces an extremely complex MS2 spectra requires a library of previously collected DDA-based MS1 spectra to resolve. The final approach is targeted acquisition, which is primarily used for absolute quantitation methods or other specialized mass spectrometry uses.[111,114]

In this chapter, we designed a synthetic tmRNA-6xHIS platform that allowed us to stabilize and isolate tmRNA-tagged proteins in *E. coli*. We verified successful introduction of 6xHIS tags from both constitutively and inducible expressed tmRNA-6xHIS constructs. We showed a broad molecular weight distribution of tagged products, and we identified over one thousand proteins in the tagged degradome under steady state conditions.

Results

Design and generation of tmRNA-6xHIS construct

To study the tmRNA degradome, the tmRNA tag sequence must be modified to stabilize tagged peptides and allow for isolation. However, the structure of tmRNA is critical for proper function and needs to be maintained in a synthetic tmRNA variant. In *E. coli*, the TRF is a 10-mer tag (ANDENYALAA) that begins in an unstructured region of the MLD and forms part of an extensive hairpin structure in the last four codons. Two sequential stop codons are positioned in the stem loop (Figure 8A). The hairpin is thought to help with proper framing and positioning of the TRF and unfold as it threads through the mRNA channel.[66,115] In addition, early codons appear to play a role in tagging efficiency. Recoding any of the first three codons resulted in decreased tagging activity, with the largest deficiency resulting from modification of the resume codons.[54] Thus the ideal isolation epitope would be 7 codons or less to fit within the *E. coli* TRF and allow for maintenance of the early codons. The 6x-histidine epitope (6x-HIS) is an attractive candidate for TRF

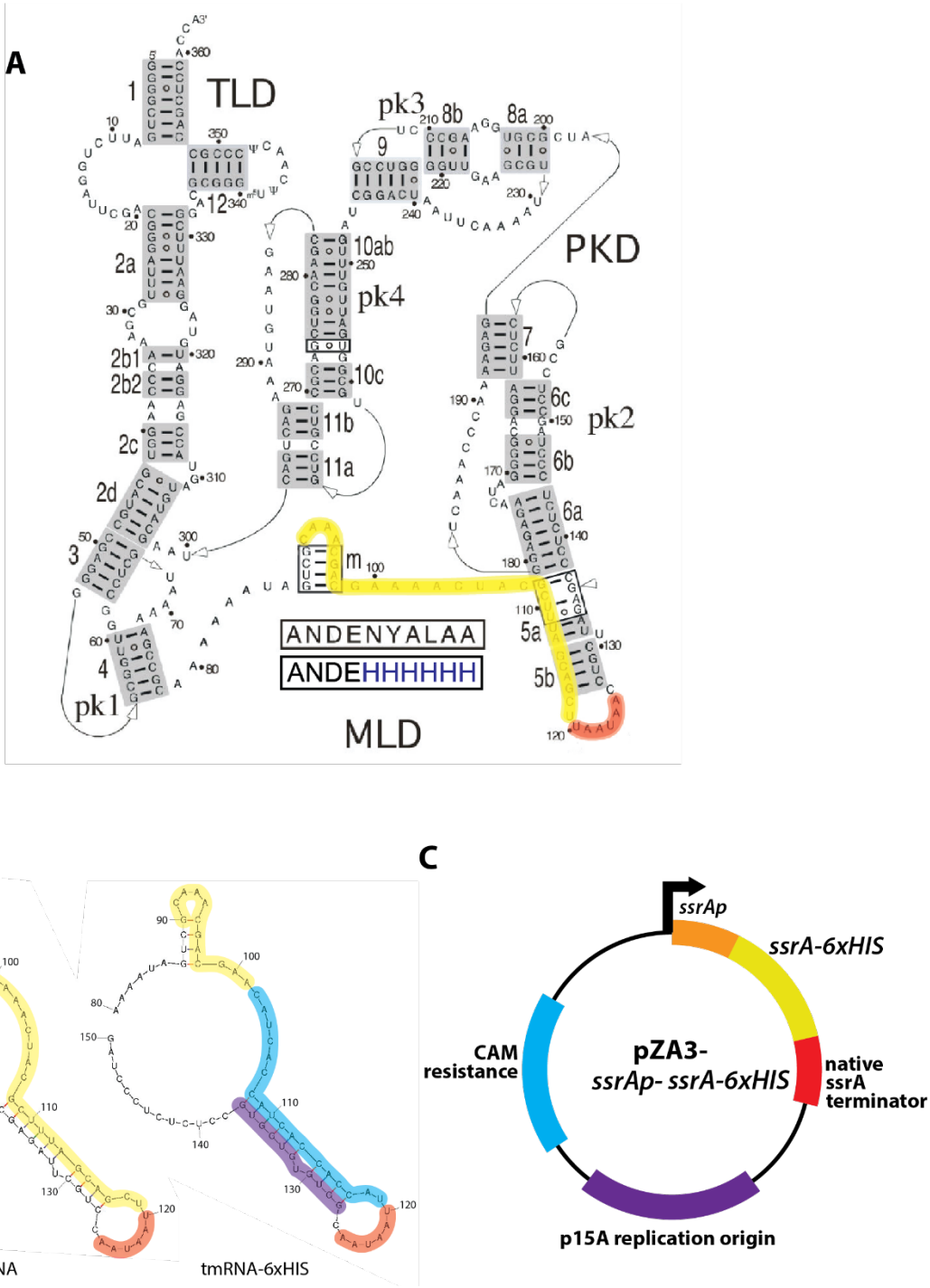

Figure 8. E. coli tmRNA-6xHIS design. (A) Native sequence-structure of *E. coli* tmRNA with the TRF (yellow) and stop codons (red). Image adapted from Burks *et. al* 2005.[7] (B) Structure of subset sequence 81-150 of native and 6xHIS modified tmRNA as predicted by mFold. (C) Plasmid map of tmRNA-6xHIS construct.

modification. The six-codon sequence length fits well within the TRF and there are numerous commercial products available for isolation and detection. Importantly previous studies have shown that 6-HIS

modification of the TRF is well tolerated in multiple bacterial species, including *E. coli*.[76,79,116] Following the design principles set forth by Roche and Sauer, we replaced the final six codons of the TRF with this modification(ANDEHHHHHH).[76] This placement prevents tag recognition by proteases and maintains the early codons for tagging efficiency. Histidine is encoded by two codons CAT and CAC with a slight codon bias for CAT (fraction of 0.57 vs 0.43).[117] Due to the slight bias, CAT was utilized wherever possible, except in cases where doing so would compromise the structure.

We used mFold to predict the structure of our engineered TRF region.[118] We selected a subset of the tmRNA sequence from 80-140 to use for structure prediction. This corresponds to the beginning of the unstructured region upstream of the TRF and extends through the complementary portion of the hairpin. The native *E. coli* tmRNA sequence subset resulted in one predicted structure that corresponded with the known structure of the region (Figure 8A). Through codon selection and compensatory modifications, we were able to design a sequence that produced one predicted structure that matched that of the native sequence (Figure 8B).

The termination sequence of *ssrA* has not been identified. Additionally, tmRNA undergoes multiple processing steps before becoming fully functional. The endonuclease RNase P cleaves the 5' terminus, while the 3' terminus is cleaved by RNase E. The result is a 363 nucleotide RNA molecule with a CCA overhang. Since the native tmRNA promoter drives high constitutive levels of expression, we used it for our initial studies.[119] To maintain both the native promoter and RNase cleavage sites, we included up to the -60 upstream 5' leader. We also included the 100-nucleotide sequence downstream of the *ssrA* gene to ensure that the native termination structure and RNase E modification sites were includerd. Finally, to allow for restriction-based cloning into a plasmid, we placed a Xho1 restriction site at the 5' end and a Mlu1 restriction site at the 3' end. Our construct was synthesized as a gene block by Integrated DNA Technology (IDT).

For our plasmid backbone, we used the PZA31-MCS plasmid from Expressys.[120] This is a medium copy plasmid using the p15A replication origin with a chloramphenicol resistance selection marker. We used a restriction enzyme-based cloning and ligation protocol to insert the synthetic tmRNA-6xHIS gene block within the MCS of the plasmid (Figure 8C). We transformed our plasmid into two different cellular

backgrounds: wildtype *E. coli* MG1655 (WT) and *E. coli* MG1655 *ΔssrA*. The *ΔssrA* strain was generated using the pKD46 Lambda-red recombinase method with a kanamycin resistance marker. Expression of our synthetic construct was well tolerated in wildtype cells (Figure 9A). As expected, *ΔssrA* cells exhibited inhibited growth kinetics. In previous studies, introduction of plasmid-based tmRNA constructs have rescued growth phenotype in *E. coli*. Unexpectedly, introduction of our synthetic construct exacerbated the growth defect.(Figure 9A)

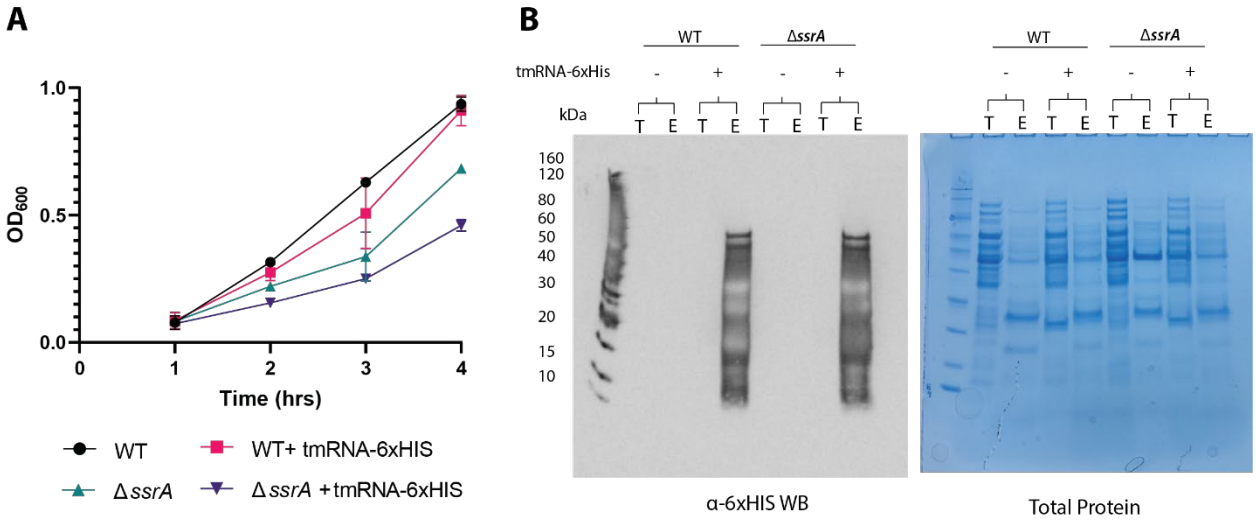

Figure 9. Comparison of expression of tmRNA-6xHIS in WT and ΔssrA cells. (A) Growth curve of strains with and without synthetic construct. (B) Gel electrophoresis analysis of total cell lysates (T) and affinity purified elution fractions (E). 2 µg of protein were loaded on each gel. α-6xHIS western blot was performed with 1:10000 dilution of antibody. Total protein was visualized using SimplyBlue Safe Stain.

Purification and assessment of 6xHIS tagging

To assess a baseline level of tagging, cells containing our synthetic construct were grown for 4.5 hours until they reached near stationary phase. Cells were then pelleted, lysed, then affinity purified, using Co^{2+} HisPur affinity columns from Thermo Fisher. Cobalt has a weaker binding interaction with the 6x-Histidine residue compared to nickel, resulting in a higher specificity of binding and ease of elution. Initially, we started with small scale purifications of several hundred micrograms of total protein lysate (~300-800 µg). However, we found that we could not reliably measure the protein concentration of the purified elution as it was close to the limit of detection (data not shown). To obtain reliable results, more than 2 mg of total protein was required. The concentration of the elution showed that approximately 2% of the total protein loaded was bound and purified by the column, suggesting low concentration of tagged proteins in the total lysate (Table

3). Most of these proteins eluted in the first elution, and generally the third elution did not yield reliable protein concentrations.

Strain	Protein Purified (ug)	Elution Fraction Concentration (ug/mL)			Total Eluted (ug)	% Eluted
		E1	E2	E3		
WT	3060.20	90.31	52.12	39.33	36.35	1.19
WT + tmRNA-6xHIS	3022.50	127.20	69.75	44.67	48.32	1.60
ΔssrA	2963.10	95.52	65.92	31.90	38.67	1.31
Δ*ssrA* + tmRNA-6xHIS	2944.50	250.76	115.68	57.54	84.80	2.88

Table 3. Protein concentrations of metal affinity purified lysates from cells containing tmRNA-6xHIS construct in wildtype and Δ*ssrA* cells.

We then verified the presence of 6xHIS tagged proteins using an α6xHIS western blot (Figure 8B). Excitingly, the elution fraction from cells containing our construct showed strong staining for 6x-HIS. There is a near continuous staining from approximately 50 kDa to 10 kDa. This suggests not only a highly diverse population of tagged proteins but also that various states of protein completeness were represented. While nearly the entire molecular weight range shows staining, there are bands with distinctly darker staining. This is particularly evident in the wildtype cells, where the bands around 30 kDa, 25 kDa, and 17 kDa have over-exposed and appear white. These bands were visible with the naked eye on the blot. We did not see any staining in total cell lysates with our construct. This was expected from the affinity purifications which suggested only a small portion of proteins were tagged.

Metal ion affinity purification of 6x-HIS tagged proteins has several known co-purification contaminants (Table 4).[108,121] In total protein gel, we saw visible bands in the elution fraction at approximately 70 kDa, 40 kDa, 25 kDa, 20 kDa, 15 kDa, and 10 kDa. These bands were seen in every purified sample at similar abundances and correspond to the weight of known contaminants. Importantly, the western blot does not show any signal in cells that do not contain our tmRNA-6xHIS construct. This suggests that while these contaminants are present in all elution fractions, they were not detected in the western blot and are not responsible for the signal we see in the cells with our construct.

In wildtype cells, our plasmid-based synthetic tmRNA coexists with the chromosomal native tmRNA. We hypothesized that this would result in competition and would produce less 6x-HIS tagging compared to *ΔssrA* cells. Data from our affinity purification shows that higher protein concentrations are purified from the *ΔssrA* cells with our construct compared to wildtype (Table 2). However, western blot analysis shows remarkably similar staining profiles in both genetic backgrounds. The wildtype cells show slightly more over-exposure compared to the knockout cells, but the staining range and banding locations are nearly identical.

Protein Name	Gene Name	Uniprot ID	Molecular Weight (kDa)
2-oxoglutarate dehydrogenase E1 component	sucA	P0AFG3	105.1
30S ribosomal protein S15	rpsO	P0ADZ4	10.3
Acetylornithine deacetylase	ArgE	Q8P8J5	42.3
Bifunctional polymyxin resistance protein ArnA	arnA	P77398	74.3
cAMP-activated global transcriptional regulator CRP	Crp	P0ACJ8	23.6
Carbonic anhydrase 2	can	P61517	25.1
Chaperonin GroEL	groEL	P0A6F5	57.3
Dihydrolipoyllysine-residue succinyltransferase component of 2-oxoglutarate dehydrogenase complex	sucB	P0AFG6	44
Ferric uptake regulation protein	Fur	P0A9A9	16.8
FKBP-type peptidyl-prolyl cis-trans isomerase SlyD	SlyD	P0A9K9	20.9
Glucose-6-phosphate 1-dehydrogenase	zwf	P0AC53	55.7
Glutamine--fructose-6-phosphate aminotransferase	GlmS	P17169	66.9
Glycogen synthase	GlgA	P0A6U8	52.8
Metal-binding protein ZinT	ZinT	P76344	24.5
RNA-binding protein Hfq	Hfq	P0A6X3	11.2
Superoxide dismutase [Cu-Zn]	sodC	P0ADGD1	17.7

Table 4. Contaminant proteins that co-elute with 6xHIS-tagged proteins in metal ion affinity purification. Table derived from Bolanos-Garcia and Davies 2006.

Comparison of tmRNA-6xHIS sequence variants

Although we used design principles set forth in Roche and Sauer's work, our tmRNA sequence differed from theirs.[76] To compare tagging, we made a subsequent tmRNA-6xHIS construct using their engineered sequence (Sauer, Figure 10A). Additionally, we modified the 3' terminus of the *ssrA* gene to reflect the consensus cleavage sequence of RNase E to determine if more efficient cleavage increase tagging (Turner-RNaseE mod).[91] Both sequence variants used the same 5' leader and 3' terminator sequences as our original construct (Turner), along with the XhoI and MluI restriction sites, and were synthesized as gene

blocks by IDT. Using restriction digest-ligation based cloning, we placed the constructs into the PZA31-MCS plasmid backbone and transformed the resulting plasmid into wildtype MG1655 cells. We confirmed that both constructs resulted in similar growth and expression tolerance to our original construct (Figure 10B). To compare 6x-HIS tagging, cell cultures were grown for 4.5 hours, pelleted, then lysed. We then isolated affinity purified 3 mg total cell lysate from each strain. Similar concentrations of protein were purified from all three constructs (Table 3). We then performed an α-6xHIS western blot and total protein analysis on 2 µg of the total protein lysate and first purified elution. While the Turner and Sauer constructs showed similar 6xHIS staining profiles, the Turner-RNaseE mod had sparser staining though it did show the same banding pattern as the other two (Figure 10C). Initially, this was surprising as the elution protein

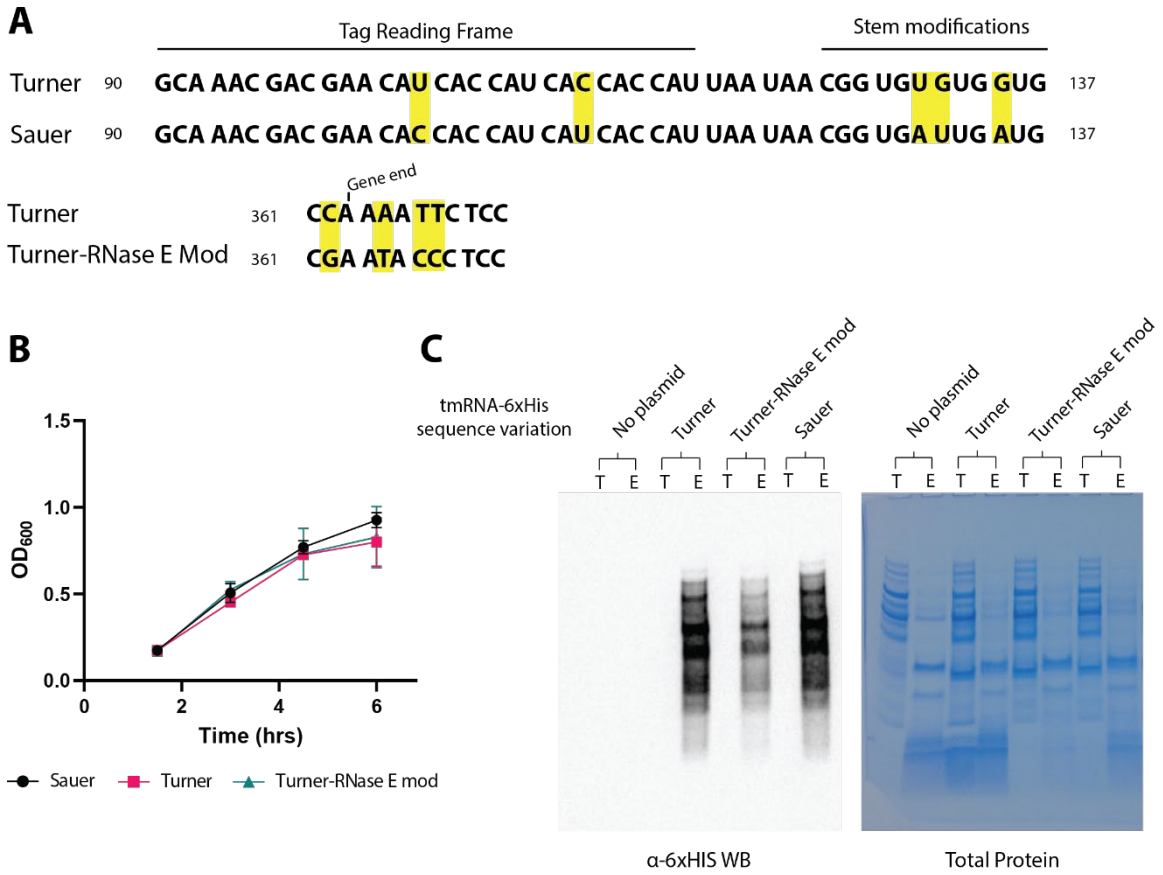

Figure 10. Comparison of tmRNA-6xHIS sequence variants. (A) Sequence variations of constructs. Sequence of Sauer construct from Roche and Sauer 2001.[6] Location of nucleotide changes highlighted in yellow. (B) Growth curve of wildtype *E. coli* cells containing each construct. (C) Gel electrophoresis analysis of total cell lysates (T) and affinity purified elution fractions (E). 2 µg of protein were loaded on each gel. α-6xHIS western blot (WB) was performed with 1:10000 dilution of antibody. Total protein was visualized using SimplyBlue Safe Stain

concentration did not suggest a lower protein concentration. However, purification from cells without plasmid showed similar protein concentrations to those with the tmRNA-6xHIS constructs. Similarly, the Coomassie total protein-stained gel showed similar abundance and banding patterns across all elution fractions. This demonstrated that affinity purification concentrations are an insufficient method of determining 6xHIS tagging amounts. It also showed that RNaseE cleavage of the 3' terminus is critical for efficient tagging. We chose to continue with the Turner construct for our work as it performed as well as the Sauer construct.

Addition of immunoprecipitation for increased purity

Recent mass spectrometry developments have increased instrument sensitivity, allowing for detection of as low as a picomole of protein.[122] However, sample purity is critical for maximizing and accurately identifying tagged peptides. Immunoprecipitation (IP) offers higher selectivity than metal ion affinity purification as it based on amino-acid motif binding rather than just charge. Some protocols suggest pre-clearing cell lysates prior to IP to increase binding capacity. To test whether this provided better recovery,

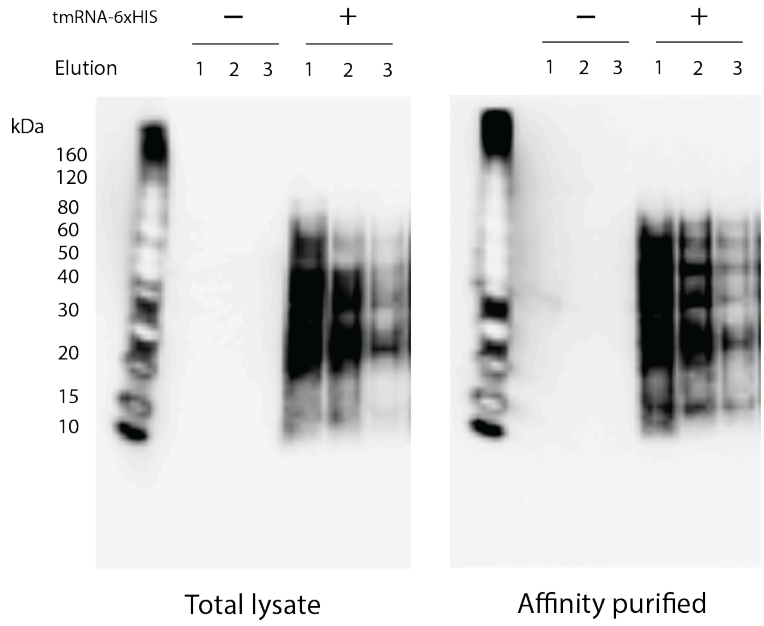

Figure 11. α-6xHIS western blot (WB) of immunoprecipitation (IP) elution fractions from total cell lysate and affinity purified elution factions. 3 mg of total cell lysate were used for IP. Affinity purified samples were generated by affinity purifying 3 mg of lysate using HisPur Cobalt affinity columns and pooling elution fractions. IPs were performed using 12 µg α-6xHIS antibody, Sepharose A beads, and a urea-based elution buffer. 52 µL of each elution faction were loaded onto the gel. WB was performed with 1:10000 dilution of antibody

we performed IP on total cell lysate and affinity purified samples. All three affinity purified elution fractions were combined prior to IP to maximize recovery of tagged proteins. We then assessed tag distribution through western blot. Since the protein concentration was below the limit of detection for all fractions, we loaded 52 µL of each fraction onto the gel. A 6xHIS tagged protein ladder was used as a positive control (Figure 11). The IP only elutions resulted in a more limited molecular weight range than previously seen in the affinity purification blots. However, the pre-cleared HisPur-IP elutions showed more evenly distributed staining and better coverage of the low molecular weight range. We chose to integrate pre-clearing the lysates using affinity purification in our workflow since it better reflected the results we saw previously.

Inducible tmRNA-6xHIS construct

Our optimization studies have utilized the native *ssrA* promoter to drive constitutive tmRNA-6xHIS expression and thus tagging. While this provides high tagged protein levels, we were unable to determine when tagging took place. This is particularly important for investigating stress responses. To address this,

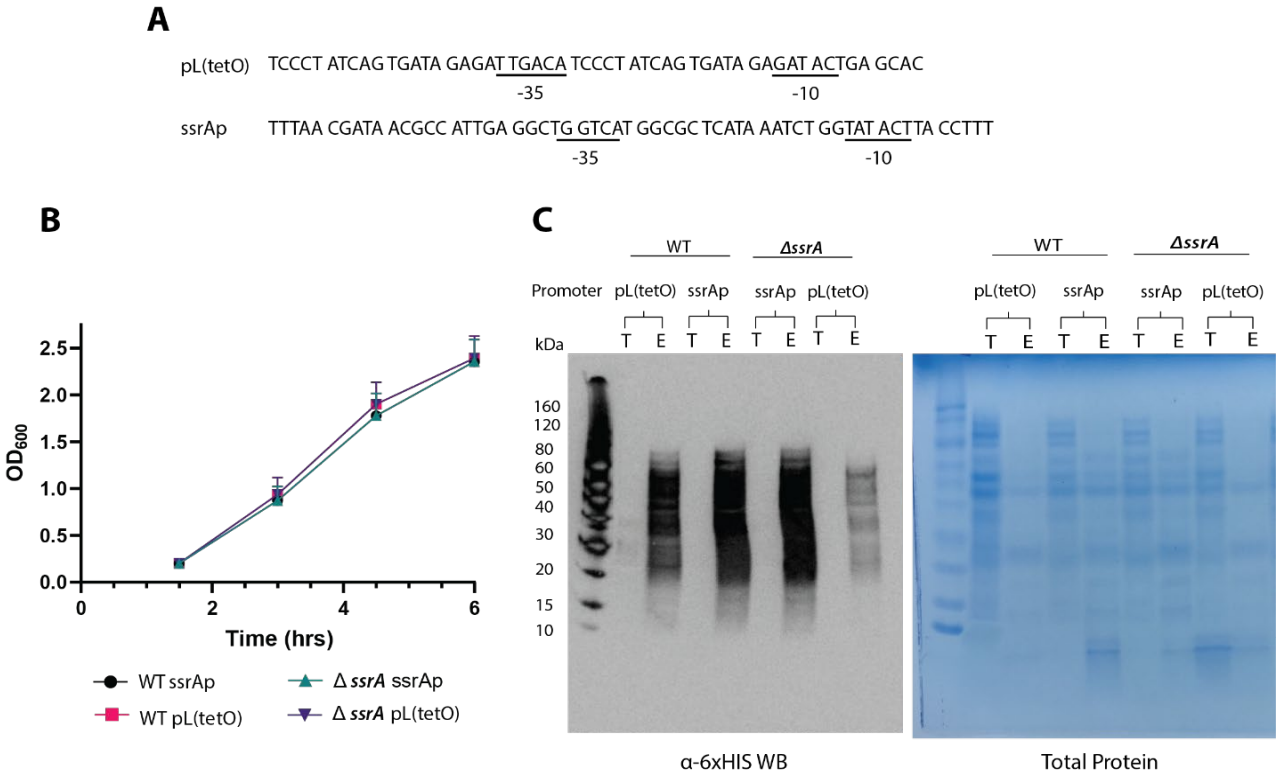

Figure 12. Comparison of promoters incorporated into tmRNA-6xHIS. (A) Sequences of promoters. (B) Growth curve of wildtype *E. coli* cells containing each construct. (C) Gel electrophoresis analysis of total cell lysates (T) and affinity purified elution fractions (E). 2 µg of protein were loaded on each gel. α-6xHIS western blot (WB) was performed with 1:10000 dilution of antibody. Total protein was visualized using SimplyBlue Safe Stain.

we replaced the native *ssrA* promoter with the pL(tetO) promoter in our tmRNA-6xHIS construct (Figure 12A).[123] We selected the pL(tetO) promoter as it would allow for a tight off-state, ensuring that any 6xHIS-tagging seen would be following induction. The tmRNA-6xHIS and 3' terminator sequences were maintained from the original construct (Turner variant). Construct was synthesized as a gene block by IDT, restriction digest-ligation cloned into the PZA31-MCS plasmid, and subsequently transformed into wildtype *E. coli* MG1655 cells and *E. coli* MG1655 *ΔssrA* cells. Expression was induced using 100 ng/μL anhydrous tetracycline (aTc) and growth was compared to cells containing the ssrAp tmRNA construct (Figure 12 B). Expression of the inducible construct was well tolerated in both genetic backgrounds and grew similarly to their ssrAp counterparts.

We wanted to compare tagging levels of the inducible construct with the ssrAp native promoter construct. Expression of the pL(tetO) construct was induced at inoculation with 100 ng/μL aTc. We then performed an α-6xHIS western blot and total protein analysis on 2 μg of the total protein lysate and first affinity purified elution (Figure 12C). In wildtype cells, 6xHIS staining was not as dark in the pL(tetO) construct, indicating fewer tagged proteins. This was not surprising since ssrAp natively drives high expression, and synthetic constructs are competing with native tmRNA for tagging. However, the molecular weight range is nearly identical in both promoters. This implies that diversity of tagged proteins is maintained with the inducible promoter, even though it is less abundant. In *ΔssrA* cells, however, the inducible promoter showed very little tagging compared with the native promoter and wildtype cells. The molecular weight range was also narrower. However, it did show a similar banding pattern to the inducible tagged cells in the wildtype. It is possible that the same diversity of tagged proteins is being tagged but are not detectable due to the lower abundance.

Discussion

We set out to design a synthetic *E. coli* tmRNA platform that would allow us to stabilize and isolate tmRNA-tagged proteins. We have created a modified tmRNA molecule that introduces a 6x-Histidine epitope. We have verified that expression of our construct is well tolerated in wildtype cells and successfully detected 6xHIS-tagged proteins using α6xHIS western blot (WB). Tagged proteins represented a broad molecular weight range, implying that there is diverse identity and completeness of proteins represented. Our work

was inspired by previous work done by Roche and Sauer who originally designed a tmRNA-6xHIS molecular for expression in *E. coli*.[76] We show that our tmRNA-6xHIS sequence variant produces a similar tagging profile to that of Roche and Sauer's variant.

In wildtype cells, our synthetic construct is competing with the native copy of tmRNA for tagging. To maximize tagging, we transformed our construct into ssrA knockout cells (*ΔssrA)*. While ssrA is not essential in *E. coli* it does result in poor growth phenotype. Previous work showed that synthetic tmRNA could rescue this. However, our experiments showed that introduction of our synthetic construct exacerbated the growth defect. We also consistently noted less abundant tagging in *ΔssrA* cells compared to wildtype. This could indicate that our synthetic construct does not perform as well as the native tmRNA and is not able to alleviate the stress associated with deletion.

Metal affinity purification of 6xHIS-tagged proteins has several co-purifying contaminant proteins. We intend to use tandem mass spectrometry to identify tagged proteins. Maximizing sample purity is critical for accurate analysis. We have shown that immunoprecipitation (IP) of lysates containing tagged proteins results in detectable staining in an α6xHIS WB. While IP on total cell lysates produced detectable staining, IP on affinity purified elutions better reflected the abundance and diversity seen in affinity purified only WB.

Finally, we created an inducible variant of our tmRNA-6xHIS construct by replacing the constitutive native *ssrA* promoter with the pL(tetOpromoter. We have shown that expression of our inducible construct is as well tolerated as the constitutively expressed construct. While the ssrAp construct resulted in higher abundance of tagged proteins, the pL(tetO) construct still induced detectable tagging and showed the same molecular weight range in wildtype cells. This implies that we are able to tag the same diversity of identity and protein completeness as with the constitutive promoter. Inducible expression of our construct will be critical for resolving changes to the degradome under stress.

Materials and Method

Bacterial strains

ΔssrA knockouts were generated using lambda-red recombinase in *E. coli* MG1655 cells.[124] Primers were designed to contain internal homology regions with the kanR-FLP cassette and external homology regions with the ssrA gene.

E. coli MG1655 cells containing our synthetic construct were inoculated 1:100 dilution into 200mL LB media. Cells were grown at 37°C shaking at 250 rpm. At OD 0.5, cells were treated with 100 ng/mL anhydrous tetracycline (aTc).

Construct generation and cloning

Engineered sequences of tmRNA-6xHIS constructs were synthesized by IDT as gBlock Gene Fragments. PZA31-MCS plasmid vectors was obtained from Expressys.

Gene blocks and vectors were digested with appropriate restriction enzymes for 30 minutes at 37ºC. Vectors were dephosphorylated with calf intestinal alkaline phosphatase (New England BioLabs [NEB] M0290). Vectors were then purified using gel electrophoresis, and the band corresponding to digested backbone were excised. Digested vector fragments were extracted from the gels using QIAquick Gel Extracton Kit (Qiagen 28706X4). Digested gene blocks were purified using the GenElute PCR Clean-up kit (Sigma Aldrich NA1020). A 3:1 molar excess of gene block to vector were used in ligation reactions along with Instant Sticky-end Ligase Master Mix (NEB M0370). Ligated constructs were then transformed into 10-beta Competent *E. coli* cells (NEB C3019). Individual colonies were selected and mini-prepped using the GenElute Miniprep Kit (Sigma Aldrich PLN70-1KT). Correct insertion of the gene block was confirmed by PCR and sequencing. Constructs were then transformed into *E. coli* MG1655 cells or *E. coli*

Transformation

50 µL of competent cells were combined with 5 µL of ligated vector-gene block, mixed gently, and incubated on ice for 30 minutes. Cells were then heat shocked at 42^{o} C for 30 seconds before being immediately cooled on ice for 5 minutes. 900 µL of Luria Broth (LB) media was then added, and cells were outgrown for 1 hour shaking at 37^{o}C. 500 µL of outgrown cells were pelleted then resuspended in 100 µL LB before plating.

Collection of total cell lysate

E. coli MG1655 cells containing our synthetic construct were inoculated 1:100 dilution into 200 mL LB media. Cells were grown at 37°C shaking at 250 rpm for 4.5 hours. Cells were pelleted at 5000 rpm in a Sorvall RC6 Plus for 10 min at 4°C, and the supernatant was decanted. Pellets were snap frozen in liquid nitrogen and incubated at -80°C for 10 min. Frozen pellets were resuspended in 3mL BPER (Thermo

Scientific 78248) and incubated at room temperature for 15 min. Lysates were centrifuged for 5 min at 16000 rpm in an Eppendorf 5415D tabletop centrifuge. Supernatent was collected as the protein lysate.

Affinity purification

3 mg of protein lysate were metal affinity purified using 0.2 mL Thermo HisPur Cobalt affinity columns (Thermo 90090). Desired amount of lysate was diluted 1:1 with Equilibrium buffer and purified in 800 µL batches. Each batch was incubated rotating for 30 min at 4°C. Purified proteins were eluted in 3 fractions of Elution Buffer.

Immunoprecipitation

Elution fractions from metal affinity purification were pooled. 12.5 µg of α-6xHis antibody (Thermo PA1-983B) was added and incubated rotating for 12 hours at 4°C. 70 µL of Sepharose A beads (Abcam AB 193256) were washed with 3 volumes of IP wash buffer (10mM Tris pH 7.4, 1mM EDTA, 1mM EGTA pH 8.0, 150mM NaCl, 1% Triton X-100) three times. The washed beads were added to the protein lysate and incubated rotating at 4°C for 4 hours. Beads were pelleted and washed 3 times with 400 µL of IP wash Buffer and once with 400 µL Pre-Urea wash buffer (50mM Tris pH 8.5, 1mM EGTA, 75mM KCl). Proteins were eluted by incubating the beads in 140 µL of Urea Elution buffer (8M urea, 20mM Tris pH 7.5, 100mM NaCl) rotating at 4°C for 30 min. Elution was performed three times.

Western blotting

2 µg of protein was separated on a 4-12% Bis-tris gel. Gel was incubated in 20% ethanol for 10 min and then transferred to nitrocellulose (IB23001) using the Invitrogen iBlot2 system. Blots were stained for total protein using the MemCode Erasable Stain (Thermo 24580). Blots were incubated for 4 hours at 4°C in blocking buffer (4% non-fat milk in TBST). α-6XHIS antibody was diluted 1:10,000 in blocking buffer and incubated for 20 hours at 4°C. Blots were washed with six times with TBST then developed using the Pierce ECL Western Blot kit.

CHAPTER 3: RAPID REMODELING OF BACTERIAL GENE EXPRESSION UNDER OXIDATIVE STRESS

Introduction

Aerobically-growing bacteria endogenously generate harmful reactive oxygen species (ROS) through the interaction of O_2 and cellular electron donors like metal centers and quionones.[125] ROS take the form of superoxide anions, hydroxyl radicals, or hydrogen peroxide and can cause widespread damage to an array of biomolecules. DNA damage and oxidation of amino acids pose dire threats to cellular function. ROS can cause breaks in DNA strands, impeding gene expression, replication, and generating mutation.[126] Meanwhile, oxidation of cysteine and methionine can result in covalent modifications that can inactive and destabilize cellular proteins.[125,127] Rapidly inactivating ROS is critical for maintaining homeostasis. Bacteria utilize superoxide dismutases and catalases which are controlled by the SoxRS and OxyR regulons.[128] SoxRS is primarily responsible for coping with superoxide stress, regulating the expression of *sodA, soxR,* and *soxS.* SoxR directly regulates the expression of SoxS, binding the to the promoter region in reduced and oxidized form and is directly responsible for resistance to the superoxide-generating compound paraquat.[127,129,130]

Oxidative stress also induces a general stress response mediated through *rpoS*. During steady state conditions in *E. coli*, transcription of most genes is controlled through RpoD (σ^{70}). Under stress conditions, including heat stress, oxidative stress, and starvation, *rpoS* is activated as an alternative sigma factor that induces expression hundreds of stress-coping genes.[131] Among these is Dps, a DNA binding protein that protects DNA from oxidative damage.[132] The general stress response is also characterized by increased proteolytic and RNase activity.[102,133]

In Chapter 2, we showed that tmRNA can be modified to introduce an isolation tag to stabilize and isolate the tmRNA degradome. Here, we show that the degradome contains a broad range of protein products that expands the information available in proteomic experiments. We demonstrate that our platform captures metabolic changes in response to oxidative stress conditions. Our results also suggest a previously unknown strategy for regulating the pentose phosphate pathway.

Results

Synthetic tmRNA-6xHIS platform

Natively, *E. coli* tmRNA introduces a 10-mer tag (ANDEYALLAA) to the C-terminus of aberrant peptides. Previous studies focused on tmRNA tag function and dynamics found that the tag's final two alanines are critical for recognition by ClpP for targeted proteolysis and that the TRF could be modified to introduce a 6xHistidine tag (6xHIS).[76,116] Building on this, we recoded the last 6 amino acids of the native tag to 6 histidines (ANDEHHHHHH). With the initial success with the native promoter, we moved to an inducible system using the pL(tetO) promoter.[123] Our construct was placed on the pZA plasmid and transformed into wildtype and Δ*ssrA* (tmRNA) *E. coli* MG1655 (Figure 13A). While tmRNA is not essential in *E. coli*, deletion

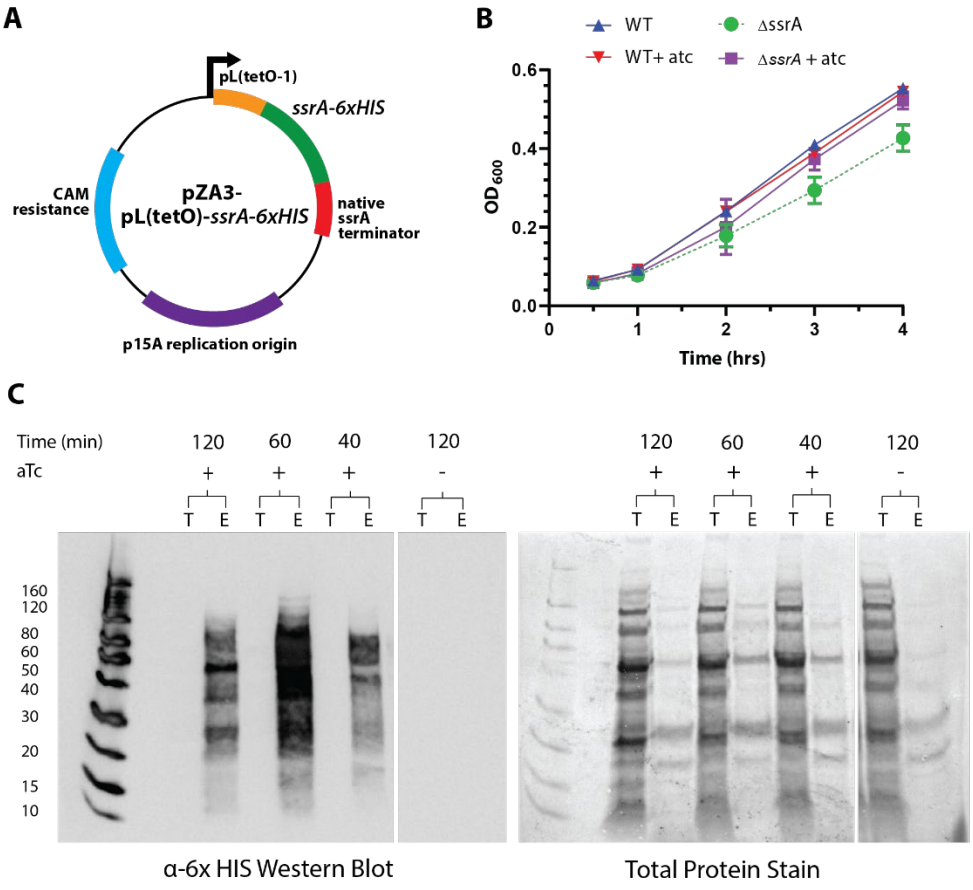

Figure 13. Inducible Synthetic tmRNA-6xHIS expression and purification (A) Plasmid map of tmRNA construct. (B) Growth curve of *E. coli* MG1655 and Δ*ssrA* cells containing our synthetic tmRNA-6xHIS construct with and without induction. Cells were induced with 100 ng/mL anhydrous tetracycline (aTc) at inoculation. (C) α-6xHIS western blot and Coomassie stain of whole cell lysate (T) and purified elution fraction (E). Cells were grown to OD_{600} 0.5 before induction. Lysates were collected at indicated times post-induction. Lysates were cobalt-affinity purified for the purified elution fractions.

causes growth defects and poor responses to stress. We assessed the cell growth with induction of our synthetic construct. Expression rescued the growth phenotype in knockout cells and was well-tolerated in wildtype cells (Figure 13B).

Resolution of existent and remodeled states requires tight regulation of construct expression. To assess the fidelity of regulation and rate of tagging, we collected lysates at several timepoints post-induction, purified using cobalt affinity columns, and analyzed with anti-6xHIS western blot. There was a broad molecular weight range of tagged products, indicating a variety of proteins being tagged. The abundance and range peaked after 60 minutes post-induction (Figure 13C). Tagging occurs quite quickly with products detectable after 20 minutes of induction. Critically, we observed tight expression regulation, with no visible tagging after 120 minutes without induction.

tmRNA-tagged proteins under steady state

Identifying the tagged proteins is crucial for examining metabolic changes under stress. To characterize the proteins tagged under steady-state and stress, we subjected *E. coli* cells containing our synthetic tmRNA construct to oxidative stress (Figure 14). Cells were grown to OD_{600} ~0.5 then treated with anhydrous tetracycline (aTc) to induce expression of our construct and/or a sublethal concentration of paraquat to induce stress. Paraquat (PQ) causes continuous production of superoxide, creating a sustained stressor.[127,134] Cells were grown for an additional hour before lysate harvest. We isolated 6xHis-tagged proteins by purifying lysates with a Cobalt-affinity column followed by anti-6xHIS immunoprecipitation. After confirming tagging via western blot, we identified the proteins and peptide products in the total proteome and tagged proteomes using tandem mass spectrometry (LC-MS/MS). The tagged and total proteomes cluster independently of one another in principle component analysis (PCA) regardless of the treatment conditions (Figure 14). Under steady state conditions, we found that there were 23 peptide products uniquely identified in the tagged fraction and 623 unique to the total proteome (Figure 15A). There were 1142 proteins identified in both fractions, which is consistent with the broad range of

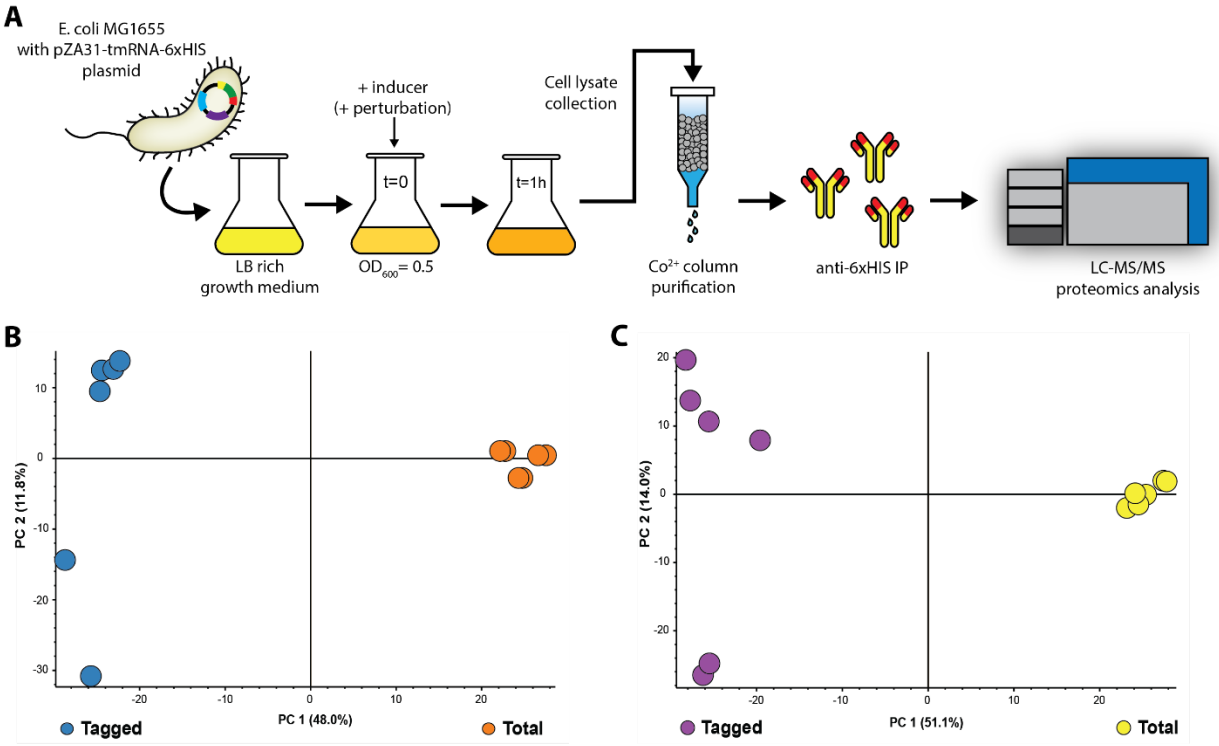

Figure 14. Experimental approach. (A) Experiment design. 200mL LB were inoculated 1:100. Cells grown to OD_{600} 0.5 and treated with aTc and/or paraquat (PQ). Cells were grown an additional hour before harvest. Lysates were cobalt-affinity purified and subsequently immunoprecipitated. Fractions were reduced, alkylated, and digested with trypsin before LC-MS/MS analysis. (B) Principle component analysis of untreated tagged and total proteomes. (C) Principle component analysis of paraquat-stressed tagged and total proteomes.

tagged products seen in the western blots (Figure 13C). Interestingly, the commonly identified products have vastly different abundances in the tagged proteome compared to the total. 182 peptide products were at least 5-fold more abundant in the tagged proteome (Figure 15). Among these were several known substrates of ClpP, previously identified by pull down assays.[126] ClpP is the primary protease responsible for degradation of the native tmRNA tag and was used as an early way of identifying tmRNA-tagged protein products. The identification of known substrates, particularly enriched in the tagged proteome, indicates that our synthetic construct is behaving as the native tmRNA.

Tagged proteins under oxidative stress

Similar results were seen under oxidative stress conditions. Of the 1762 proteins identified, 28 were unique to the tagged proteome and 517 to the total (Figure 15C). We identified markers of oxidative stress,

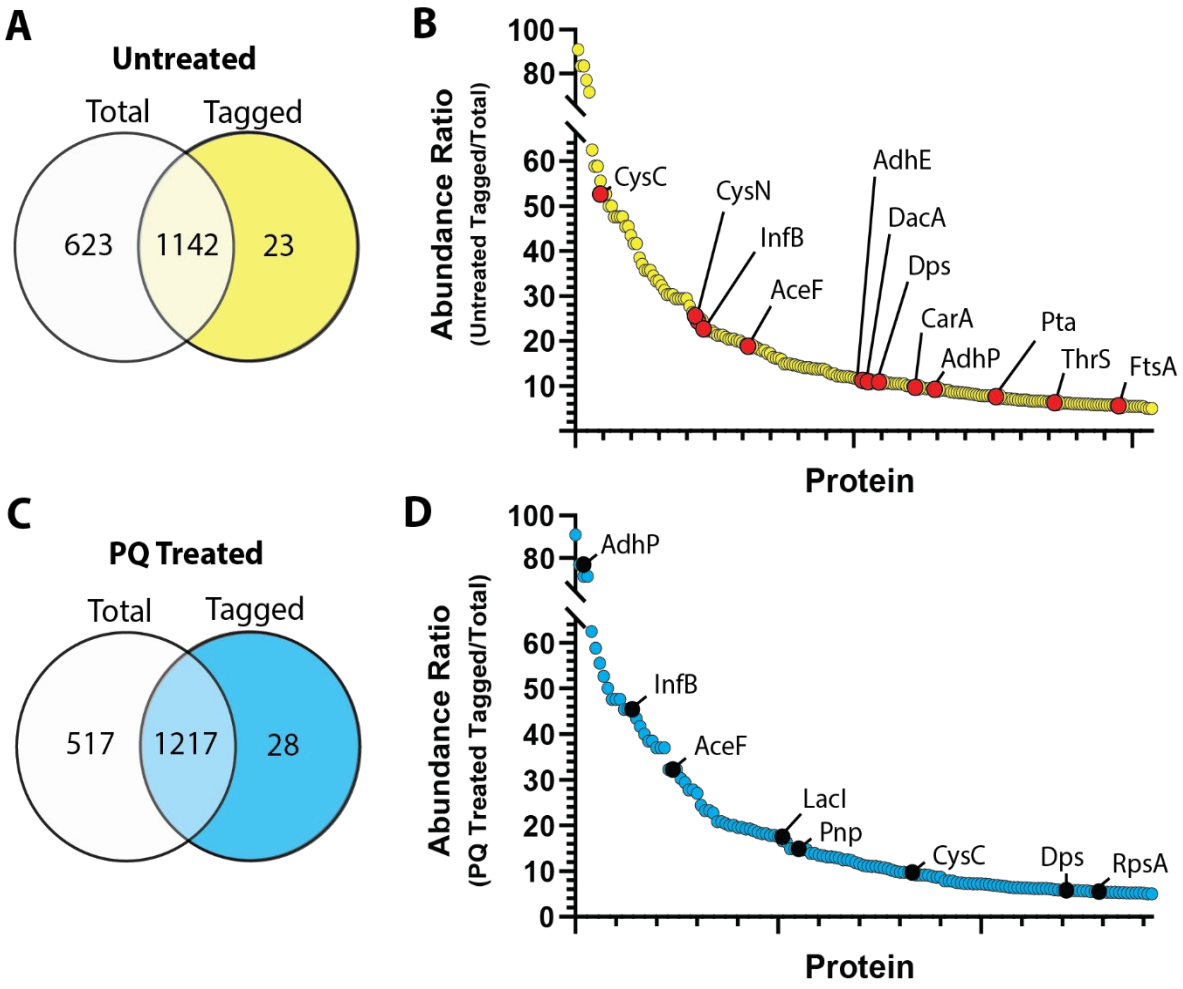

Figure 15. Mass spectrometry analysis of tagged and total proteomes. (A) Identified proteins in untreated sample fractions. (B) Protein abundance ratios of the tagged proteome over the total proteome in untreated, steady state samples. Known ClpP substrates are identified. (C) Identified proteins in paraquat-treated sample fractions. (D) Fold abundance enrichment of the tagged proteome over the total proteome of paraquat-treated samples. Known ClpP substrates are identified.

including *soxRS, katEG,* and *ahpFC* (Table 4). We again observed differences in abundances of the commonly identified peptide products with 180 products being at least 5-fold more abundant in the tagged proteome (Figure 15D). Among these enriched proteins, we still identified known ClpP substrates, including some identified in untreated cells. However, we see changes in the abundance ratios of the common proteins under paraquat stress. Taken together, these results indicate that the tagged proteome expands the coverage of the total proteome, provides unique abundance information, and captures changes occurring under stress.

Shifts in the degradome during oxidative stress

A hallmark of the bacterial stress response is the activation of RNases, which cleave mRNAs in both a stochastic and directed manner.[92,103] Since tmRNA requires RNA cleavage to integrate into the ribosome, we should see a shift in the tagged proteome under stress conditions. We compared the peptide products identified in the tagged subproteome under steady-state and paraquat-treatment. We identified more uniquely tagged peptide products under oxidative stress, with 213 unique to paraquat-treated and 129 unique to steady-state (Figure 16A). This is consistent with increased RNase activity. We also observed shifts in abundances of the 1032 commonly identified peptide products. There were 83 peptide products that were at least 5-fold more abundant and 69 that were at least 5-fold less abundant under oxidative

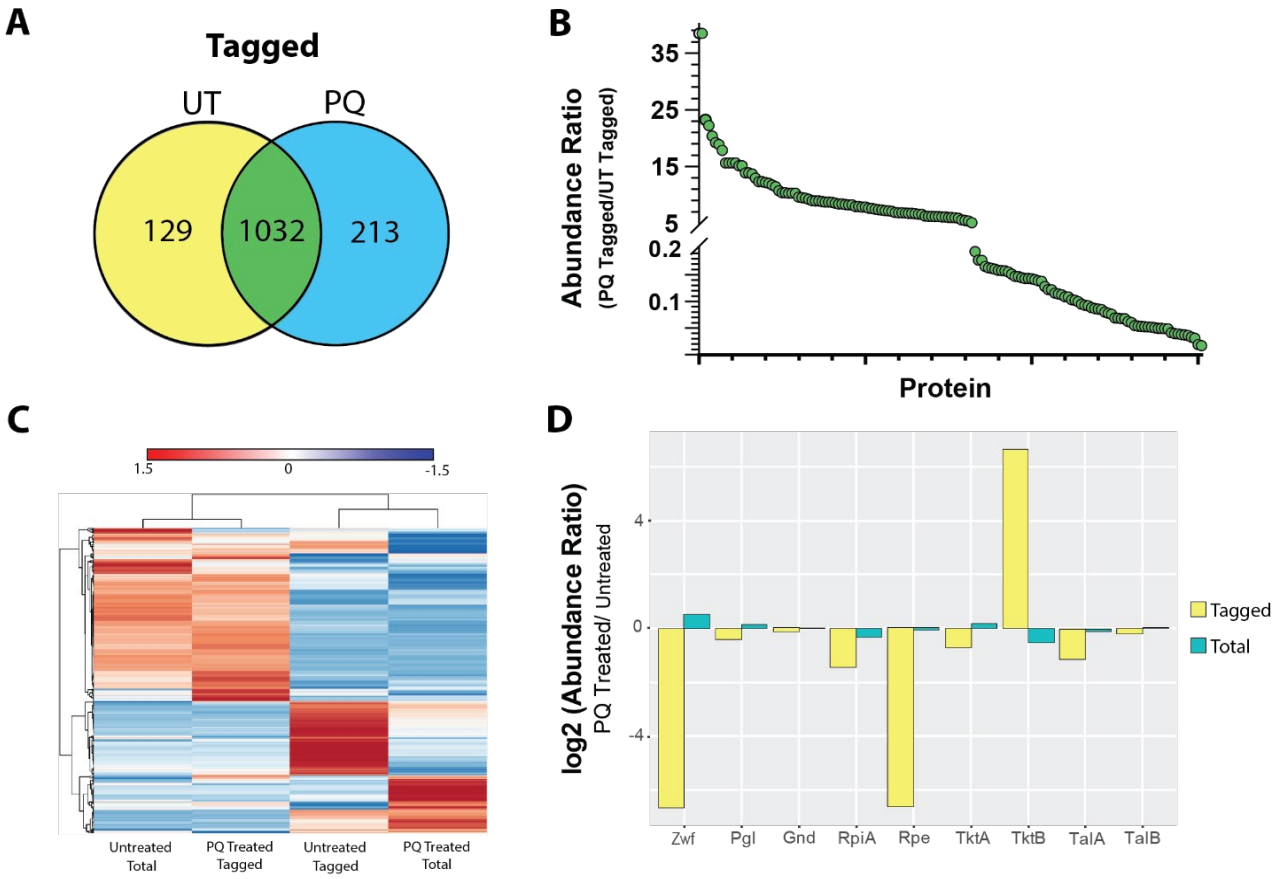

Figure 16. Mass spectrometry analysis of tagged proteomes at steady state and under stress. (A) Uniquely identified proteins in each proteome. (B) Fold abundance enrichment in the paraquat-treated proteome of commonly identified proteins. (C) Hierarchical clustering of proteins identified in each fraction. D) Fold abundance enrichment in paraquat-treated cells of proteins from the pentose phosphate pathways in the tagged and total proteome.

stress (16B). These findings demonstrate that there are shifts in the tagging profiles with the application of stress. The differential enrichments suggest that these shifts are protein specific.

A key goal of this system is to fill the information gap between transcription and translation. This is of particular importance in cells responding to environmental challenge. Metabolism and its associated proteins are among the highest abundant in the degradome. Under oxidative stress, catabolic pathways are particularly well represented in the tagged subproteome. Interestingly, the total proteome showed enrichment primarily of anabolic pathways. Some of the anabolic pathways most prominently represented had their catabolic counterparts enriched in the tagged subproteome. This suggests that our platform well represents the metabolic genes and captures shifts in metabolic pathway usage. One of the most interesting shifts was in the first enzymatic step in the pentose phosphate pathway. We found that paraquat challenge increased the abundance of Zwf by approximately 2-fold. This result was not surprising given that oxidative stress increases demand for NADPH to maintain glutathione balance. However, in the degradome, Zwf was significantly less abundant under paraquat treatment (Figure 16D). This result suggests that pentose phosphate pathway activity is regulated not only by metabolic feedback inhibition, but also by regulated proteolysis of Zwf, which is reversed under oxidative stress conditions.

Discussion

In this study, we demonstrate that tmRNA can be modified to introduce 6xHistidine tags in an untargeted way. We show that expression of a synthetic tmRNA-6xHIS construct can be controlled with an inducible promoter and that detectable tagging occurs quite rapidly following induction. We demonstrate that this platform captures known substrates of native tmRNA and expands the coverage of traditional proteomics experiments. We demonstrate that our platform output provides good coverage of metabolic genes and captures changes in pathway prioritization. Excitingly, tmRNA has a near ubiquitous presence in sequenced bacteria, meaning that our construct can be modified and expanded for use in any bacterial environment.

Our platform could also provide novel insight into translation dynamics. The critical function of natural tmRNA is to resolve stalled translation events and maintain a functional ribosome pool. Translation can stall for a variety of reasons, including non-stop mRNAs, programmed stall sites, and rare codons.[48,80,135,136]

It was previously accepted that tmRNA required an empty ribosomal A-site to act, meaning that only nonstop transcripts would be tagged.[92,137,138] However, recent work revealed tmRNA intervention can also occur on intact transcripts.[139] This new insight greatly expands the phenomena our platform is able to capture. This is particularly useful in studying bacterial stress responses where translation is moderated by changes to gene expression and the intracellular environment. For example, during starvation, there is a combination of limited nutrient availability and increased expression of RNases.[103,105,140] RNases are implicated in regulating the expression of some genes post-transcriptionally through cleavage events.[141] Our platform provides a way to capture the effects of both facets with one measurement.

Materials and Methods

Culturing

E. coli MG1655 cells containing our synthetic construct were inoculated 1:100 dilution into 200mL LB media. Cells were grown at 37°C shaking at 250 rpm. At OD 0.5, cells were treated with 100 ng/mL anhydrous tetracycline (aTc) and 10 μM paraquat where noted. Cells were grown an additional 1 hour. Cells were pelleted at 5000 rpm in a Sorvall RC6 Plus for 10 min at 4°C, and the supernatant was decanted. Pellets were snap frozen in liquid nitrogen and incubated at -80°C for 10 min. Frozen pellets were resuspended in 3mL BPER (Thermo Scientific 78248) and incubated at room temperature for 15 min. Lysates were centrifuged for 5 min at 16000 rpm in an Eppendorf 5415D tabletop centrifuge. Supernatent was collected as the protein lysate.

Affinity Purification

3 mg of protein lysate were metal affinity purified using 0.2 mL Thermo HisPur Cobalt affinity columns (Thermo 90090). Desired amount of lysate was diluted 1:1 with Equilibrium buffer and purified in 800 μL batches. Each batch was incubated rotating for 30 min at 4°C. Purified proteins were eluted in 3 fractions of Elution Buffer.

Immunoprecipitation

Elution fractions from metal affinity purification were pooled. 12.5 μg of α-6xHis antibody (Thermo PA1-983B) was added and incubated rotating for 12 hours at 4°C. 70 μL of Sepharose A beads (Abcam AB 193256) were washed with 3 volumes of IP wash buffer (10mM Tris pH 7.4, 1mM EDTA, 1mM EGTA pH

8.0, 150mM NaCl, 1% Triton X-100) three times. The washed beads were added to the protein lysate and incubated rotating at 4°C for 4 hours. Beads were pelleted and washed 3 times with 400 µL of IP wash Buffer and once with 400 µL Pre-Urea wash buffer (50mM Tris pH 8.5, 1mM EGTA, 75mM KCl). Proteins were eluted by incubating the beads in 140 µL of Urea Elution buffer (8M urea, 20mM Tris pH 7.5, 100mM NaCl) rotating at 4°C for 30 min. Elution was performed three times.

Mass spectrometry analysis

The 110 µL of the first immunoprecipitation elution and 2 µg of total protein lysate were prepared for mass spectrometry. Samples were reduced with 10 mM of DTT at 60°C for 45 min and alkylated with 15mM iodoacetamide at room temperature for 30 min. Samples were then digested with trypsin/LysC (Promega V5073) at 1:20 for 4 hours at 37C. Purified elutions were then diluted with 1mL of 25mM ammonium bicarbonate (for <1M concentration of urea) and digested overnight. Samples were dried down, resuspended in 20 µL of 0.1% formic acid, and desalted using Pierce C18 spin tips (Thermo 84850). Samples were dried and resuspended in 20 µL of 0.1% formic acid and spiked with 0.5 µL of 10x iRT retention peptide mix (Biogynosis KI3002-1).

NanoLC MSMS analysis was carried out with a Thermo Scientific Fusion Lumos tribrid mass spectrometer interfaced to a UltiMate3000 RSLCnano HPLC system. 1 µg of the tryptic digest was loaded and desalted in an Agilent Zorbax 300 SB-C18 trapping column (0.3 × 5 mm) at 5 µL/min for 5 min. Peptides were then eluted into Thermo Scientific Accalaim PepMap™ 100, 2 µm, 100 Å, 75 µm × 250 mm and chromatographically separated using a binary solvent system consisting of A: 0.1% formic acid and 2.5% acetonitrile and B: 0.1% formic acid and 75% acetonitrile at a flow rate of 300 nL/min. A gradient was run from 1% B to 50%B over 40 minutes, followed by a 5-minute wash step with 99% B and 10-minute equilibration at 1% B before the next sample was injected. Precursor masses were detected in the Orbitrap at R=120,000 (m/z 200). Fragment masses were detected in linear ion trap at unit mass resolution. Data dependent MSMS was carried with top of speed setting, cycle time was 3 sec with dynamic exclusion of 30 sec.

Protein identification and relative quantification were carried out using Proteome Discoverer software package (Thermo Scientific). Raw data was searched against an E. coli protein database from Uniprot

(2016-07-14) along with a contaminant protein database with both Sequest HT and Mascot search engines. Cysteine carbomidomethylation was set as fixed modification. Methionine oxidation and Glutamine deamidation were set as variable modifications. Trypsin was set as the digestion enzyme and allowed for 2 missed cleavages. Peptide mass tolerance was ±10 ppm, fragment mass tolerance was ±0.8 Da. Target peptide FDR was set to 0.01 (strict) and 0.05 (relaxed).

For relative quantification, label free quantification (LFQ) was carried out using MINORA feature detection followed by quantification with precursor intensity of unique and razor peptides. Peptides with variable modifications were excluded from quantification. A protein is not quantified if it is only detected in one replicate. Group abundance ratios were calculated using the pairwise approach.

Western Blotting

2 µg of protein was separated on a 4-12% Bis-tris gel. Gel was incubated in 20% ethanol for 10 min and then transferred to nitrocellulose (IB23001) using the Invitrogen iBlot2 system. Blots were stained for total protein using the MemCode Erasable Stain (Thermo 24580). Blots were incubated for 4 hours at 4°C in blocking buffer (4% non-fat milk in TBST). α-6XHIS antibody was diluted 1:10,000 in blocking buffer and incubated for 20 hours at 4°C. Blots were washed with six times with TBST then developed using the Pierce ECL Western Blot kit.

CHAPTER 4: PROTEOMIC ANALYSIS OF TMRNA DEGRADOME UNDER TRANSLATIONAL STRESS

Introduction

Bacterial survival hinges on the ability to rapidly respond to changes in the environment, particularly nutrient availability. Starvation conditions trigger the stringent response, a stress response modulated by (p)ppGpp produced by RelA.[142,143] Nutrient deficiency creates a surplus of uncharged tRNAs, which begin binding in the A-site of the ribosome. RelA senses the binding and rapidly begins producing (p)ppGpp. The accumulation of (p)ppGpp triggers wide-spread translational shut down and reduced overall mRNA levels through decreased synthesis and increased degradation.[93,140,144]

RNase toxins are key players in translational shut down and mRNA degradation.[105] Type II toxin systems are thought to be activated during the stringent response through increased Lon-mediated degradation of repressor antitoxins. RelE has been indicated as playing a critical role in shutting down translation and turning off (p)ppGpp production due to its ribosome-dependent cleavage mechanism. RelE cleaves mRNA within the ribosomal A site, preventing binding of uncharged tRNAs and further RelA activity.[90,104,145–147] RNase cleavage often results in non-stop mRNAs and stalled translational complexes. tmRNA has been shown to play a critical role during stringent response in recycling these stalled ribosomes and ensuring rapid degradation of cleaved RNAs and resulting aberrant peptides.[148,149]

As we showed in chapter 2, tmRNA can be modified to introduce synthetic peptide tags *in vivo* and that this modified platform could provide novel insight to stress responses.[77,137] This platform is particularly useful for studying the effect of RNase activation due to tmRNA's role in resolving stalled translational complexes caused by mRNA cleavage. In this study, we utilize a synthetic tmRNA-6xHIS to the effects of RNase activation on translation. We show that RelE plays a critical role in regulating the translation of ribosomal proteins.

Results

Effect of serine hydroxamate in wildtype and ΔrelE cells

We previously showed that expression of our synthetic tmRNA-6xHIS construct was well tolerated in wildtype MG1655 *E. coli* cells (Figure 13). To verify expression tolerance, we transformed the tmRNA-6XHIS plasmid-based construct into *ΔrelE* MG1655 *E. coli* cells and monitored growth following induction of expression of our construct with anhydrous tetracycline (aTc; Figure 17A). We did not observe any defects in growth kinetics or behavior in *ΔrelE* cells compared with wildtype, indicating plasmid and tmRNA-6xHIS expression are tolerated.

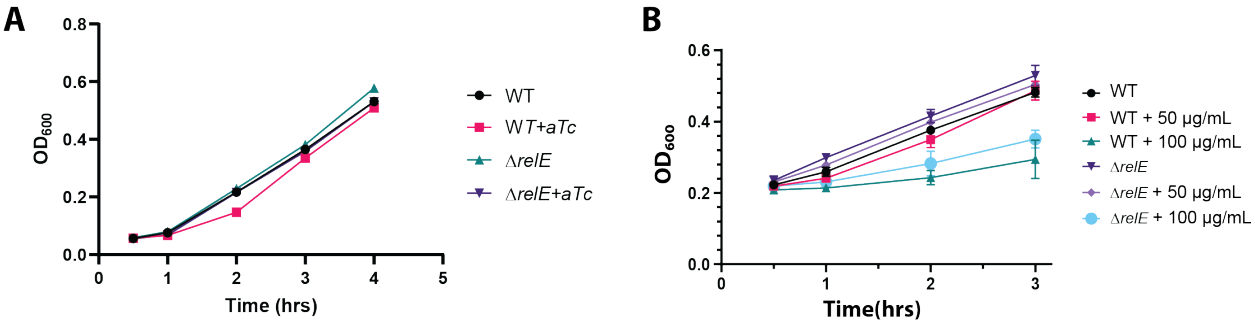

Figure 17. Expression tolerance of tmRNA-6xHIS and dose response curve of wildtype and ΔrelE cells. (A) Growth curve of strains with and without expression induction of our construct. Expression was induced using 100 ng/mL aTc. (B) Dose response curve of strains in response to SHX.

To simulate amino acid starvation and induce the stringent response, we used serine hydroxamate (SHX), an antimetabolite that inhibits seryl-tRNA synthetase activity to block charging of serine onto tRNAs. Previous studies have shown dose-dependent responses in cells challenged with SHX. To determine an optimal, non-lethal concentration of SHX, cells containing tmRNA-6xHIS were grown to OD_{600} ~0.5 then simultaneously induced tmRNA-6xHIS expression and challenged with SHX (Figure 17B). Both strains responded similarly to SHX exposure. Cells challenged with 50ug/mL of SHX recovered growth within 1 hour. We observed the most pronounced effect in response to 100 µg/mL SHX, with growth defects persisting up to 4 hours post-exposure.

Shifts in size of tmRNA-tagged proteins under SHX-challenge

We next asked to what extent SHX stress impacts the distribution of proteins requiring tmRNA-mediated intervention in wildtype and *ΔrelE* cells. To elucidate this set of proteins, which we refer to as the

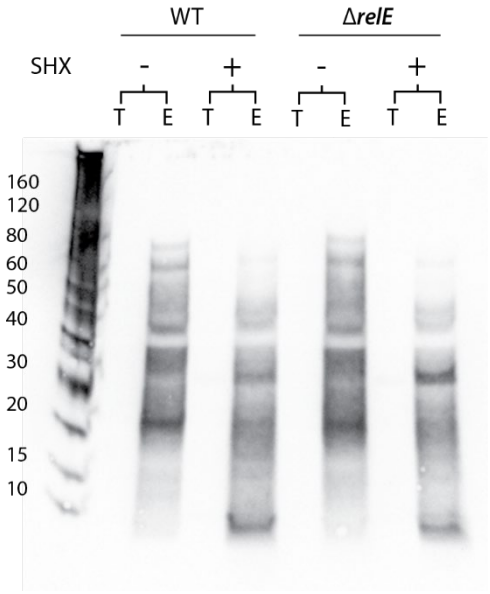

Figure 18. 6xHIS tagging in WT and ΔrelE cells in response to SHX treatment. α-6xHIS western blot of whole cell lysate (T) and purified elution fraction (E). Cells were grown to OD_{600} 0.5 before induction with aTc and challenge with 100 µg/mL SHX. Cells were grown for an additional hour before lysate collection. 2 µg of protein was loaded onto the gel.

degradome, cells were grown as described and challenged with 100 µg/mL SHX. We previously showed that peak tmRNA-tagging occurred at 1 hour post-induction (Figure 14C). Protein lysates were extracted and purified to isolate the 6xHIS tagged proteins by cobalt-affinity purification. Western blot analysis of the purified fractions showed broad molecular range distribution of tagged products with and without SHX-treatment (Figure 18). Under steady-state conditions, the majority of tagged proteins fall between 80 kDa and 20 kDa. In response to SHX treatment, the molecular weight distribution shifts with most tagged proteins smaller than 40 kDa and a distinct, dark band at 10 kDa. Interestingly, wildtype cells have an even distribution of proteins, while *ΔrelE* cells have an additional dark band at around 40 kDa. RNase toxin activation would result in increased shortened, non-stop mRNA transcripts. These non-stop transcripts would create stalled translation complexes requiring tmRNA-mediated resolution. The molecular weight shift of tagged proteins suggests that tmRNA is intervening on smaller mRNA fragments following SHX exposure, which is consistent with increased RNase cleavage.

Degradome proteins under SHX-challenge

To characterize changes to the total proteome and degradome of SHX challenged cells, respectively, we collected total lysate and purified tagged proteins for identification using LC-MS/MS and performed label free quantification. Unchallenged total lysates showed a shared stable proteome, with majority of proteins

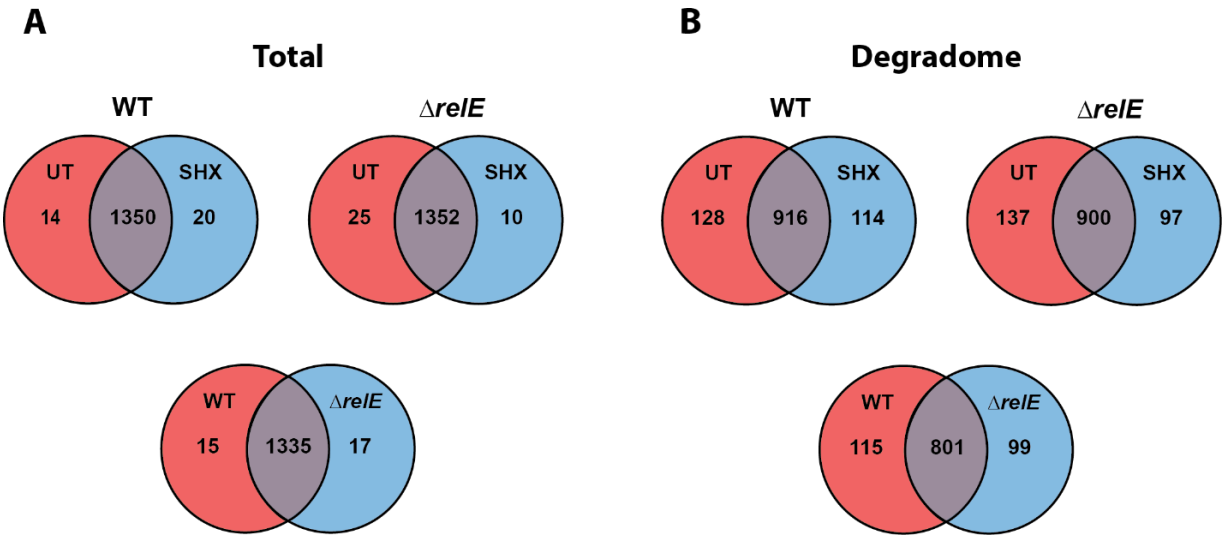

Figure 19. Venn diagram showing of overlap of identified proteins in serine hydroxamate treated (SHX) and untreated (UT) in wildtype (WT) and Δ*relE* cells. Proteins were identified using mass spectrometry. (A) Proteins identified in the total cell lysates. (B) Proteins identified in the tagged degradomes.

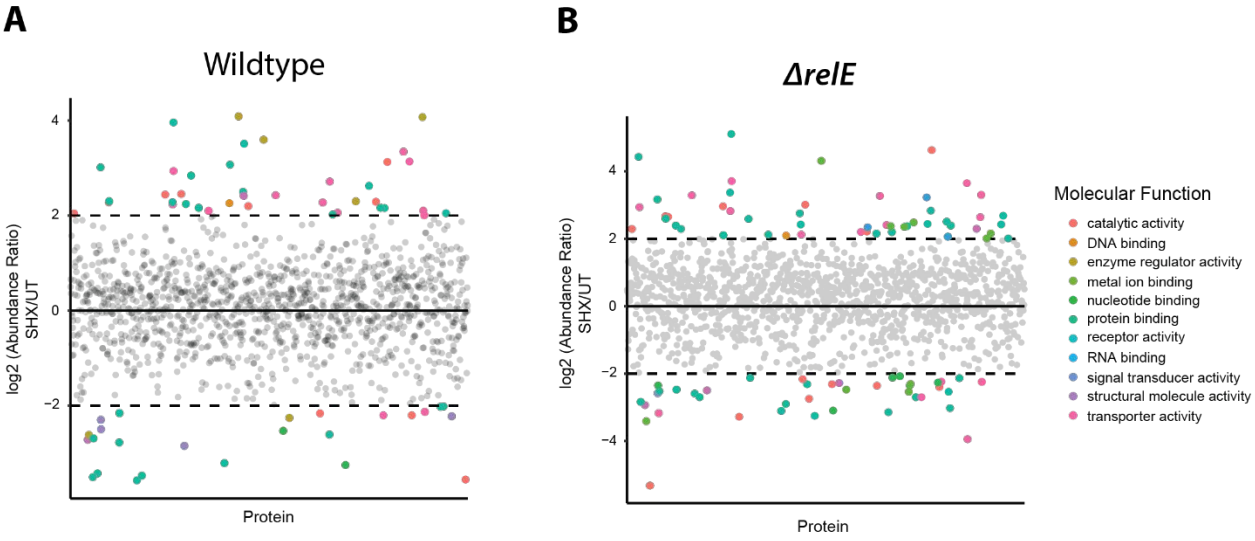

Figure 20. Mass spectrometry analysis of total proteomes under translational stress. Log2 abundance ratios of proteins identified in the serine hydroxamate treated (SHX) and untreated (UT) total proteome. Abundance ratios were determined using Proteome Discoverer. (A) Proteins identified in wildtype cells. (B) Proteins identified in Δ*relE* cells.

identified in both strains (Figure 19A). Interestingly, the total proteome composition did not change following SHX challenge. Of the 1391 overall proteins identified, 1335 were found in unchallenged and challenged cells of both broad strains. While there was a consistent population of identified proteins, there were some abundance shifts in response to SHX. Approximately 10% of identified proteins had significant differential abundance in SHX-challenged cells compared to unchallenged cells (136 in wildtype and 177 in *ΔrelE;* Figure 20). These results show that SHX exposure does not cause broadscale shifts in the proteome

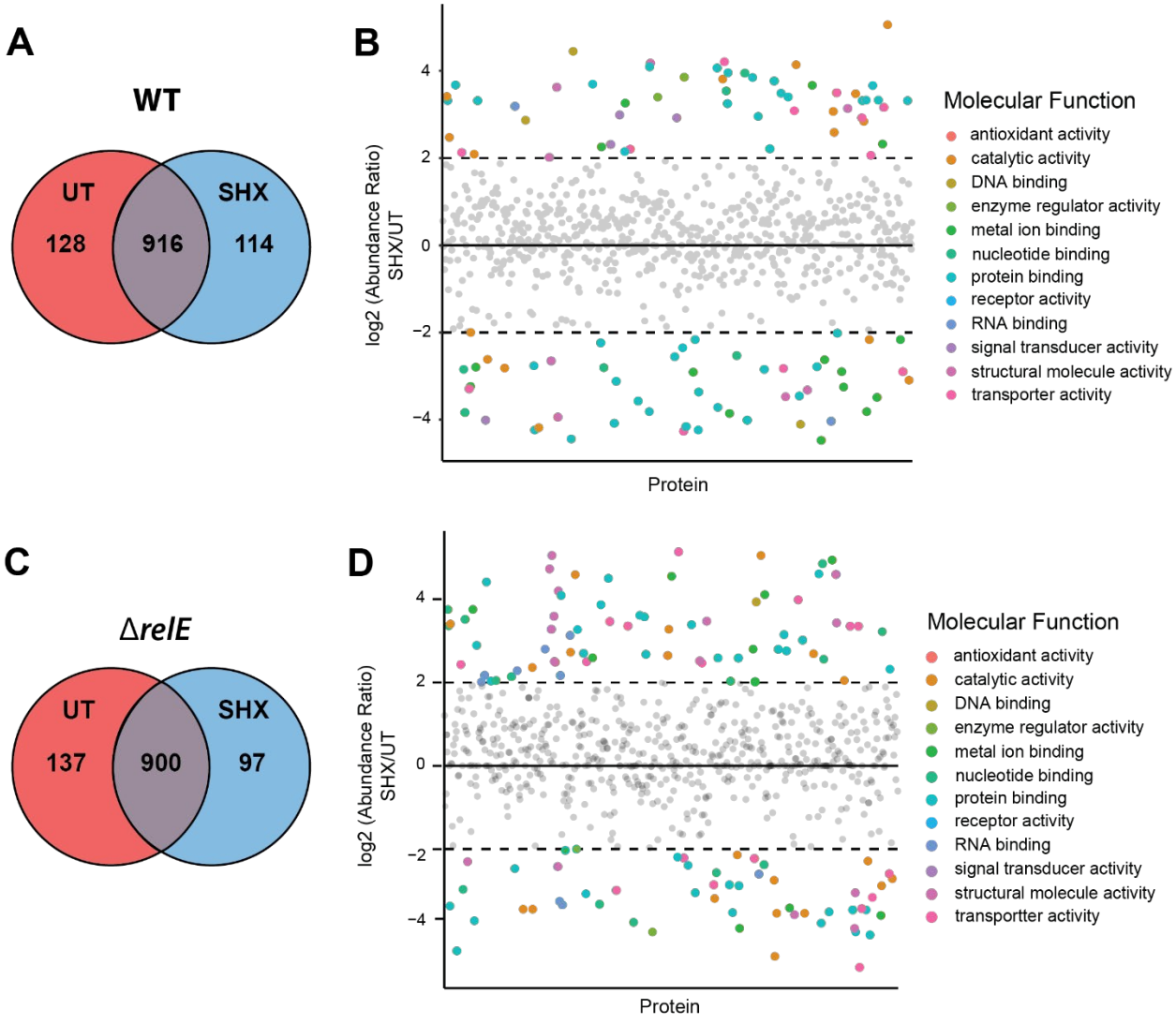

Figure 21. Mass spectrometry analysis of tagged degradomes under translational stress. (A) Overlap of identified proteins of SHX and UT in wildtype cells. (B) Log2 abundance ratios of proteins identified in SHX and UT degradomes from wildtype cells. Abundance ratios were determined using Proteome Discoverer. (C) Overlap of identified proteins of SHX and UT in Δ*relE* cells. (D) Log2 abundance ratios of proteins identified in SHX and UT degradomes from Δ*relE* cells. Abundance ratios were determined using Proteome Discoverer.

composition but does affect the overall abundance of a subset of proteins. The tagged degradomes showed a similar protein overlap. Challenged and unchallenged cells shared 916 proteins in wildtype and 900 in *ΔrelE*, with 801 proteins identified in all conditions (Figure 19B). However, both tagged degradomes showed widespread abundance shifts following SHX challenge. Over 50% of proteins (473 in wildtype and 525 in *ΔrelE*) showed a significant differential abundance in SHX-challenged cells compared with untreated (Figure 21). The enriched proteins represent a broad variety of molecular functions. Interestingly, the population of enriched degradome proteins is largely distinct from those in the total proteome, with 55 in wildtype and 61 in *ΔrelE* proteins shared between fractions. Taken together, these results suggest that there are changes in translational dynamics that are not captured in the total proteome.

Ribosomal protein abundance changes in the degradome

Gene ontology (GO) enrichment analysis of the significantly enriched degradome proteins showed that proteins relating to cellular metabolism and alpha-amino acid metabolism were significantly

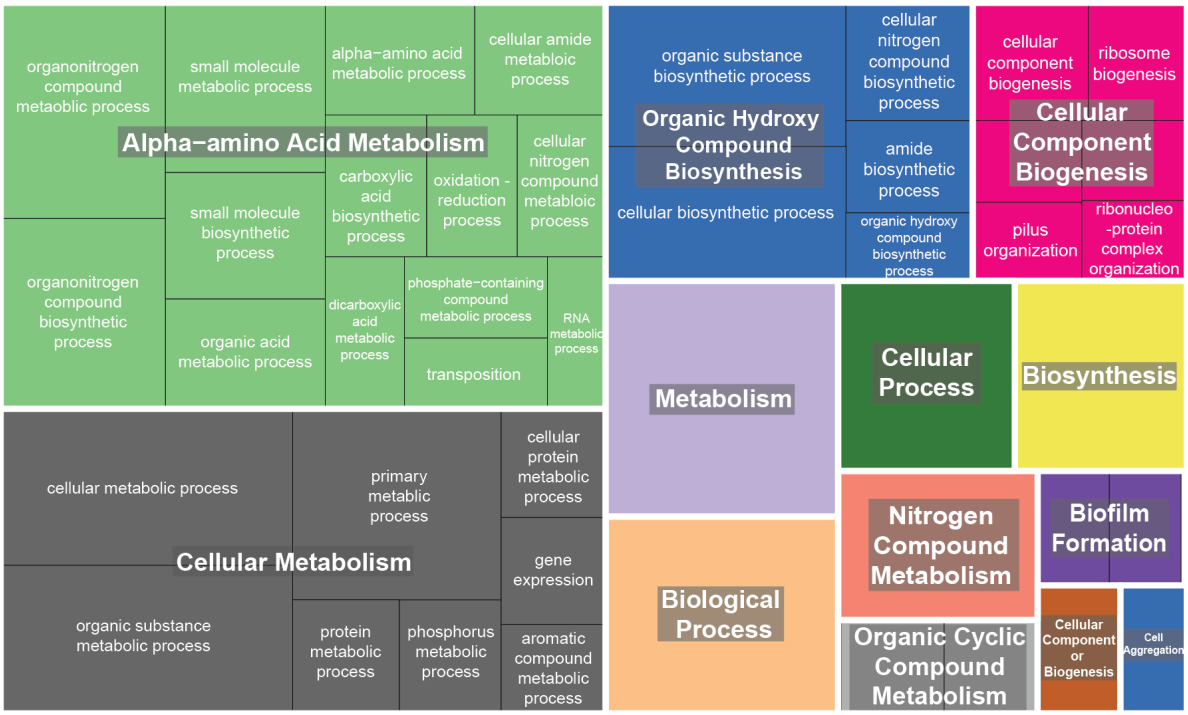

Figure 22. Gene ontology analysis of significantly enriched proteins in the degradome. Proteins with a log2 abundance ratio greater than 2 or less than -2 were selected for analysis. Analysis was performed using PANTHER and GO terms were consolidated using Revigo. Size of blocks indicate prevalence of representation.

overrepresented (Figure 22). GO enrichment analysis also indicated ribosome biogenesis proteins were highly represented in enriched degradome proteins. To further investigate this, we compared the

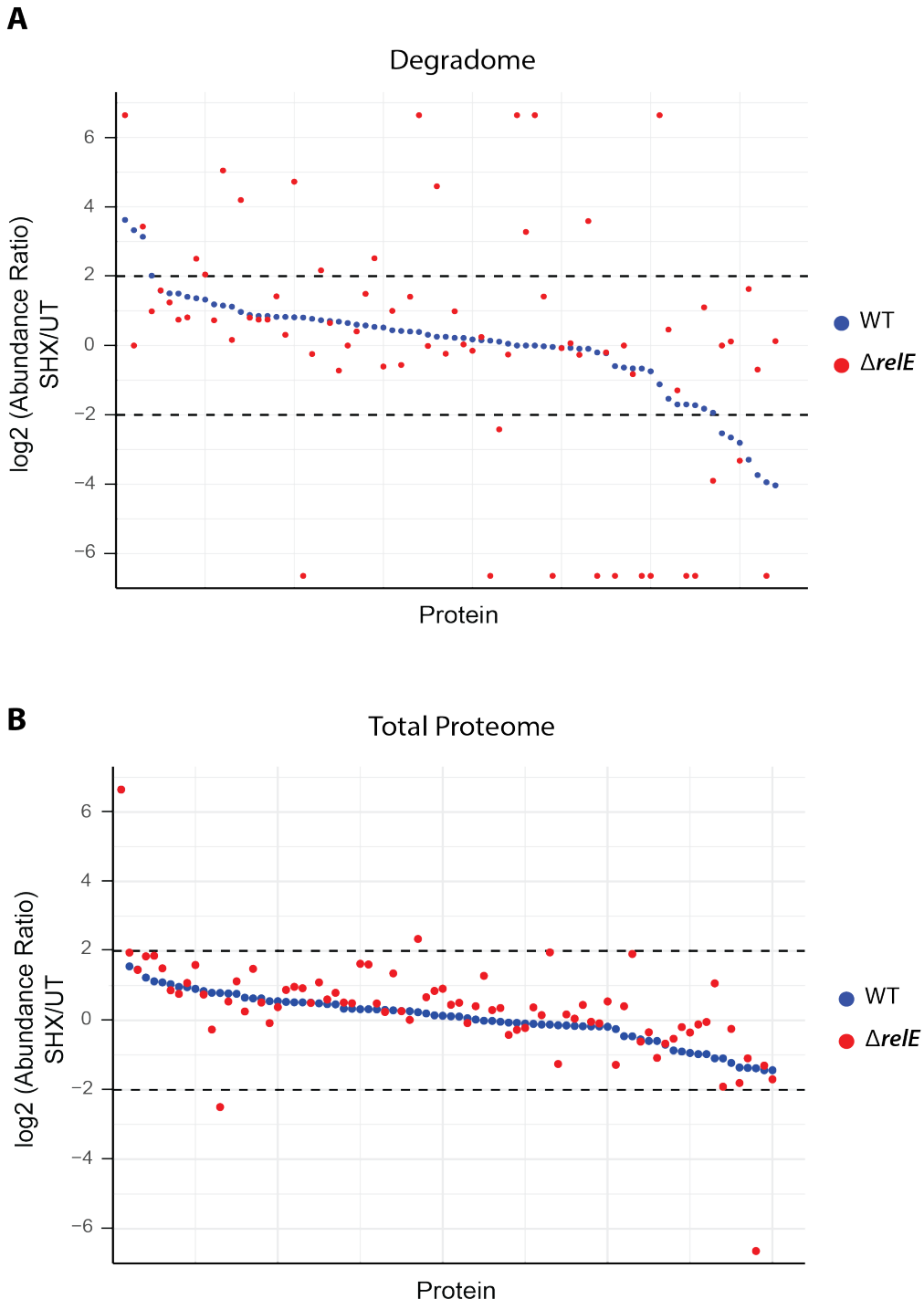

Figure 23. Abundance ratios of ribosomal proteins under stress. Log2 abundance ratios of proteins identified in SHX and UT degradomes from wildtype cells. Abundance ratios were determined using Proteome Discoverer. Dashed lines represent abundance significance threshold. (A)Ribosomal proteins identified in the tagged degradome. (B) Ribosomal proteins identified in the total proteome.

abundance ratios of all identified ribosomal proteins in response to SHX-treatment (Figure 23A). Wildtype ribosomal proteins have a range of abundance ratios, though only 11 show significant abundance difference in response to SHX treatment. However, we see a drastically different profile in *ΔrelE* cells with 29 having a significant abundance difference. Excitingly, nearly every ribosomal protein shows a disparate abundance ratio compared to its wildtype counterpart. These disparate changes appear to be protein-specific and unique to the degradome (Figure 23B). This could indicate that RelE activation and cleavage plays a role in post-transcriptionally moderating ribosomal protein abundance and translation.

Discussion

In this study, we use a synthetic tmRNA platform to study changes to translational dynamics during nutritional stress in wildtype and *ΔrelE E. coli* cells. Challenge with 100 µg/mL SHX impedes growth for 4 hours in both strains. Mass spectrometry analysis showed that the composition of the total proteome and the degradome were very stable with most proteins identified in both strains and challenged conditions. Mass spectrometry quantification showed shifts in protein abundance in response to SHX-treatment. Protein abundance shifts were drastically more prevalent in the tagged degradomes compared to total proteomes. Western blot analysis also showed smaller molecular weight proteins in SHX-challenged degradomes comparison to unchallenged. The significant overlap of identified proteins indicates that the shifts in size and abundance are not due to changing proteome composition.

RNase activation is a key aspect of the stringent response, resulting in increased mRNA cleavage.[142,147,147,148] With the increased cleavage rate, tmRNA may have to intervene earlier in translation, resulting in smaller tagged peptide products. Increased cleavage could also contribute to the differences in abundance changes between total proteomes and tagged degradomes. RNases have been indicated as a means of post-transcriptionally regulating gene expression during stress.[141] Even with our synthetic system present, total proteome analysis generally did not capture tmRNA-tagged proteins as they are a small fraction of all proteins in the cell. Abundance shifts in the degradome could be indicative of transcripts that are increasingly targeted for cleavage, particularly by RNases with sequence specificity.

Translational shutdown is a key aspect of the stringent response. Cessation is accomplished through a multi-pronged inhibition of transcription and translation machinery, activation of RNases, and inhibition of

ribosome maturation.[93,140,150] Ribosome assembly and maturation is highly regulated, often requiring sequential protein binding and conformation-specific protein release.[93] (p)ppGpp binds to several of the conformational checkpoint proteins to alter their kinetics and binding.[151–153] This leads to sequestration of immature ribosome components, dissociation of mature ribosomes, and decreased activation of hibernating ribosomes.[152,154,155] In addition, translational shutdown impacts the availability of ribosomal proteins, further exacerbating the assembly arrest and shifting stoichiometry of sequestered and free components. (p)ppGpp-activated Lon degrades free ribosomal proteins to recycle and conserve amino acids.[93,144,151]

Lon is also responsible for activation of RNases toxins through degradation of the antitoxins. RNase cleavage further assists in translational shutdown through the generation of non-stop mRNAs.[140] RelE in particular plays a very important role moderating the stringent response. RelE cleaves within the A-site of the ribosome, which is thought to prevent uncharged tRNAs from binding and subsequent RelA recognition and (p)ppGpp production.[104,145,156] A-site cleavage also directly stalls ongoing translation and allows tmRNA tagging and protease recycling. Additionally, RelE also exhibits a mild sequence preference which may allow it to act as a post-transcriptional expression regulator and target a subset of RNAs for cleavage.[147] During the stringent response, ribosomal proteins are not needed in the same concentration as during steady state. With a functional RelE, ribosomal protein abundance in the degradome largely did not change following SHX treatment. In the deletion mutant, ribosomal proteins showed much greater abundance variation in the degradome. However, these changes were not reflected in the total proteome abundances. These variations could be the result of poor translational shut down in the absence of RelE. Previous studies showed that RelE cleaves tmRNA following SHX treatment. However, our data did not indicate any differences that could be attributed to differential functional tmRNA-6XHIS concentrations between strains. The stringent response activates a host of RNases beyond RelE. While previous studies have shown that RelE alone was not responsible for (p)ppGpp accumulation profiles, RelE may play the most direct role in efficiently ceasing translation and regulating translation components.[150]

This study provides novel insight into translational regulation by RelE during the stringent response, particularly ribosomal protein translation. RelE is one of many RNase toxins activated during the stringent response. A recent study showed that while RelE deletion alone did not significantly alter (p)ppGpp

production, deletion of 10 type II toxin-antitoxin systems resulted in prolonged accumulation. RNase toxins exhibit a broad range of sequence preference and cleavage conditions. The relative contribution of each RNase and proportion of stochastic and directed cleavage remains unclear. Our platform provides a unique opportunity to map the location of RNase cleavage and monitor effects on translation dynamics in a holistic, undirected manner. Understanding the relative contribution of each RNase and stressor-specific changes in their behavior could reveal previously unknown aspects of the stress response.

Material and Methods

Culturing

E. coli MG1655 cells containing our synthetic construct were inoculated 1:100 dilution into 200 mL LB media. Cells were grown at 37°C shaking at 250 rpm. At OD 0.5, cells were challenged with 100 ng/mL anhydrous tetracycline (aTc) and 100ug/mL serine hydroxamate where noted. Cells were grown an additional 1 hour. Cells were pelleted at 5000 rpm in a Sorvall RC6 Plus for 10 min at 4°C, and the supernatant was decanted. Pellets were snap frozen in liquid nitrogen and incubated at -80°C for 10 min. Frozen pellets were resuspended in 3 mL BPER (Thermo Scientific 78248) and incubated at room temperature for 15 min. Lysates were centrifuged for 5 min at 16000 rpm in an Eppendorf 5415D tabletop centrifuge. Supernatent was collected as the protein lysate.

Affinity Purification

3 mg of protein lysate were metal affinity purified using 0.2 mL Thermo HisPur Cobalt affinity columns (Thermo 90090). Desired amount of lysate was diluted 1:1 with Equilibrium buffer and purified in 800 µL batches. Each batch was incubated rotating for 30 min at 4°C. Purified proteins were eluted in 3 fractions of Elution Buffer.

Immunoprecipitation

Elution fractions from metal affinity purification were pooled. 12.5 µg of α-6xHis antibody (Thermo PA1-983B) was added and incubated rotating for 12 hours at 4°C. 70 µL of Sepharose A beads (Thermo) were washed with 3 volumes of IP wash buffer (10mM Tris pH 7.4, 1mM EDTA, 1mM EGTA pH 8.0, 150mM NaCl, 1% Triton X-100) three times. The washed beads were added to the protein lysate and incubated rotating at 4°C for 4 hours. Beads were pelleted and washed 3 times with 400 µL of IP wash Buffer and

once with 400 µL Pre-Urea wash buffer (50mM Tris pH 8.5, 1mM EGTA, 75mM KCl). Proteins were eluted by incubating the beads in 140 µL of Urea Elution buffer (8M urea, 20mM Tris pH 7.5, 100mM NaCl) rotating at 4°C for 30 min. Elution was performed three times.

Mass Spectrometry Analysis

The 110 µL of the first immunoprecipitation elution and 2 µg of total protein lysate were prepared for mass spectrometry. Samples were reduced with 10mM of DTT at 60C for 45 min and alkylated with 15mM iodoacetamide at room temperature for 30 min. Samples were then digested with trypsin/LysC (Promega V5073) at 1:20 for 4 hours at 37C. Purified elutions were then diluted with 1 mL of 25mM ammonium bicarbonate (for <1M concentration of urea) and digested overnight. Samples were dried down, resuspended in 20 µL of 0.1% formic acid, and desalted using Pierce C18 spin tips (Thermo 84850). Samples were dried and resuspended in 20 µL of 0.1% formic acid and spiked with 0.5 µL of 10x iRT retention peptide mix (Biogynosis KI3002-1).

NanoLC MSMS analysis was carried out with a Thermo Scientific Fusion Lumos tribrid mass spectrometer interfaced to a UltiMate3000 RSLCnano HPLC system. 1 µg of the tryptic digest was loaded and desalted in an Agilent Zorbax 300 SB-C18 trapping column (0.3 × 5 mm) at 5 µL/min for 5 min. Peptides were then eluted into Thermo Scientific Accalaim PepMap™ 100, 2 µm, 100 Å, 75 µm × 250 mm and chromatographically separated using a binary solvent system consisting of A: 0.1% formic acid and 2.5% acetonitrile and B: 0.1% formic acid and 75% acetonitrile at a flow rate of 300 nL/min. A gradient was run from 1% B to 50%B over 40 minutes, followed by a 5-minute wash step with 99% B and 10-minute equilibration at 1% B before the next sample was injected. Precursor masses were detected in the Orbitrap at R=120,000 (m/z 200). Fragment masses were detected in linear ion trap at unit mass resolution. Data dependent MSMS was carried with top of speed setting, cycle time was 3 sec with dynamic exclusion of 30 sec.

Protein identification and relative quantification were carried out using Proteome Discoverer software package (Thermo Scientific). Raw data was searched against an E. coli protein database from Uniprot (2016-07-14) along with a contaminant protein database with the Sequest HT search engine. Cysteine carbomidomethylation was set as fixed modification. Methionine oxidation and Glutamine deamidation were

set as variable modifications. Trypsin was set as the digestion enzyme and allowed for 2 missed cleavages. Peptide mass tolerance was ±10 ppm, fragment mass tolerance was ±0.8 Da. Target peptide FDR was set to 0.01 (strict) and 0.05 (relaxed). Protein identifications required a minimum of 2 unique peptides. For relative quantification, label free quantification (LFQ) was carried out using MINORA feature detection followed by quantification with precursor intensity of unique and razor peptides. Peptides with variable modifications were excluded from quantification. A protein is not quantified if it is only detected in one replicate. Group abundance ratios were calculated using the pairwise approach. Proteins were considered to be significantly differential if the log2 of the group abundance ratio was greater than 2 or less than -2.

Gene ontology enrichment analysis was performed on proteins with a significant abundance ratio of SHX-challenged over unchallenged in either wildtype or *ΔrelE* cells using PANTHER. GO term consolidation was performed using REVIGO.

Western Blotting

2 µg of protein was separated on a 4-12% Bis-tris gel. Gel was incubated in 20% ethanol for 10 min and then transferred to nitrocellulose (IB23001) using the Invitrogen iBlot2 system. Blots were stained for total protein using the MemCode Erasable Stain (Thermo 24580). Blots were incubated for 4 hours at 4°C in blocking buffer (4% non-fat milk in TBST). α-6XHIS antibody was diluted 1:10,000 in blocking buffer and incubated for 20 hours at 4°C. Blots were washed with six times with TBST then developed using the Pierce ECL Western Blot kit.

CHAPTER 5: SUMMARY AND FUTURE DIRECTIONS

Antimicrobial resistance has become a global threat to human health through increasing prevalence and diversity of resistant organisms and stagnating development of new therapeutic compounds. There is a need to develop alternative approaches to address the rising crisis. While primary compound-target interactions are well characterized, the downstream gene expression and metabolic changes they induce in bacteria are not well understood. A deeper understanding of the bacterial stress response mechanisms could provide novel targets against bacterial pathogens.

In bacteria, transcription and translation two key regulation points of gene expression are coordinated to occur simultaneously. This coordination allows for rapid changes in gene expression but does not allow for quality control checks, exposing both systems to perturbations. This is particularly prevalent under stress conditions where changes in transcription-translational kinetics, nutrient availability, and degradation enzymes can result in catastrophically stalled translational complexes. Resolving stalled translational complexes is critical for bacterial survival. Bacteria have evolved a specialized RNA system, transfer messenger RNA (tmRNA), that resolves stalled complexes and targets the aberrant peptides for degradation. Studying proteins that tmRNA tags, the tmRNA degradome, could provide new insight in bacterial stress mechanisms.

In this work, we set out to develop a synthetic *E. coli* tmRNA construct that would allow for the stabilization and isolation of tagged proteins under stress conditions. We successfully engineered a tmRNA variant that introduces a 6x-Histidine epitope to the C-terminus of tagged proteins (tmRNA-6xHIS). We demonstrated that expression of our construct is tolerated in wildtype and tmRNA knockout (*ΔssrA*) cells. We have successfully isolated 6xHIS-tagged proteins through affinity purification and immunoprecipitation. We showed that tagged proteins represent a broad molecular weight range, implying a diverse population of identity and completeness of tagged proteins. We successfully connected our construct to an inducible expression promoter that would allow for temporal resolution of tagged proteins. We showed that 6x-HIS tagging could be detected in as little as 20 minutes after expression induction, with maximum tagging occurring after 1 hour.

Using mass spectrometry under steady-state conditions, we identified over 1100 proteins in the tmRNA degradome, confirming the diversity of tagged proteins. As a proof of concept, ClpP is one of the proteases known for degrading tmRNA-tagged proteins. In our degradome, we identified multiple known ClpP substrates, demonstrating that our synthetic construct is tagging similar proteins to the native construct. We then compared the similarities between composition of the degradome versus that of the total proteome. Of the 1164 proteins identified, only 23 were unique to the degradome. This demonstrated that analysis of the degradome is not only reflective of the composition of the total proteome but also can increase the coverage of the proteome. When abundances of proteins in the degradome were compared to the total cell lysate, we observed unique, protein-specific abundance relationship. This implies that tmRNA does not act equally on every transcript and therefore could provide insight into translational dynamics and translational regulation of gene expression.

Under oxidative stress, we saw a similar diverse composition of degradome proteins with over 1000 proteins identified. However, tagged protein profiles were markedly different under stress conditions compared to steady state. We identified an increased diversity of both unique and overrepresented peptides in our tagged degradome, indicating wide-spread mRNA damage. We continued to identify ClpP substrates in the degradome. Excitingly, we observed that the degradome to total proteome abundance ratio of several ClpP substrates shifted drastically under oxidative stress. This implies that under stress conditions the gene expression may be regulated by non-stop decay.

Activation of RNases is a critical aspect of the stress response, particularly in response to nutrient starvation. While a host of RNases are activated during the stringent response, RelE plays a key role in shutting down translation through cleavage within the A-site of the ribosome and generation of nonstop translational complexes. This also closely ties to tmRNA-mediated rescue, as it requires and empty A-site before accommodation into the ribosome. We studied the relationship between RelE and the tagged degradome under conditions of nutrient starvation through treatment with serine hydroxamate. In response to SHX, we observed significant changes in protein abundances in the tagged degradome in wildtype and *ΔrelE* cells. In western blotting, we also noted that there was a shift in the molecular weight range of tagged proteins biasing toward smaller molecular weights. Together this indicated that we were capturing changes

to gene expression through RNase cleavage and non-stop decay. Most excitingly, we observed massive abundance shifts of ribosomal proteins in the degradome of *ΔrelE* cells. These same changes were not observed in either the wildtype degradome or the total proteome of either genetic background. This indicates that RelE may play a critical role in regulating the translation and expression of ribosomal proteins under nutrient stress.

Our work provides insight into hidden aspects of the bacterial stress response. However, further investigation is needed to draw more definitive biological conclusions. One promising lead from our data is the potential regulation of the pentose phosphate pathway (PPP). Our data showed that many of the PPP proteins, including *zwf* the first committed enzymatic step, became significantly less abundant in the degradome under oxidative stress. This was accompanied by a modest increase of the protein in the total proteome. It has been shown that cells increase metabolic flux through the PPP to increase the cellular pool of NADPH in response to oxidative stress. Our data implies that this flux may be linked to non-stop decay of PPP proteins under steady state conditions that rapidly decreases in response to oxidative stress. It is unclear whether the metabolic flux through the pathway or the level of anti-oxidative NADPH levels are the critical response. To further investigate this, an integrative multi-omics study could be performed to assess the level of PPP transcripts, total protein, degradome, and NADPH. Additionally, further metabolomic study could reveal whether NADPH is particularly important to oxidative stress response or if there is just a widespread increase of cellular antioxidants.

Our data also indicated a link between RelE and regulation of ribosomal protein translation under amino acid stress. In *ΔrelE E. coli* cells, we observed drastic changes to ribosomal protein abundance in the degradome that were not seen in wildtype cells or the total proteome. This suggests that RelE may play a role in regulating the amount of non-stop decay on ribosomal proteins and general shut down of translation. RNase toxins have been implicated in post-transcriptional regulation of gene expression under stress conditions. Under amino acid stress, a host of RNases, including RelE and MazF, are activated, but it is unclear what role each contributes to degradation and gene expression regulation. To further investigate this, deletion mutants of individual or multiple RNases could be used to monitor changes to the degradome with a particular focus in ribosomal proteins. This could be coupled with ribosomal profiling and

quantification of rRNA to gain a better understanding of the of the impact on the abundance of functional ribosomes. Some RNases, like RelE, exhibit sequence specificity for cleavage. A synthetic tmRNA-6xHIS platform could provide the opportunity to map the location of RNase cleavage. This could be examined in RNase deletion mutants to investigate the possibility and extent of post-transcriptional control of gene expression.

One limitation of our work is that we were not able to confirm 6xHIS tagging with our mass spectrometry work. This stems from the approach we took to our proteomics work. We used a bottom-up approach where proteins are digested into peptides prior to tandem mass spectrometry analysis. Within the mass spectrometer, peptides are fragmented, and their mass-to-charge ratio (m/z) is measured to generate a MS2 spectra. Fragmentation patterns are dictated from by the composition peptide, and thus the sequence can be derived from the characteristic m/z peaks produced. It is possible to interpret MS2 spectra manually, but even a single mass spectrometry experiment can generate tens of thousands of MS2 spectra. To interpret these in an efficient, high throughput manner, search algorithms are used in conjunction with a reference proteome. In our work, we used the Swiss-Prot reference proteome from *E. coli* K12 along with a contaminant reference proteome. The contaminant reference proteome contained protein sequences of exogenous proteins that commonly contaminate samples such as bovine serum alubumin, Sepharose A, and human keratin proteins. The search algorithm performs a theoretical protein digest on the provided reference proteome and generates MS2 spectra with fragmentation patterns matching the resulting peptides. The experimental MS2 spectra are then compared with the theoretical MS2 to identify most likely peptide sequences. Any peptide sequence that does not match a sequence from the reference proteome is not returned in the final identification.

This is a particular problem for our platform as any tagged protein would have a modified C-terminal sequence compared to the reference proteome. This means any tag sequence will not be identified through the standard search method. To combat this, we tried an alternative search method that allowed for a variable C-terminal modification of 1340 Da (the molecular weight of AANDEHHHHHH). This method does not identify this peptide sequence, only the mass. Even so, we were not able to identify any tagged peptides.

There are several chemical reasons that could account for the lack of detection. The size of tagged peptides could be too large. In bottom-up experiments, proteins are commonly digested with trypsin which cleaves at arginine (R) and lysine (K). In many species, the distribution of R and K in the proteome create an average protein length of 10-14 amino acids.[157,158] This is the ideal length for efficient ionization and resolvable MS2 fragmentation patterns. Peptides tagged by tmRNA-6xHIS would be nearly double that length, which could interfere ionization and prevent entry into the mass spectrometer. Additionally, the charge 6xHIS epitope may interfere with liquid chromatography (LC) separation. LC-MS/MS methods generally use a gradient of acetonitrile along with a C18 column to separate peptides by hydrophobicity. Composition of the gradient and flow rate can be altered to change peptide separation. The concentration of charge at the C-terminal tail of tagged peptides likely affected when the peptide eluted from the column. This charge concentration may have also affected ionization, though this is unlikely.

To address these issues, I engineered two trypsin-cleavable 6xHIS tag variants. Previous studies have shown that the early codons, particularly the resume codon, are critical for tagging efficiency, and the C-terminal codons are critical for recognition by proteases.[53,62,73,159] To allow for maintenance of the early codons, I recoded the TRF to ANDKHHHHHH. There is concern that the proximity of the highly charged 6xHIS epitope will interfere with tryspin cleavage, so an additional alternative construct was made with ARDEHHHHHH. Constructs utilized the ssrAp promoter and 3' terminator region used in ssrAp-tmRNA-6xHIS construct. Constructs were synthesized as a gene block by IDT, placed into the PZA31-MCS plasmid backbone, and transformed into wildtype MG1655 *E. coli* cells. We confirmed that expression of both constructs was well tolerated (Figure 24A).

We compared tagging profiles of our protease cleavable variants to our original construct. Cells containing our constructs were grown for 4.5 hours before being pelleted and lysed. 3 mg of lysates were then affinity purified using HisPur Cobalt columns. 2 µg of protein from the total lysate and purified first elution were analyzed by α6xHIS western blot and total protein gel staining (Figure 24B). Tagging levels and profiles of the protease cleaveable variants were very similar to our original construct. Interestingly, the ARDE variant showed slightly higher tagging levels compared to ANDK. This is surprising since previous data indicated that the second codon affected tagging efficiency.

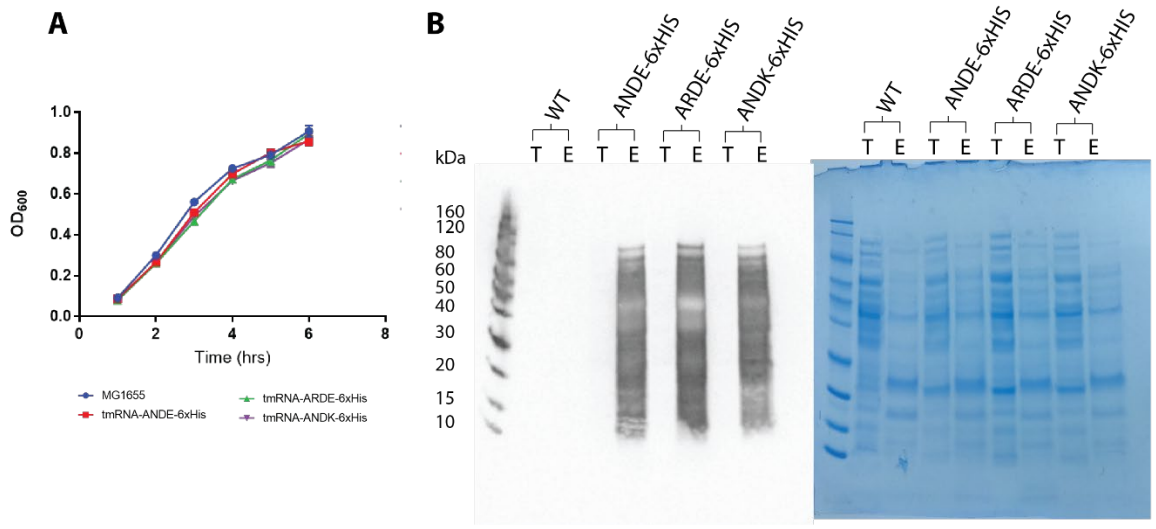

Figure 24. Protease cleavable tmRNA-6xHIS variants. (A) Growth curve of strains. (B) α-6xHIS western blot and comassie stain of whole cell lysate (T) and purified elution fraction (E). Total protein stain performed using SimplyBlue SafeStain.

We then prepared lysates from our protease cleavable constructs for LC-MS/MS analysis. Affinity purified elutions were pooled and immunoprecitated with 12 µg of α6xHIS antibody (Thermo PA1-983B) as previously described. 110 µL of the first IP elution and 2 µg of total protein were then reduced, alkylated, and digested with tryspin/LysC as previously described before LC-MS/MS analysis. To identify peptides from our raw mass spectrometry data, we allowed for variable C-terminal modifications of 244.28 Da (-AR) and 445.49 Da (-ANDK). Since the search algorithm only identifies modification by weight, verifying presence of representative peptide fragments is critical. Unfortunately, this approach was not successful. The algorithm identified many proteins with an -AR modification. However, these already had a canonical -AR sequence and were not the result of tagging. There were a few proteins identified as having the -ANDK modification, but from the state of the MS2 spectra, I could not verify that these contained fragments that matched an ANDK tag.

For our proteomics work, we used data-dependent acquisition (DDA) for generation of MS2 spectra. Using this method, only a subset of the peptides is selected for fragmentation based on abundance. This approach requires having multiple copies of the same peptide that elute from the chromatography column simultaneously. However, tmRNA can act anywhere along the length of protein, so tag insertion could have a very broad distribution. A shift of tagging position by one amino acid would produce a peptide of a different

mass, which would be measured separately by the mass spectrometer. Given this, we would expect to only detect tagged peptides that experience high levels of catastrophic stalling during translation. The lack of detection could imply that even on common catastrophic stall sites, the peptide abundance is too low to be selected for fragmentation.

While identifying a tagged peptide was interesting for characterization of our system, identifying tagging locations could provide key insights to cellular function. Evidence suggests that activation RNases is used as a way for post-transcriptionally modifying gene expression.[91,141] Understanding where cleavage occurs could provide novel insight into gene expression regulation, the role of RNase in stress response, and post-transcriptional gene regulation through non-stop decay.

One option for identifying tagging location would be to generate a theoretical tagged reference proteome where the reference proteome includes the tagged sequence. The most extensive option would be to simulate tag insertion at every single amino acid position within the proteome. Given that the *E. coli* Uniprot reference proteome contains more than 5000 proteins, it is not the most efficient option. A smaller subset of tagging locations based on the literature and previous mass spectrometry experiments could be a more viable option. These could include tagging at termination codons, known stall sequences like SecM, or locations with rare codons.

An alternative approach to using DDA is to use data-independent acquisition (DIA). In DIA, every precursor peptide ion is selected for fragmentation. This produces a highly multiplexed MS2 spectra that can be difficult to interpret. Previously, interpretation of DIA spectra required a library of DDA spectra that were processed through conventional search algorithms. Recent advancements have allowed for the generation of theoretical DDA spectra that can be used to resolve the DIA spectra and searched through conventional search algorithms. This would still require additional research into fragmentation patterns of tagged peptide to identify tagging locations. A synthetic non-stop or heavy stall-inducing construct could be developed to characterize tmRNA-tagged peptide fragmentation patterns. From these characteristic fragmentation patterns, combination DIA-targeted acquisition approach could be developed that would allow for the identification and possibly even quantification of tagging.

Our work developing a synthetic tmRNA platform has opened the door to new insights into the bacterial stress response. These insights could be used to inform and develop novel strategies for addressing the antibiotic crisis. For example, bacteria experience oxidative stress following exposure antimicrobial compounds. Our data indicates that the pentose phosphate pathway may play a key role in that response through increased production of NADPH or increased expression of PPP proteins. One potential path to a novel antimicrobial could be through investigating the impact of PPP inhibition or sequestration of NADPH or other cellular antioxidants. This would require extensive additional research, but broad degradome surveys could provide starting points.

One of the most exciting aspects of this platform is its versatility. Nearly every sequenced bacterium contains tmRNA with each being unique to its species. This allows for investigation into a broad range of bacterial species, including resistant pathogens. Additionally, it could be possible to use this method to study a complex culture of multiple species in an *in vivo* environment through modification of each species tmRNA. This platform can be used to investigate a near limitless number of conditions and settings to provide information that cannot be captured using any other methods.

APPENDIX A: LIST OF TMRNA CONSTRUCT SEQUENCES

Construct	Tag Peptide Sequence	Promoter	Sequence
ssrAp-tmRNA-6xHIS (Turner)	ANDEHHHHHH	ssrAp	ATTCACTCGAGCGAATAAAAATCAGGCTACATGGGTGCTAAATCTTTAACGATAA CGCCATTGAGGCTGGTCATGGCGCTCATAAATCTGGTATACTTACCTTTACACAT TGGGGCTGATTCTGGATTCGACGGGATTTGCGAAACCCAAGGTGCATGCCGAG GGGCGGTTGGCCTCGTAAAAAGCCGCAAAAAATAGTCGCAAACGACGAACATC ACCATCACCACCATTAATAACGGTGTGTGGTGCCTCTCTCCCTAGCCTCCGCTC TTAGGACGGGGATCAAGAGAGGTCAAACCCAAAAGAGATCGCGTGGAAGCCCT GCCTGGGGTTGAAGCGTTAAAACTTAATCAGGCTAGTTTGTTAGTGGCGTGTCC GTCCGCAGCTGGCAAGCGAATGTAAAGACTGACTAAGCATGTAGTACCGAGGA TGTAGGAATTTCGGACGCGGGTTCAACTCCCGCCAGCTCCACCAAAATTCTCCA TCGGTGATTACCAGAGTCATCCGATGAAGTCCTAAGAGCCCGCACGGCGCAAG CCCTGCGGGCTTTTTTGTGCCCTCAAGCTTACGCGTCCTAGGCTTAT
ssrAp-tmRNA-6xHIS (Sauer)	ANDEHHHHHH	ssrAp	ATTCACTCGAGCGAATAAAAATCAGGCTACATGGGTGCTAAATCTTTAACGATAA CGCCATTGAGGCTGGTCATGGCGCTCATAAATCTGGTATACTTACCTTTACACAT TGGGGCTGATTCTGGATTCGACGGGATTTGCGAAACCCAAGGTGCATGCCGAG GGGCGGTTGGCCTCGTAAAAAGCCGCAAAAAATAGTCGCAAACGACGAACACC ACCATCATCACCATTAATAACGGTGATTGATGCCTCTCTCCCTAGCCTCCGCTCT TAGGACGGGGATCAAGAGAGGTCAAACCCAAAAGAGATCGCGTGGAAGCCCTG CCTGGGGTTGAAGCGTTAAAACTTAATCAGGCTAGTTTGTTAGTGGCGTGTCCG TCCGCAGCTGGCAAGCGAATGTAAAGACTGACTAAGCATGTAGTACCGAGGAT GTAGGAATTTCGGACGCGGGTTCAACTCCCGCCAGCTCCACCAAAATTCTCCAT CGGTGATTACCAGAGTCATCCGATGAAGTCCTAAGAGCCCGCACGGCGCAAGC CCTGCGGGCTTTTTTGTGCCCTCAAGCTTACGCGTCCTAGGCTTAT
ssrAp-tmRNA-6xHIS (Turner-RNase E mod)	ANDEHHHHHH	ssrAp	ATTCACTCGAGCGAATAAAAATCAGGCTACATGGGTGCTAAATCTTTAACGATAA CGCCATTGAGGCTGGTCATGGCGCTCATAAATCTGGTATACTTACCTTTACACAT TGGGGCTGATTCTGGATTCGACGGGATTTGCGAAACCCAAGGTGCATGCCGAG GGGCGGTTGGCCTCGTAAAAAGCCGCAAAAAATAGTCGCAAACGACGAACATC ACCATCACCACCATTAATAACGGTGTGTGGTGCCTCTCTCCCTAGCCTCCGCTC TTAGGACGGGGATCAAGAGAGGTCAAACCCAAAAGAGATCGCGTGGAAGCCCT GCCTGGGGTTGAAGCGTTAAAACTTAATCAGGCTAGTTTGTTAGTGGCGTGTCC GTCCGCAGCTGGCAAGCGAATGTAAAGACTGACTAAGCATGTAGTACCGAGGA TGTAGGAATTTCGGACGCGGGTTCAACTCCCGCCAGCTCCACGAATACCCTCCA TCGGTGATTACCAGAGTCATCCGATGAAGTCCTAAGAGCCCGCACGGCGCAAG CCCTGCGGGCTTTTTTGTGCCCTCAAGCTTACGCGTCCTAGGCTTAT
pL(tetO)-tmRNA-6xHIS	ANDEHHHHHH	pL(tetO)	attcaCTCGAGTCCCTATCAGTGATAGAGATTGACATCCCTATCAGTGATAGAGAT ACTGAGCACAcacattGGGGCTGATTCTGGATTCGACGGGATTTGCGAAACCCAA GGTGCATGCCGAGGGGCGGTTGGCCTCGTAAAAAGCCGCAAAAAATAGTCGCA AACGACGAACATCACCATCACCACCATTAATAACGGTGTGTGGTGCCTCTCTCC CTAGCCTCCGCTCTTAGGACGGGGATCAAGAGAGGTCAAACCCAAAAGAGATC GCGTGGAAGCCCTGCCTGGGGTTGAAGCGTTAAAACTTAATCAGGCTAGTTTGT TAGTGGCGTGTCCGTCCGCAGCTGGCAAGCGAATGTAAAGACTGACTAAGCAT GTAGTACCGAGGATGTAGGAATTTCGGACGCGGGTTCAACTCCCGCCAGCTCC ACCAAAATTCTCCATCGGTGATTACCAGAGTCATCCGATGAAGTCCTAAGAGCC CGCACGGCGCAAGCCCTGCGGGCTTTTTTGTGCCCTCAATTTGTCCCGCGAAG TCCGACGCGTcttat
ssrAp-tmRNA-AR-6xHIS	ARDEHHHHHH	ssrAp	attcactcgagCGAATAAAAATCAGGCTACATGGGTGCTAAATCTTTAACGATAACGC CATTGAGGCTGGTCATGGCGCTCATAAATCTGGTATACTTACCTTTACACATTGG GGCTGATTCTGGATTCGACGGGATTTGCGAAACCCAAGGTGCATGCCGAGGGG CGGTTGGCCTCGTAAAAAGCCGCAAAAAATAGTCGCACGCGACGAACATCACC ATCACCACCATTAATAACGGTGTGTGGTGCCTCTCTCCCTAGCCTCCGCTCTTA GGACGGGGATCAAGAGAGGTCAAACCCAAAAGAGATCGCGTGGAAGCCCTGCC TGGGGTTGAAGCGTTAAAACTTAATCAGGCTAGTTTGTTAGTGGCGTGTCCGTC CGCAGCTGGCAAGCGAATGTAAAGACTGACTAAGCATGTAGTACCGAGGATGTA GGAATTTCGGACGCGGGTTCAACTCCCGCCAGCTCCACCAAAATTCTCCATCGG TGATTACCAGAGTCATCCGATGAAGTCCTAAGAGCCCGCACGGCGCAAGCCCT GCGGGCTTTTTTGTGCCCTCaagcttACGCGTCCTAGGcttat
ssrAp-tmRNA-DK-6xHIS	ANDKHHHHHH	ssrAp	attcactcgagCGAATAAAAATCAGGCTACATGGGTGCTAAATCTTTAACGATAACGC CATTGAGGCTGGTCATGGCGCTCATAAATCTGGTATACTTACCTTTACACATTGG GGCTGATTCTGGATTCGACGGGATTTGCGAAACCCAAGGTGCATGCCGAGGGG CGGTTGGCCTCGTAAAAAGCCGCAAAAAATAGTCGCAAACGACAAACATCACCA TCACCACCATTAATAACGGTGTGTGGTGCCTCTCTCCCTAGCCTCCGCTCTTAG GACGGGGATCAAGAGAGGTCAAACCCAAAAGAGATCGCGTGGAAGCCCTGCCT GGGGTTGAAGCGTTAAAACTTAATCAGGCTAGTTTGTTAGTGGCGTGTCCGTCC GCAGCTGGCAAGCGAATGTAAAGACTGACTAAGCATGTAGTACCGAGGATGTA GGAATTTCGGACGCGGGTTCAACTCCCGCCAGCTCCACCAAAATTCTCCATCGG TGATTACCAGAGTCATCCGATGAAGTCCTAAGAGCCCGCACGGCGCAAGCCCT GCGGGCTTTTTTGTGCCCTCaagcttACGCGTCCTAGGcttat

BIBLIOGRAPHY

1. Staphylococcus aureus in Healthcare Settings | HAI | CDC. https://www.cdc.gov/hai/organisms/staph.html (2020).
2. Gourkhede, D. *et al.* Antimicrobial resistance in bacteria- its origin and evolution: A review. *International Journal of Livestock Research* **11**, (2021).
3. Hutchings, M. I., Truman, A. W. & Wilkinson, B. Antibiotics: past, present and future. *Current Opinion in Microbiology* **51**, 72–80 (2019).
4. Monserrat-Martinez, A., Gambin, Y. & Sierecki, E. Thinking Outside the Bug: Molecular Targets and Strategies to Overcome Antibiotic Resistance. *International Journal of Molecular Sciences* **20**, 1255 (2019).
5. Wong, J. Dr. Alexander Fleming and the discovery of penicillin. *Primary Care Update for OB/GYNS* **10**, 124–126 (2003).
6. Bennett, J. W. & Chung, K.-T. Alexander Fleming and the discovery of penicillin. in *Advances in Applied Microbiology* vol. 49 163–184 (Academic Press, 2001).
7. Geddes, A. 80th Anniversary of the discovery of penicillin: An appreciation of Sir Alexander Fleming. *International Journal of Antimicrobial Agents* **32**, 373 (2008).
8. Cirillo, V. J. Two faces of death: fatalities from disease and combat in America's principal wars, 1775 to present. *Perspect Biol Med* **51**, 121–133 (2008).
9. Centers for Disease Control and Prevention (U.S.). *Antibiotic resistance threats in the United States, 2019*. https://stacks.cdc.gov/view/cdc/82532 (2019) doi:10.15620/cdc:82532.
10. Counsell, D. J. Intoxicants in Ancient Egypt: The Application of Modern Forensic Analytical Techniques to Ancient Artefacts and Mummified Remains in the Evaluation of Drug Use by an Ancient Society: A Historical and Scientific Investigation. (The University of Manchester (United Kingdom)).

11. Nelson, M. L., Dinardo, A., Hochberg, J. & Armelagos, G. J. Brief communication: Mass spectroscopic characterization of tetracycline in the skeletal remains of an ancient population from Sudanese Nubia 350–550 CE. *American Journal of Physical Anthropology* **143**, 151–154 (2010).
12. Tetracycline-Labeled Human Bone from Ancient Sudanese Nubia (A.D. 350). https://www.science.org/doi/abs/10.1126/science.7001623.
13. Haas, L. F. Papyrus of Ebers and Smith. *Journal of Neurology, Neurosurgery & Psychiatry* **67**, 578–578 (1999).
14. Wainwright, M. Moulds in Folk Medicine. *Folklore* **100**, 162–166 (1989).
15. Horcajada, J. P. *et al.* Epidemiology and Treatment of Multidrug-Resistant and Extensively Drug-Resistant Pseudomonas aeruginosa Infections. *Clinical Microbiology Reviews* **32**, e00031-19 (2019).
16. Gullberg, E., Albrecht, L. M., Karlsson, C., Sandegren, L. & Andersson, D. I. Selection of a Multidrug Resistance Plasmid by Sublethal Levels of Antibiotics and Heavy Metals. *mBio* **5**, e01918-14 (2014).
17. McCarthy, A. J. & Lindsay, J. A. The distribution of plasmids that carry virulence and resistance genes in Staphylococcus aureus is lineage associated. *BMC Microbiology* **12**, 104 (2012).
18. Haaber, J., Penadés, J. R. & Ingmer, H. Transfer of Antibiotic Resistance in Staphylococcus aureus. *Trends in Microbiology* **25**, 893–905 (2017).
19. Antimicrobial resistance a 'global health emergency,' UN, ahead of awareness week. *UN News* https://news.un.org/en/node/1025511/antimicrobial-resistance-a-global-health-emergency-un-ahead-of-awareness-week-2.
20. BBC One - Planet Earth, Caves. *BBC* https://www.bbc.co.uk/programmes/b0074sh2.
21. Carlsbad, M. A. 3225 N. P. H. & Us, N. 88220 P. 575 785-2232 C. Lechuguilla Cave - Carlsbad Caverns National Park (U.S. National Park Service). https://www.nps.gov/cave/learn/nature/lechuguilla_cave.htm.

22. Bhullar, K. *et al.* Antibiotic Resistance Is Prevalent in an Isolated Cave Microbiome. *PLOS ONE* **7**, e34953 (2012).

23. Embley, T. M. & Stackebrandt, E. The molecular phylogeny and systematics of the actinomycetes. *Annual Review of Microbiology* **48**, 257–290 (1994).

24. Streptomyces as symbionts: an emerging and widespread theme? | FEMS Microbiology Reviews | Oxford Academic. https://academic.oup.com/femsre/article/36/4/862/521102.

25. Natural products in soil microbe interactions and evolution. *Natural Product Reports* **32**, 956–970 (2015).

26. Peterson, E. & Kaur, P. Antibiotic Resistance Mechanisms in Bacteria: Relationships Between Resistance Determinants of Antibiotic Producers, Environmental Bacteria, and Clinical Pathogens. *Frontiers in Microbiology* **9**, (2018).

27. Walker, M. S. & Walker, J. B. Streptomycin Biosynthesis and Metabolism: ENZYMATIC PHOSPHORYLATION OF DIHYDROSTREPTOBIOSAMINE MOIETIES OF DIHYDROSTREPTOMYCIN-(STREPTIDINO)PHOSPHATE AND DIHYDROSTREPTOMYCIN BY STREPTOMYCES EXTRACTS. *Journal of Biological Chemistry* **245**, 6683–6689 (1970).

28. Cox, G. & Wright, G. D. Intrinsic antibiotic resistance: Mechanisms, origins, challenges and solutions. *International Journal of Medical Microbiology* **303**, 287–292 (2013).

29. Sattler, S. A. *et al.* Characterizations of Two Bacterial Persulfide Dioxygenases of the Metallo-β-lactamase Superfamily *. *Journal of Biological Chemistry* **290**, 18914–18923 (2015).

30. Schindler, B. D. & Kaatz, G. W. Multidrug efflux pumps of Gram-positive bacteria. *Drug Resistance Updates* **27**, 1–13 (2016).

31. Yu, L. *et al.* Molecular cloning and functional characterization of an ATP-binding cassette transporter OtrC from Streptomyces rimosus. *BMC Biotechnology* **12**, 52 (2012).

32. Nikaido, H. Multidrug Resistance in Bacteria. *Annu Rev Biochem* **78**, 119–146 (2009).

33. Liu, B. & Pop, M. ARDB—Antibiotic Resistance Genes Database. *Nucleic Acids Research* **37**, D443–D447 (2009).

34. Burmeister, A. R. Horizontal Gene Transfer. *Evol Med Public Health* **2015**, 193–194 (2015).

35. Arnold, B. J., Huang, I.-T. & Hanage, W. P. Horizontal gene transfer and adaptive evolution in bacteria. *Nat Rev Microbiol* **20**, 206–218 (2022).

36. Walsh, C. & Wencewicz, T. *Antibiotics: Challenges, Mechanisms, Opportunities*. (John Wiley & Sons, 2020).

37. Loman, N. J. & Pallen, M. J. Twenty years of bacterial genome sequencing. *Nat Rev Microbiol* **13**, 787–794 (2015).

38. Payne, D. J., Gwynn, M. N., Holmes, D. J. & Pompliano, D. L. Drugs for bad bugs: confronting the challenges of antibacterial discovery. *Nat Rev Drug Discov* **6**, 29–40 (2007).

39. Wenzel, R. P. The Antibiotic Pipeline - Challenges, Costs, and Values. *The New England Journal of Medicine* **351**, 523–6 (2004).

40. Ling, L. L. *et al.* A new antibiotic kills pathogens without detectable resistance. *Nature* **517**, 455–459 (2015).

41. Vishwakarma, R. K. & Brodolin, K. The σ Subunit-Remodeling Factors: An Emerging Paradigms of Transcription Regulation. *Frontiers in Microbiology* **11**, (2020).

42. Österberg, S., Peso-Santos, T. del & Shingler, V. Regulation of Alternative Sigma Factor Use. *Annual Review of Microbiology* **65**, 37–55 (2011).

43. Roberts, J. W. Mechanisms of Bacterial Transcription Termination. *Journal of Molecular Biology* **431**, 4030–4039 (2019).

44. McGary, K. & Nudler, E. RNA polymerase and the ribosome: the close relationship. *Current Opinion in Microbiology* **16**, 112–117 (2013).

45. Martinez-Rucobo, F. W. & Cramer, P. Structural basis of transcription elongation. *Biochimica et Biophysica Acta (BBA) - Gene Regulatory Mechanisms* **1829**, 9–19 (2013).

46. Kohler, R., Mooney, R. A., Mills, D. J., Landick, R. & Cramer, P. Architecture of a transcribing-translating expressome. *Science* **356**, 194–197 (2017).

47. Feaga HA, Viollier PH, Keiler KC. Release of Nonstop Ribosomes Is Essential. *mBio* **5**, e01916-14 (2014).

48. Buskirk, A. R. & Green, R. Ribosome pausing, arrest and rescue in bacteria and eukaryotes. *Phil. Trans. R. Soc. B* **372**, 20160183 (2017).

49. Shimizu, Y. ArfA Recruits RF2 into Stalled Ribosomes. *Journal of Molecular Biology* **423**, 624–631 (2012).

50. Muto, A. *et al.* Requirement of transfer-messenger RNA for the growth of Bacillus subtilis under stresses. *Genes to Cells* **5**, 627–635 (2000).

51. Keiler, K. C. & Shapiro, L. tmRNA Is Required for Correct Timing of DNA Replication in Caulobacter crescentus. *J. Bacteriol.* **185**, 573–580 (2003).

52. Shin, J.-H. & Price, C. W. The SsrA-SmpB Ribosome Rescue System Is Important for Growth of Bacillus subtilis at Low and High Temperatures. *J. Bacteriol.* **189**, 3729–3737 (2007).

53. Keiler, K. C., Shapiro, L. & Williams, K. P. tmRNAs that encode proteolysis-inducing tags are found in all known bacterial genomes: A two-piece tmRNA functions in Caulobacter. *PNAS* **97**, 7778–7783 (2000).

54. Lee, S., Ishii, M., Tadaki, T., Muto, A. & Himeno, H. Determinants on tmRNA for initiating efficient and precise trans-translation: Some mutations upstream of the tag-encoding sequence of Escherichia coli tmRNA shift the initiation point of trans-translation in vitro. *RNA* **7**, 999–1012 (2001).

55. KoMINE YU, Kitabatake M, Yokogawa T, Nishikawa K, Inokuchi H. A tRNA-like structure is present in 10Sa RNA, a small stable RNA from Escherichia coli. | PNAS. *PNAS* **91**, 9223–9227 (1994).

56. Gueneau de Novoa, P. & Williams, K. P. The tmRNA website: reductive evolution of tmRNA in plastids and other endosymbionts. *Nucleic Acids Res* **32**, D104–D108 (2004).

57. Hudson, C. M. & Williams, K. P. The tmRNA website. *Nucleic Acids Res* **43**, D138–D140 (2015).

58. Burks, J., Zwieb, C., Müller, F., Wower, I. & Wower, J. Comparative 3-D Modeling of tmRNA. *BMC Molecular Biology* **6**, 14 (2005).

59. Barends, S., Wower, J. & Kraal, B. Kinetic Parameters for tmRNA Binding to Alanyl-tRNA Synthetase and Elongation Factor Tu from Escherichia coli. *Biochemistry* **39**, 2652–2658 (2000).

60. Wower, I. K., Zwieb, C. & Wower, J. Contributions of Pseudoknots and Protein SmpB to the Structure and Function of tmRNA in trans-Translation. *J. Biol. Chem.* **279**, 54202–54209 (2004).

61. Wower, I. K., Zwieb, C. & Wower, J. Escherichia coli tmRNA lacking pseudoknot 1 tags truncated proteins in vivo and in vitro. *RNA* **15**, 128–137 (2009).

62. Cheng, K. *et al.* tmRNA·SmpB complex mimics native aminoacyl-tRNAs in the A site of stalled ribosomes. *Journal of Structural Biology* **169**, 342–348 (2010).

63. Gutmann, S. *et al.* Crystal structure of the transfer-RNA domain of transfer-messenger RNA in complex with SmpB. *Nature* **424**, 699–703 (2003).

64. Konno, T., Kurita, D., Takada, K., Muto, A. & Himeno, H. A functional interaction of SmpB with tmRNA for determination of the resuming point of trans-translation. *RNA* **13**, 1723–1731 (2007).

65. Kurita, D., Miller, M. R., Muto, A., Buskirk, A. R. & Himeno, H. Rejection of tmRNA·SmpB after GTP hydrolysis by EF-Tu on ribosomes stalled on intact mRNA. *RNA* **20**, 1706–1714 (2014).

66. Rae, C. D., Gordiyenko, Y. & Ramakrishnan, V. How a circularized tmRNA moves through the ribosome. *Science* **363**, 740–744 (2019).

67. Miller, M. R. *et al.* The role of SmpB and the ribosomal decoding center in licensing tmRNA entry into stalled ribosomes. *RNA* **17**, 1727–1736 (2011).

68. Miller, M. R. & Buskirk, A. R. An unusual mechanism for EF-Tu activation during tmRNA-mediated ribosome rescue. *RNA* **20**, 228–235 (2014).

69. Richards J, Mehta P, Karzai AW. RNase R degrades non-stop mRNAs selectively in an SmpB-tmRNA-dependent manner. *Molecular Microbiology* **62**, 1700–1712 (2006).

70. Venkataraman, K., Zafar, H. & Karzai, A. W. Distinct tmRNA sequence elements facilitate RNase R engagement on rescued ribosomes for selective nonstop mRNA decay. *Nucleic Acids Res* **42**, 11192–11202 (2014).

71. Keiler, K. C., Waller, P. R. H. & Sauer, R. T. Role of a Peptide Tagging System in Degradation of Proteins Synthesized from Damaged Messenger RNA. *Science* **271**, 990–993 (1996).

72. Parsell, D. A., Silber, K. R. & Sauer, R. T. Carboxy-terminal determinants of intracellular protein degradation. *Genes Dev.* **4**, 277–286 (1990).

73. Gottesman, S., Roche, E., Zhou, Y. & Sauer, R. T. The ClpXP and ClpAP proteases degrade proteins with carboxy-terminal peptide tails added by the SsrA-tagging system. *Genes Dev.* **12**, 1338–1347 (1998).

74. Flynn JM, Levchenko I, Seidel M, Wickner SH, Sauer RT, Baker TA. Overlapping recognition determinants within the ssrA degradation tag allow modulation of proteolysis. *PNAS* **98**, 10584–10589 (2001).

75. Choy, J. S., Aung, L. L. & Karzai, A. W. Lon Protease Degrades Transfer-Messenger RNA-Tagged Proteins. *J. Bacteriol.* **189**, 6564–6571 (2007).

76. Roche, E. D. & Sauer, R. T. Identification of Endogenous SsrA-tagged Proteins Reveals Tagging at Positions Corresponding to Stop Codons. *J. Biol. Chem.* **276**, 28509–28515 (2001).

77. Hong, S.-J., Lessner, F. H., Mahen, E. M. & Keiler, K. C. Proteomic identification of tmRNA substrates. *PNAS* **104**, 17128–17133 (2007).

78. MuZhi, P., YanQiong, T., HongQian, T., Xiang, M. & Zhu, L. Construction of tmRNA mutant applied for the identification of trans-translation substrates in Aeromonas veronii. *Genomics and Applied Biology* **38**, 1636–1642 (2019).

79. Fujihara, A. *et al.* Detection of tmRNA-mediated trans-translation products in Bacillus subtilis. *Genes to Cells* **7**, 343–350 (2002).

80. Li, X., Hirano, R., Tagami, H. & Aiba, H. Protein tagging at rare codons is caused by tmRNA action at the 3' end of nonstop mRNA generated in response to ribosome stalling. *RNA* **12**, 248–255 (2006).

81. Li, X., Yokota, T., Ito, K., Nakamura, Y. & Aiba, H. Reduced action of polypeptide release factors induces mRNA cleavage and tmRNA tagging at stop codons in Escherichia coli. *Molecular Microbiology* **63**, 116–126 (2007).

82. Moore, S. D. & Sauer, R. T. Ribosome rescue: tmRNA tagging activity and capacity in Escherichia coli. *Molecular Microbiology* **58**, 456–466 (2005).

83. Janssen, B. D., Garza-Sánchez, F. & Hayes, C. S. A-Site mRNA Cleavage Is Not Required for tmRNA-Mediated ssrA-Peptide Tagging. *PLOS ONE* **8**, e81319 (2013).

84. Keiler, K. C. & Feaga, H. A. Resolving Nonstop Translation Complexes Is a Matter of Life or Death. *Journal of Bacteriology* **196**, 2123–2130 (2014).

85. The N-Terminus of GalE Induces tmRNA Activity in Escherichia coli | PLOS ONE. https://journals.plos.org/plosone/article?id=10.1371/journal.pone.0015207.

86. Kramer, G., Boehringer, D., Ban, N. & Bukau, B. The ribosome as a platform for co-translational processing, folding and targeting of newly synthesized proteins. *Nat Struct Mol Biol* **16**, 589–597 (2009).

87. Ito, K. & Chiba, S. Arrest Peptides: Cis-Acting Modulators of Translation. *Annual Review of Biochemistry* **82**, 171–202 (2013).

88. Tian, C. *et al.* Rapid Curtailing of the Stringent Response by Toxin-Antitoxin Module-Encoded mRNases. *Journal of Bacteriology* **198**, 1918–1926 (2016).

89. Christensen, S. K., Pedersen, K., Hansen, F. G. & Gerdes, K. Toxin–antitoxin Loci as Stress-response-elements: ChpAK/MazF and ChpBK Cleave Translated RNAs and are Counteracted by tmRNA. *Journal of Molecular Biology* **332**, 809–819 (2003).

90. Christensen, S. K. & Gerdes, K. RelE toxins from Bacteria and Archaea cleave mRNAs on translating ribosomes, which are rescued by tmRNA. *Molecular Microbiology* **48**, 1389–1400 (2003).

91. Ehretsmann, C. P., Carpousis, A. J. & Krisch, H. M. Specificity of Escherichia coli endoribonuclease RNase E: in vivo and in vitro analysis of mutants in a bacteriophage T4 mRNA processing site. *Genes Dev.* **6**, 149–159 (1992).

92. Garza-Sánchez, F., Shoji, S., Fredrick, K. & Hayes, C. S. RNase II is important for A-site mRNA cleavage during ribosome pausing. *Molecular Microbiology* **73**, 882–897 (2009).

93. Bennison, D. J., Irving, S. E. & Corrigan, R. M. The Impact of the Stringent Response on TRAFAC GTPases and Prokaryotic Ribosome Assembly. *Cells* **8**, 1313 (2019).

94. Agirrezabala, X. *et al.* The ribosome triggers the stringent response by RelA via a highly distorted tRNA. *EMBO reports* **14**, 811–816 (2013).

95. Buskirk, A. R. & Green, R. Ribosome pausing, arrest and rescue in bacteria and eukaryotes. *Phil. Trans. R. Soc. B* **372**, 20160183 (2017).

96. Grabow, W. & Jaeger, L. RNA modularity for synthetic biology. *F1000Prime Rep* **5**, 46 (2013).

97. Pardee, K. *et al.* Paper-based synthetic gene networks. *Cell* **159**, 940–954 (2014).

98. Kim, J. & Franco, E. RNA nanotechnology in synthetic biology. *Current Opinion in Biotechnology* **63**, 135–141 (2020).

99. Schmidt, C. M. & Smolke, C. D. RNA Switches for Synthetic Biology. *Cold Spring Harb Perspect Biol* **11**, a032532 (2019).

100. Chappell, J., Watters, K. E., Takahashi, M. K. & Lucks, J. B. A renaissance in RNA synthetic biology: new mechanisms, applications and tools for the future. *Current Opinion in Chemical Biology* **28**, 47–56 (2015).

101. Hayes, C. S. & Keiler, K. C. Beyond ribosome rescue: tmRNA and co-translational processes. *FEBS Letters* **584**, 413–419 (2010).

102. Gottesman, S. Roles of mRNA stability, translational regulation, and small RNAs in stress response regulation. in *Bacterial Stress Responses* 506 (ASM Press, 2011).

103. Starosta, A. L., Lassak, J., Jung, K. & Wilson, D. N. The bacterial translation stress response. *FEMS Microbiol Rev* **38**, 1172–1201 (2014).

104. Christensen, S. K., Mikkelsen, M., Pedersen, K. & Gerdes, K. RelE, a global inhibitor of translation, is activated during nutritional stress. *PNAS* **98**, 14328–14333 (2001).

105. Cook, G. M. *et al.* Ribonucleases in bacterial toxin–antitoxin systems. *Biochimica et Biophysica Acta (BBA) - Gene Regulatory Mechanisms* **1829**, 523–531 (2013).

106. Ma, N. J., Hemez, C. F., Barber, K. W., Rinehart, J. & Isaacs, F. J. Organisms with alternative genetic codes resolve unassigned codons via mistranslation and ribosomal rescue. *Elife* **7**, (2018).

107. Huang, C., Wolfgang, M. C., Withey, J., Koomey, M. & Friedman, D. I. Charged tmRNA but not tmRNA-mediated proteolysis is essential for *Neisseria gonorrhoeae* viability. *The EMBO Journal* **19**, 1098–1107 (2000).

108. Bolanos-Garcia, V. M. & Davies, O. R. Structural analysis and classification of native proteins from E. coli commonly co-purified by immobilised metal affinity chromatography. *Biochimica et Biophysica Acta (BBA) - General Subjects* **1760**, 1304–1313 (2006).

109. Dupree, E. J. *et al.* A Critical Review of Bottom-Up Proteomics: The Good, the Bad, and the Future of This Field. *Proteomes* **8**, 14 (2020).

110. Gool, A. *et al.* Analytical techniques for multiplex analysis of protein biomarkers. *Expert Review of Proteomics* **17**, 1–17 (2020).

111. Chen, C., Hou, J., Tanner, J. J. & Cheng, J. Bioinformatics Methods for Mass Spectrometry-Based Proteomics Data Analysis. *International Journal of Molecular Sciences* **21**, 2873 (2020).

112. Searle, B. C. Scaffold: A bioinformatic tool for validating MS/MS-based proteomic studies. *Proteomics* **10**, 1265–1269 (2010).

113. Eng, J. K., McCormack, A. L. & Yates, J. R. An approach to correlate tandem mass spectral data of peptides with amino acid sequences in a protein database. *J. Am. Soc. Mass Spectrom.* **5**, 976–989 (1994).

114. Data-Independent Acquisition Mass Spectrometry-Based Proteomics and Software Tools: A Glimpse in 2020 - Zhang - 2020 - PROTEOMICS - Wiley Online Library. https://analyticalsciencejournals.onlinelibrary.wiley.com/doi/full/10.1002/pmic.201900276?casa_token=zQpPXGdTXhkAAAAA%3ASxVUQ44CjksSxqggwHnYgrkXiRjAxoD761J0l08sVpahjDJDBgUadNeBF0b9Q4FvTbvdwiUB4TD7ez-A.

115. Valle, M. *et al.* Visualizing tmRNA Entry into a Stalled Ribosome. *Science* **300**, 127–130 (2003).

116. Hong, S.-J., Lessner, F. H., Mahen, E. M. & Keiler, K. C. Proteomic identification of tmRNA substrates. *PNAS* **104**, 17128–17133 (2007).

117. Codon Usage Frequency Table(chart)-Genscript. https://www.genscript.com/tools/codon-frequency-table.

118. Zuker, M. Mfold web server for nucleic acid folding and hybridization prediction. *Nucleic Acids Res* **31**, 3406–3415 (2003).

119. Vvedenskaya, I. O. *et al.* Growth phase-dependent control of transcription start site selection and gene expression by nanoRNAs. *Genes Dev* **26**, 1498–1507 (2012).

120. EXPRESSYS - Tools & Reagents. http://expressys.com/main_tools.html.

121. Andersen, K. R., Leksa, N. C. & Schwartz, T. U. Optimized E. coli expression strain LOBSTR eliminates common contaminants from His-tag purification. *Proteins* **81**, 1857–1861 (2013).

122. Orbitrap Tribrid Mass Spectrometers - US. https://www.thermofisher.com/us/en/home/industrial/mass-spectrometry/liquid-chromatography-mass-spectrometry-lc-ms/lc-ms-systems/orbitrap-lc-ms/orbitrap-tribrid-mass-spectrometers.html.

123. Lutz, R. & Bujard, H. Independent and tight regulation of transcriptional units in Escherichia coli via the LacR/O, the TetR/O and AraC/I1-I2 regulatory elements. *Nucleic Acids Res* **25**, 1203–1210 (1997).

124. Datsenko, K. A. & Wanner, B. L. One-step inactivation of chromosomal genes in Escherichia coli K-12 using PCR products. *Proc Natl Acad Sci U S A* **97**, 6640–6645 (2000).

125. Ezraty, B., Gennaris, A., Barras, F. & Collet, J.-F. Oxidative stress, protein damage and repair in bacteria. *Nat Rev Microbiol* **15**, 385–396 (2017).

126. Neher, S. B. *et al.* Proteomic Profiling of ClpXP Substrates after DNA Damage Reveals Extensive Instability within SOS Regulon. *Molecular Cell* **22**, 193–204 (2006).

127. Paraquat: model for oxidant-initiated toxicity. | Environmental Health Perspectives | Vol. 55, No. https://ehp.niehs.nih.gov/doi/abs/10.1289/ehp.845537.

128. Chiang, S. M. & Schellhorn, H. E. Regulators of oxidative stress response genes in Escherichia coli and their functional conservation in bacteria. *Archives of Biochemistry and Biophysics* **525**, 161–169 (2012).

129. Nunoshiba, T., deRojas-Walker, T., Wishnok, J. S., Tannenbaum, S. R. & Demple, B. Activation by nitric oxide of an oxidative-stress response that defends Escherichia coli against activated macrophages. *Proc Natl Acad Sci U S A* **90**, 9993–9997 (1993).

130. Manchado, M., Michán, C. & Pueyo, C. Hydrogen peroxide activates the SoxRS regulon in vivo. *J Bacteriol* **182**, 6842–6844 (2000).

131. Schellhorn, H. E. Function, Evolution, and Composition of the RpoS Regulon in Escherichia coli. *Frontiers in Microbiology* **11**, (2020).

132. Gottesman, S. Trouble is coming: Signaling pathways that regulate general stress responses in bacteria. *Journal of Biological Chemistry* **294**, 11685–11700 (2019).

133. Kuroda, A. *et al.* Role of Inorganic Polyphosphate in Promoting Ribosomal Protein Degradation by the Lon Protease in E. coli. *Science* **293**, 705–708 (2001).

134. Iron mediates paraquat toxicity in Escherichia coli. - ScienceDirect. https://www.sciencedirect.com/science/article/pii/S002192581867111X.

135. Sunohara, T., Jojima, K., Yamamoto, Y., Inada, T. & Aiba, H. Nascent-peptide-mediated ribosome stalling at a stop codon induces mRNA cleavage resulting in nonstop mRNA that is recognized by tmRNA. *RNA* **10**, 378–386 (2004).

136. Wilson, D. N., Arenz, S. & Beckmann, R. Translation regulation via nascent polypeptide-mediated ribosome stalling. *Current Opinion in Structural Biology* **37**, 123–133 (2016).

137. Hayes, C. S. & Sauer, R. T. Cleavage of the A Site mRNA Codon during Ribosome Pausing Provides a Mechanism for Translational Quality Control. *Molecular Cell* **12**, 903–911 (2003).

138. Sunohara, T., Jojima, K., Tagami, H., Inada, T. & Aiba, H. Ribosome Stalling during Translation Elongation Induces Cleavage of mRNA Being Translated in Escherichia coli*. *Journal of Biological Chemistry* **279**, 15368–15375 (2004).

139. Janssen, B. D., Garza-Sánchez, F. & Hayes, C. S. A-Site mRNA Cleavage Is Not Required for tmRNA-Mediated ssrA-Peptide Tagging. *PLOS ONE* **8**, e81319 (2013).

140. Tian, C. *et al.* Rapid Curtailing of the Stringent Response by Toxin-Antitoxin Module-Encoded mRNases. *Journal of Bacteriology* **198**, 1918–1926 (2016).

141. Bertram, R. & Schuster, C. F. Post-transcriptional regulation of gene expression in bacterial pathogens by toxin-antitoxin systems. *Front. Cell. Infect. Microbiol.* **4**, (2014).

142. Agirrezabala, X. *et al.* The ribosome triggers the stringent response by RelA via a highly distorted tRNA. *EMBO reports* **14**, 811–816 (2013).

143. Atkinson, G. C., Tenson, T. & Hauryliuk, V. The RelA/SpoT Homolog (RSH) Superfamily: Distribution and Functional Evolution of ppGpp Synthetases and Hydrolases across the Tree of Life. *PLOS ONE* **6**, e23479 (2011).

144. Irving, S. E., Choudhury, N. R. & Corrigan, R. M. The stringent response and physiological roles of (pp)pGpp in bacteria. *Nature Reviews Microbiology* 1–16 (2020) doi:10.1038/s41579-020-00470-y.

145. Goeders, N., Drèze, P.-L. & Melderen, L. V. Relaxed Cleavage Specificity within the RelE Toxin Family. *J. Bacteriol.* **195**, 2541–2549 (2013).

146. Hwang, J.-Y. & Buskirk, A. R. A ribosome profiling study of mRNA cleavage by the endonuclease RelE. *Nucleic Acids Res* **45**, 327–336 (2017).

147. Pedersen, K. *et al.* The Bacterial Toxin RelE Displays Codon-Specific Cleavage of mRNAs in the Ribosomal A Site. *Cell* **112**, 131–140 (2003).

148. Li, X., Yagi, M., Morita, T. & Aiba, H. Cleavage of mRNAs and role of tmRNA system under amino acid starvation in Escherichia coli. *Molecular Microbiology* **68**, 462–473 (2008).

149. Chadani, Y. *et al. trans*-translation-mediated tight regulation of the expression of the alternative ribosome-rescue factor ArfA in *Escherichia coli*. *Genes & Genetic Systems* **86**, 151–163 (2011).

150. Boutte, C. C. & Crosson, S. Bacterial lifestyle shapes the regulation of stringent response activation. *Trends Microbiol* **21**, 174–180 (2013).

151. Kanjee, U., Ogata, K. & Houry, W. A. Direct binding targets of the stringent response alarmone (p)ppGpp. *Molecular Microbiology* **85**, 1029–1043 (2012).

152. Barker, M. M., Gaal, T., Josaitis, C. A. & Gourse, R. L. Mechanism of regulation of transcription initiation by ppGpp. I. Effects of ppGpp on transcription initiation in vivo and in vitro1 1Edited by R. Ebright. *Journal of Molecular Biology* **305**, 673–688 (2001).

153. Paul, B. J. *et al.* DksA: A Critical Component of the Transcription Initiation Machinery that Potentiates the Regulation of rRNA Promoters by ppGpp and the Initiating NTP. *Cell* **118**, 311–322 (2004).

154. Jenvert, R.-M. K. & Schiavone, L. H. Characterization of the tRNA and ribosome-dependent pppGpp-synthesis by recombinant stringent factor from Escherichia coli. *The FEBS Journal* **272**, 685–695 (2005).

155. Vinogradova, D. S. *et al.* How the initiating ribosome copes with ppGpp to translate mRNAs. *PLOS Biology* **18**, e3000593 (2020).

156. Christensen, S. K. & Gerdes, K. Delayed-relaxed response explained by hyperactivation of RelE. *Molecular Microbiology* **53**, 587–597 (2004).

157. Han, M.-J. & Lee, S. Y. The Escherichia coli Proteome: Past, Present, and Future Prospects. *Microbiology and Molecular Biology Reviews* **70**, 362 (2006).

158. Swaney, D. L., Wenger, C. D. & Coon, J. J. Value of Using Multiple Proteases for Large-Scale Mass Spectrometry-Based Proteomics. *J. Proteome Res.* **9**, 1323–1329 (2010).

159. Moore SD, Sauer RT. Ribosome rescue: tmRNA tagging activity and capacity in Escherichia coli. **58**, 456–466 (2005).